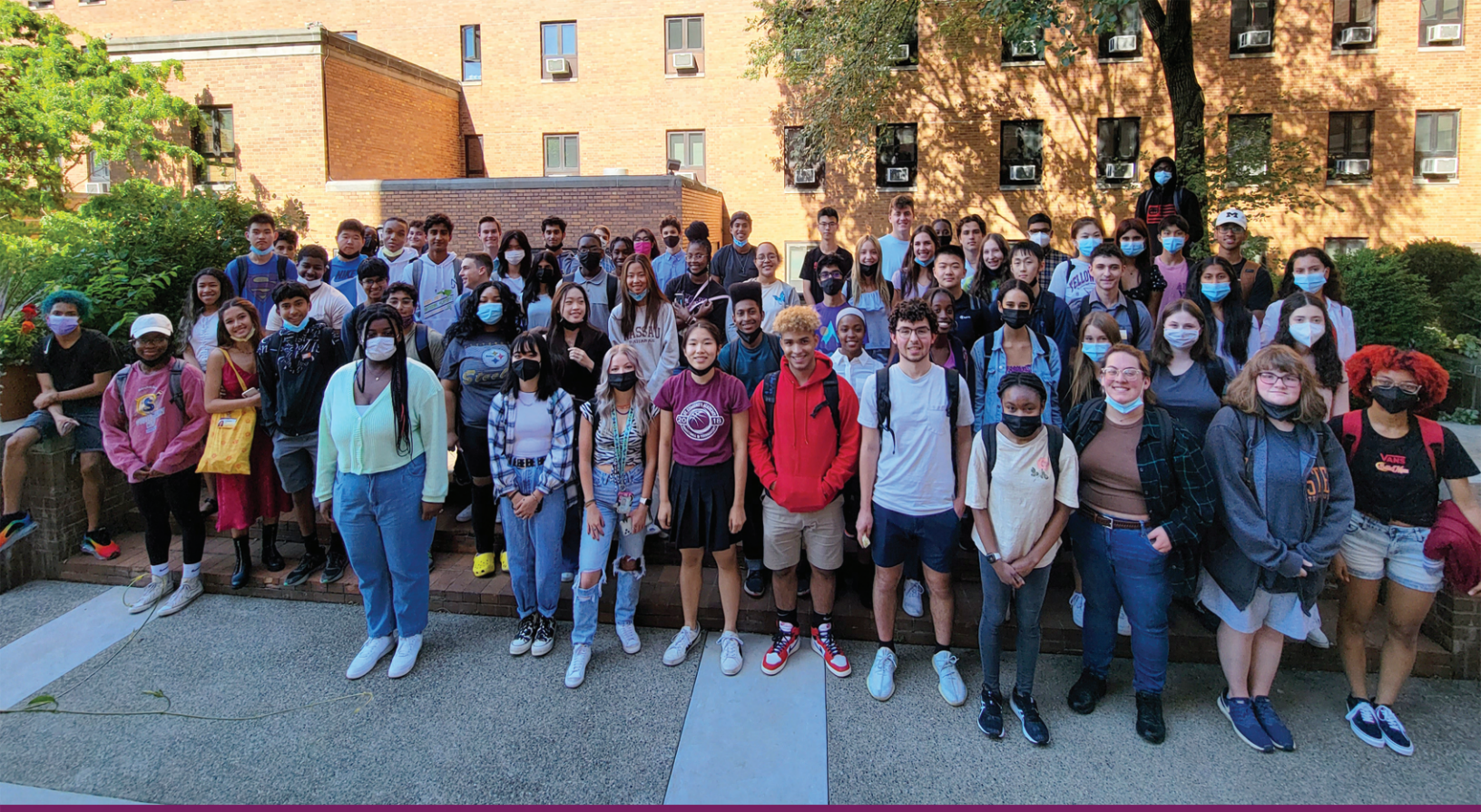

UPMC HILLMAN CANCER CENTER ACADEMY

Abstract Book

Friday, August 5th, 2022

UPMC
LIFE CHANGING MEDICINE

University of Pittsburgh

Welcome

Thank you for joining us today to honor our hard-working scholars and laboratories from the Hillman Academy! We strive to provide cutting-edge research and career preparatory experiences to a diverse group of highly motivated high school students who are interested in pursuing higher education and careers in STEM fields. In this hands-on summer program, scholars are placed in laboratories directed by dedicated faculty and trainee mentors across the University of Pittsburgh Campus.

Over the course of its history, the Hillman Academy has become an award-winning science, technology, engineering, and mathematics (STEM) program that prepares students for successful college careers and beyond. The Academy was initiated in 2009 under the directorship of Michael Lotze, MD and has grown to the program it is today with generous support from the NIH, Doris Duke Charitable Foundation, Jack Kent Cooke Foundation, UPMC, Hillman Foundation, Ear and Eye Foundation, Beckwith Funds, Stan Marks Foundation, Pitt, grateful parents and patients, and the many University faculty, trainees, and staff who give selflessly of their time.

Please join us in honoring these students and mentors, as well as, the hard work they did this summer to complete an authentic research project. We are so glad that you chose to join us today and are pleased that you have given your scholar a chance to work with our talented faculty, students, and fellows!

Hillman Academy Staff:

Program Director: David Boone

Associate Director: Joseph Ayoob

Program Coordinator: Solomon Livshits

Project Manager: Steven Jones

Site Directors:

Cancer Biology (CB): Dr. Deborah Galson and Dr. Malabika Sen

Computer Science, Biology and Biomedical Informatics (CoSBBI): Dr. David Boone

Computational Biology (CompBio): Dr. Joseph C. Ayoob and Dr. David Koes

Immunology and Cancer Immunotherapy (ICI): Dr. Tullia Bruno and Dr. Greg Delgoffe

Ophthalmology (OPT): Dr. Yuanyuan Chen

Surgery: Dr. Steven Evans

Tech Drive X (TDX): Dr. Andrew Duncan and Serafina Lanna

Women's Cancer Research Center (WCRC): Dr. Jennifer Xavier

Thank you

This program was made possible with the help of the following people and organizations.

Funding

National Institutes of Health (NIH)

National Cancer Institute Youth Enjoy Science Program

Doris Duke Charitable Foundation (DDCF)

The Beckwith Institute

Hillman Foundation

Shadyside Hospital Foundation

Ear and Eye Foundation

NIH CURE - past

UPMC Center for Engagement and Inclusion – past

Jack Kent Cooke Foundation

Stan Marks Foundation

University of Pittsburgh

UPMC Parking and Security – past

Grateful parents and patients

Partners

Fund for the Advancement of Minority Education (FAME)

Homeless Children's Education Fund (HCEF)

Pittsburgh Public Schools (PPS)

Remake Learning

MPowerhouse

STEM PUSH Network

Partners (cont.)

Precollege STEM Programs at Pitt

The Citizen Science Lab

Gene Team

BioZone

Community Engagement Centers

Propel Schools

Hillman Academy Leadership Team

Dr. Robert Ferris

Dr. Devin Dressman

Dr. Chad Ellis

Dr. Christopher Bakkenist

Dr. David Boone

Dr. Joe Ayoob

Site Heads

Dr. Joe Ayoob

Dr. David Boone

Dr. Tullia Bruno

Dr. Yuanyuan Chen

Dr. Greg Delgoffe

Dr. Andrew Duncan

Dr. Steven Evans

Dr. Deborah Galson

Dr. David Koes

Serafina Lanna

Dr. Malabika Sen

Dr. Jennifer Xavier

Administration

Ivet Bahar

Michael Becich

Greg Cooper

Genine Bartolotta

Josh Bennis

Andrea Brasili

Kathy Brickett

Rob Ceccehetti

Dianna Fennell

Carrie Fogel

Harry Hochheiser

Steven Jones

Barbara Karnbauer

Geeta Kaul

Adam Kohlhaas

Robert Kornosky

Vladislav Leskovtec

Alison Lithgow

Solomon Livshits

Andrew Orenberg

Toni Porterfield

Rayleigh Reynolds

Stacey Rizzo

José-Alain Sahel

Madison Seaver

Craig Smith

Lawney Snyder

Lola Thompson

Gina Toy-Cutler

Administration (cont.)

Darryl Washington

Technology

Anthony Bell

Laura Brun

Scot Dunsmore

Keith Durst

HDS and Interpreters

Jayde Eng

John Blasco

Marcus Springer

Josh Stresing

Doris Duke Scholars

Ivy Baker

Pablo Coen-Pirani

Michelle Orioha

Yash Patel

Instructors

Phuong Mai

Andrew Orenberg

Laura Savariau

Megan Yates

TECBio REU @ Pitt Mentoring Committee

Rose Evard

Maya Iwabuchi

Anamarie Martinez-Turak

Carli Newman

Madeline Ohl

Makayla Reed

Jane Siwek

Speakers, Lecturers, and Guests

Jorge Antonio Gumucio

Rebecca Auron

Hamzah Aweidah

Joe Ayoob

Riyue Bao

Jenna Barbour

Michael Becich

Ruel Beresford

David Boone

Rich Boyce

Myrna Brignol

Tullia Bruno

Timothy Burns

Paul Cantalupo

Anne-Ruxandra Carvunis

Speakers, Lecturers, and Guests (cont.)

Brittany Chamberlain

Kun-Che Chang

Shaquille Charles

Keith Callenberg

Scott Cohen

Steven Evans

Deborah Galson

Dr. Aditi Gurkar

MaCalus Hogan

Dennis Hsu

Mahnoor Imran

Vishal Jhanji

Jacquita Johnson

Steven Jones

Aiden Lakshman

Sanghoon Lee

Chenyu Li

Solomon Livshits

John Maier

Lisa McIlvreid

Daisy Okpa

Andrew Orenberg

Eddie Perez

Vanessa Reyes

William Reynolds

Maxwell Reynolds

Dr. Stacey Rizzo

Taylor Robinson

Joy Roy

April Sagan

Bee Schindler

Clarence Scott

Malabika Sen

Remi Shittu

Elizabeth Shunk

Sanya Taneja

Nilgun Tasdemir

Shikhar Uttam

Abhishek Vats

Lawrence Vernetti

Andreas Vogt

Rebecca Watters

Sierra Wilson

Professional Development Seminar Series Speakers

Joe Ayoob

Office of Diversity Equity and Inclusion in the Health Sciences– Bee Schindler

TRIO Student Support Services – James Scott, Jenna Barbour, and Liz Shunk

Taylor Robinson and David Donehue – past students

Public Health Panel – Myrna Brignol, Ruel Beresford, Jacquita Johnson, Jorge Antonio Gumucio, and Daisy Okpa

Atomic Hands and ASL Clear- Scott Cohen

Surgeons – MaCalus Hogan, Steven Evans, Vanessa Reyes, Mahnoor Imran, and Shaquille Charles

Tullia Bruno

Solomon Livshits

Davin Sweeney

Mentors

Thanks to the 100s of mentors across campus each of which is recognized on the individual student abstracts and site schedules!

Offices and Departments

University of Pittsburgh

UPMC Hospital System

UPMC Hillman Cancer Center

Children's Hospital

Pitt School of Medicine

Ear and Eye Institute

UPMC Security Office

UPMC Volunteer office

Disability Resources and Services

Pitt IT/ Technology Help Desk

Panther Central

Department of Biomedical Informatics

Department of Ophthalmology

Computational and Systems Biology

Department of Immunology

Department of Pathology

Department of Surgery

Magee Women's Cancer Research Institute

McGowan Institute of Regenerative Medicine

University Counsel

And the many other departments that support this program.

UPMC HCC Summer Academy
Cancer Biology Site 2022 Research Symposium

August 5, 2022, 8:30 am-12:45 pm
Auditorium in Assembly Building on 5051 Center Ave
Zoom Link - https://pitt.zoom.us/j/96664887654 Passcode: 089238

8:30AM **Welcoming Remarks**

CB Site Education Team:
Deborah L. Galson, PhD, CB Site Director
Malabika Sen, PhD, CB Site Co-Director
Andrew Orenberg, Grad. Student, CB Site Teaching Assistant

8:45 AM- 12:45 PM CB Scholar Research Presentations (10 min talks)

8:45 AM #1 Leviticus McGraw-Sapp
Lab: Timothy F. Burns, MD, PhD; Lab Mentor: Vinod Kumar, PhD

9:00 AM #2 Daniel Guo
Lab: Shou-Jiang Gao, PhD; Lab Mentor: Wen Meng, PhD

9:15 AM #3 Catherine Maldia
Lab: Shou-Jiang Gao, PhD; Lab Mentor: Wen Meng, PhD

9:30 AM #4 Jibraan Rahman
Lab: Shivendra Singh, PhD; Lab Mentor: Krishna Beer Singh, PhD

9:45 AM #5 Audrey Munro-Neely
Lab: Lin Zhang, PhD; Lab Mentor: Sui Sui Hao, PhD

10:00 AM #6 Maria Silvaggio
Lab: Kurt R. Weiss, MD; Lab Mentor: Tanya Heim, MS

10:15 AM #7 Donovan Allen
Lab: Taofeek Owonikoko, MD, PhD; Lab Mentor: John Schmitz, PhD

10:30-10:45 AM ---------- BREAK ----------

10:45 AM #8 Daniel Wang
Lab: Kathryn Demanelis, PhD

11:00 AM #9 Jason Chen
Lab: Wei Du, MD, PhD; Lab Mentor: Limei Wu, PhD

11:15 AM #10 Ethan Minzer
Lab: Wei Du, MD, PhD; Lab Mentor: Neha Atale, PhD

11:30 AM #11 Nancy Chen
Lab: Yvonne Chao, MD, PhD;
Lab Mentors: Haizhou Liu, PhD & Sheeba John Mary, PhD

11:45 AM #12 Mohammed Al-Nagash
Lab: Haitao Guo, PhD; Lab Mentor: Elena Kim, PhD

12:00 PM #13 Anthony Kalvi
Lab: Jian Yu, PhD; Lab Mentor: Brian Leibowitz, PhD

12:15 PM #14 Hillary Boyzo
Lab: Hatice Osmanbeyoglu, PhD; Lab Mentor: April Sagan, PhD

12:30 PM #15 Yash Patel *DDCF Undergraduate Intern
Lab: Hatice Osmanbeyoglu, PhD; Lab Mentor: Sanghoon Lee, PhD

12:45 PM ------ LUNCHEON (Atrium/Crane Shed)------

2:00 PM ACADEMY-WIDE CLOSING CEREMONY (Auditorium)

Hillman Academy – Computational Biology (CompBio)

2022 Research Symposium

August 5, 2022, 10:00 AM to 12:05 PM

8th floor classroom Murdoch Building (3420 Fifth Ave)

https://pitt.zoom.us/j/95184305664. Passcode: science

10:15 AM **Introduction**

COBRA Scholars Research Presentations

10:20 AM **Maria Ramos**

Mentor: Daniel Yuan

10:35 AM **Akiva Rosenzweig**

Mentor: Ali Sinan Saglam

10:50 AM **Neil Porwal**

Mentors: Tyler Lovelace and Minxue Jia

11:05 AM **Break**

11:20 AM **Fatimah Bisiriyu, Sophia Song, Ananya Vyas**

Mentor: Dr. David Koes

11:35 AM **Oluwatobiloba Olaore**

Mentor: Mr. Anupam Banerjee

11:50 AM **Ivan Revis**

Mentor: Dante Poe

12:05 PM **Orion Douglas**

Mentor: Dr. Maria Chikina

Hillman Academy - CoSBBI
2022 Research Symposium
August 5, 2022, 8:00 AM
The Offices at Baum, Room 407 A/B
https://us02web.zoom.us/j/85754282549?pwd=elordlNjOE43cFNXOEM4M3RhNGRjZz09

8:00 AM **Welcoming Remarks**
David Boone, PhD

8:05 AM **CoSBBI Scholars Research Presentations – Session 1**

8:05 AM **Katherine Hu**
Mentors: Drs. Xinghua Lu and Lujia Chen

8:20 AM **Arya Mehta**
Mentor: Dr. Pradeep Raamana

8:35 AM **Kevin Lu**
Mentors: Drs. Xinghua Lu and Lujia Chen

8:50 AM **Olutoba Ojo**
Mentors: Dr. Uma Chandran and Alex Chang

9:05 AM **Johnathan Sheerrill**
Mentor: Dr. Catherine Bender

9:20 AM **Shaun Fernando**
Mentors: Dr. Dana Bovbjerg and Jessica Manculich

9:35 AM **BREAK**

9:40 AM **CoSBBI Scholars Research Presentations – Session 2**

9:40 AM **Aiden Dorneich**
Mentors: Drs. Murat Akcakaya and Busra Tugce Susam

9:55 AM **Elizabeth Bair**
Mentor: Dr. Andrew King

10:10 AM **Preetam Jukalkar**
Mentors: Dr. Liang Zhan and Xiyao Fu

10:25 AM **Anyssa Oden**
Mentors: Dr. Steven Abramowitch and Shaniel Bowen

10:40 AM **Richael Saka**
Mentor: Dr. Olga Kravchenko

10:55 AM **Samantha Fernsebner and Zivia Gale**
Mentors: Drs. Daniel Lundberg and Adebowale Ogunjirin

11:15 AM **BREAK**

11:20 AM **CoSBBI Scholars Research Presentations – Session 3**

11:20 AM **Ryan Krishna**
Mentor: Dr. Balaji Palanisamy

11:35 AM **Valerie DeVos**
Mentor: Dr. Rich Boyce

11:50 AM **Ivy Baker – Doris Duke Undergraduate**
Mentor: Dr. Rich Boyce

12:05 AM **Pablo Coen-Pirani – Doris Duke Undergraduate**
Mentors: Dr. Xia Jiang and Chuhan Xu

12:20 PM **Ansh Goyal**
Mentors: Dr. Rafael Ceschin, William Reynolds, and Joy Roy

12:35 PM **Tejas Mitra**
Mentors: Dr. In Hee Lee and Ehab Hamed

12:50 PM **Lunch – Baum 4th floor foyer and 407A/B RSVP REQUIRED**

2:00 PM **Hillman Academy Graduation**
Assembly Building – 5051 Center Ave or **Zoom for students**:
https://us02web.zoom.us/j/86021100717?pwd=dmVQQ0NvYzFnMUVIOUxKWFdwd2U5UT09
YouTube for others: https://www.youtube.com/watch?v=mCHMby8VqTg

Hillman Academy – Immunology and Cancer Immunotherapy (ICI)

2022 Research Symposium

August 5, 2022, 8:30 AM to 12:30 PM
Cancer Pavilion - Herberman Conference Center 202a
https://pitt.zoom.us/j/93436767243

8:30 AM **Breakfast**

9:00 AM **Welcome video by Greg Delgoffe and Tullia Bruno**

ICI Scholars Research Presentations

9:15 AM **Alessandra Azure**
Delgoffe Lab

9:30 AM **Marcus Waller**
Turnquist Lab

9:45 AM **Iliyan Nazarali**
Das Lab

10:00 AM **Grace Ketler**
Bruno Lab

10:15 AM **Break**

10:30 AM **Jenna Trent**
Ferris Lab

10:45 AM **Sulwe Kauffman-Okoko**
Soloff Lab

11:00 PM **Kamili Wiley**
Gottschalk Lab

11:15 AM **Helen Zhang**
Gottschalk Lab

11:30 AM **Break**

11:45 AM **Lea Omer**
Ito Lab

12:00 PM **Jhanvi Sharma**
Kohan Lab

12:15 PM **Closing remarks by Ian MacFawn, Brydie Huckestein and, Stephanie Grebinoski**

12:30 AM **Grab and go lunch**

We want to thank the Hillman Cancer Center and Department of Immunology for being supportive of our site and our mission to train the next generation of scientists. We also want to thank the mentors, both principal investigators and lab mentors that have spent so much time with the kids this summer. Finally, we want to thank all the students for working so hard this summer!

Hillman Academy – Ophthalmology (OPT)

Hillman Summer Students Research Presentations

August 5, 2022, 9:00 AM to 12:00 PM

EEI 936

https://pitt.zoom.us/j/99934918582

Each session will be started by a brief intro of each student by his/her mentor followed by a 10 min presentation leaving 2 min Q&A.

9:30-9:45 am Start the OPT site meeting

9:45-10:00 am Skyler Spears (Mentors: Drs. Vishal Jhani and Gary Hin-Fai Yam)

10:00-10:15 am Jasmine Horton (Mentor: J. Patrick Mayo)

10:15-10:30 am Marcus Jones (Mentor: Dr. Shaohua Pi)

10:30-10:45 am Daniel Komlosi (Mentor: Dr. Robert M. Shanks)

10:45-11:00 am Jonathan Li (Mentor: Dr. Yuanyuan Chen)

11:00-11:15 am Samuel Wilson (Mentor: Dr. Yiqin Du)

11:15-12:00 pm Lunch

Hillman Academy – Surgery

Hillman Academy Final Presentations

August 5, 2022, 9:00 AM to 12:00 PM

UPMC Presbyterian Hospital F1273

https://bit.ly/3SsIYds Passcode: cyjMmh

9:00 AM **Opening Remarks**

Surgery Scholars Research Presentations

9:10 AM **Jeremiah Satcho**

Mentor: Dr. Amer Zureikat

9:25 AM **Sean Russell**

Mentor: Dr. Christine Leeper

9:40 AM **Michael Ulis**

Mentor: Dr. Joseph Church

9:55 AM **Lucy Pu**

Mentor: Dr. Rajeev Dhupar

10:10 AM **Rae'Nell Durham**

Mentor: Dr. Joshua Brown

10:25 AM **Aniya Hall**

Mentor: Dr. Nathan Liang

10:40 PM **Closing Remarks**

TECH DRIVE X

2022 Research Symposium • Hillman Academy

August 5, 2022

Bridgeside Point II, Room 503, 450 Technology Drive, Pittsburgh, PA 15219
Virtual: https://pitt.zoom.us/j/92797539563

8:45 AM **Welcome**
Dr. Andrew Duncan & Serafina Lanna, TDX Site Heads

9:00 AM **Oral Presentations** (10 min. presentations + 5 min. questions); introductions by lab mentors

9:00 AM **Franco Alvarez**
Lab & Mentor, Dr. Matt Steinhauser

9:15 AM **Sophia Alvarez**
Lab, Dr. Ioannis Zervantonakis; *Mentor,* Dorota Jazwinska

9:30AM **Elise Chu**
Lab, Dr. Bill Chen; *Mentors,* Aine Boudreau, Dr. Travis Lear

9:45 AM **Griffin Hurt**
Lab, Dr. Ioannis Zervantonakis; *Mentor,* Matt Poskus

10:00 AM **Priyasha Itani**
Lab, Dr. Justin Weinbaum; *Mentor,* Isabelle Chickanosky

10:15 AM **Tabo Mkandawire**
Lab, Dr. Fabrisia Ambrosio; *Mentors,* Gabrielle Gilmer, Dr. Zachary Hettinger

10:30 AM **BREAK**

10:45 AM **Oluwatomisin Olaore**
Lab, Drs. Yuan Liu, Jay Tan; *Mentor,* Qing Cao

11:00 AM **Arnav Patel**
Lab, Dr. Jonathan Vande Geest; *Mentors,* Ali Behrangzade, Hirut Kollech, Katarina Martinet, Remi Shittu, Gabrielle Wilson

11:15 AM **Narendra Ray**
Lab, Dr. Spandan Maiti; *Mentor,* Ronald Fortunato

11:30 AM **Sidharth Sadashiv**
Lab , Dr. Andreas Vogt; *Mentor,* Laura Vollmer

11:45 AM **Nikita Venkatasamy**
Lab, Dr. George Hussey; *Mentor,* Dr. William D'Angelo

12:00 PM **Julian Westray**
Lab, Dr. Vaughn Cooper; *Mentor,* Abigail Matela

12:15 PM **Luncheon – Bridgeside Point II, 5th floor lunchroom**

2:00 PM **Closing Ceremony**
Assembly Building, First Floor Auditorium
5051 Centre Ave, Pittsburgh, PA 15213

WCRC HCC Academy

Room: 2001 Assembly Building

Zoom link: https://pitt.zoom.us/j/95027069803

10:00-12:00PM AM - Introduction and Hillman Academy Scholar Research Presentations

Welcome: Site Director: Jennifer Xavier, PhD

Enysah Roberts
PI: Adrian Lee PhD, Steffi Oesterreich PhD
Mentor: Neil Carleton

Isaiah Hooks
PI: Adrian Lee PhD, Steffi Oesterreich PhD
Mentors: Olivia McGinn PhD, Lauren Brown

Olivia St Esprit
PI: Carola Neumann, MD
Mentors: Lisa Hong

Donise Griffin
PI: Nadine Hempel PhD
Mentor: Sierra White, PhD

Joi Anthony-Gray
PI: Kathrine Aird PhD
Mentor: Apoorva Uboveja, PhD

Sofi Adams
PI: Margaret Rosenzweig RN, PhD

Michelle Orioha
PI: Lan Coffman, MD PhD
Mentor: Huda Aditya PhD, Len Frisbee

Closing: Site Director: Jennifer Xavier, PhD

12:00 PM – Lunch


Results

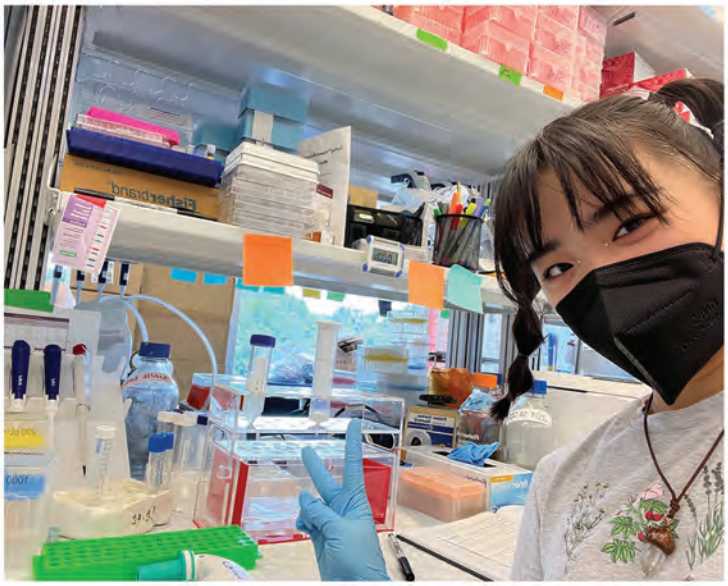

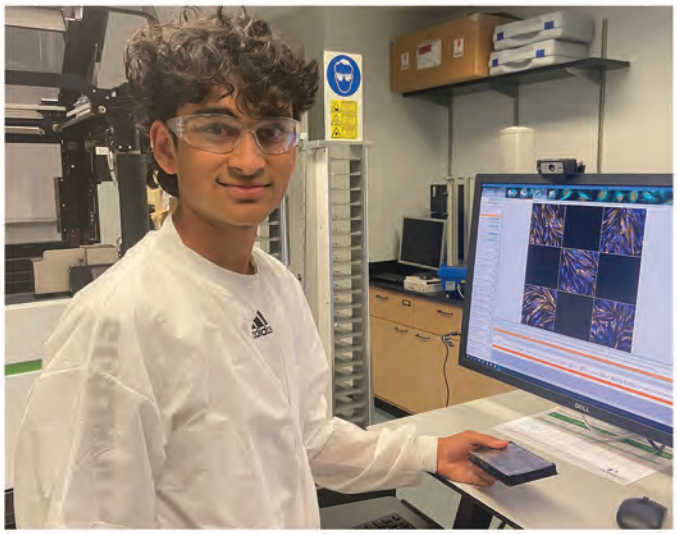


UPMC
LIFE CHANGING MEDICINE
Effects of
Osteoblas

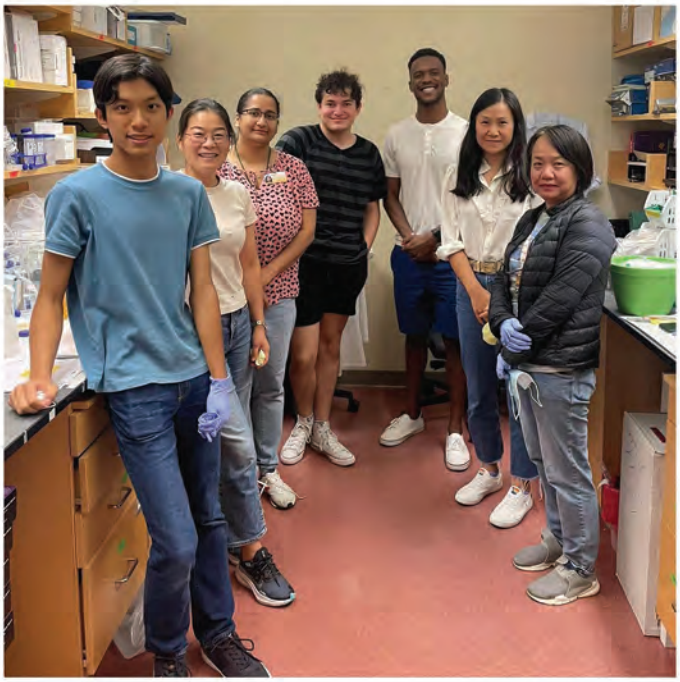

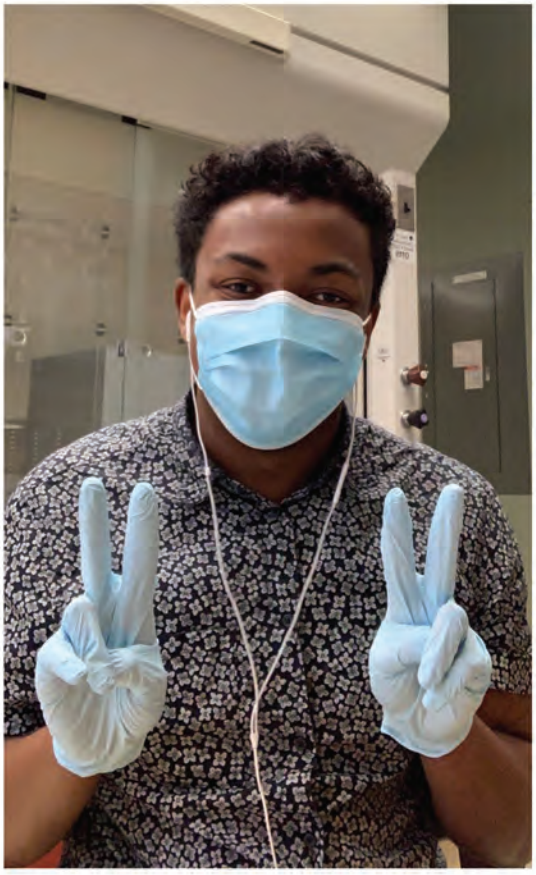

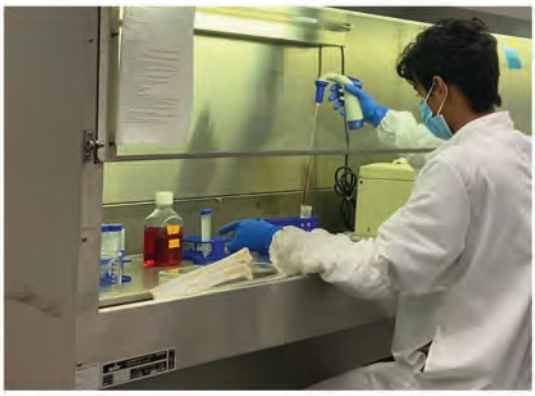

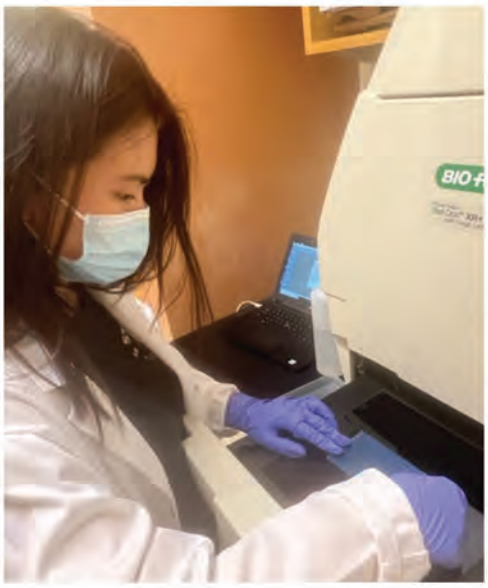


WOMEN

Mental Health Disparities Between Deaf and Hard of Hearing & Hearing Peers

Scholar: Ivy Baker
College: Pennsylvania College of Technology, Williamsport, PA
Mentor: Dr. Richard Boyce
Site: Biomedical Informatics – CoSBBI

Background: Many barriers to treatment confront persons who identify as deaf, Deaf, or Hard of Hearing (d/DHH) and who also have mental health disorders, including bipolar, major depressive disorder, and PTSD. Lack of knowledge about Deaf culture and American Sign Language, discomfort with going to counseling with an interpreter because of privacy concerns are just some issues that d/DHH patients with mental health conditions face.

Objective: This project studies differences in mental health treatment between d/DHH and hearing people with respect to mental health treatment using a database called All of Us (AoU). AoU is a national cohort study currently seeking to enroll 1 million patients who are highly diverse (race, ethnicity, gender identity, socioeconomic status, etc.), including d/DHH people.

Methods: Using the AoU workbench, cohort definitions were created to identify participants who were d/DHH, and/or had depression. Summary statistics using the first diagnosis of depression were used to compare the participants in each cohort by demographics, socio-economic status, health utilization, and responses to survey questions. Differences were summarized and discussed with a clinical expert to arrive at possible explanations.

Results: 18294 AoU participants were identified as d/DHH and 310776 as hearing. Participants with a diagnosis of any form of depression totaled 7043 (38.4%) for d/DHH and 46577 (15.0%) for hearing. The most common form of depression for d/DHH was Depressive disorder (48.7%) followed by Major depression, single episode (24.5%) while for hearing participants it was reversed with Major depression, single episode at 39.2% vs 35.7%.

Conclusions: Initial evidence suggests there might be significant differences in the prevalence of depression in the AoU dataset between d/DHH and hearing participants. We are in the process of completing the analysis of treatment pathways between cohorts.

Empirical Study of Overfitting in Deep Learning Prediction Models for Breast Cancer Metastasis

Scholar: Pablo Coen-Pirani

College: University of Southern California, Los Angeles, CA

PI: Xia Jiang, PhD

Mentors: Xia Jiang, Chuhan Xu

Site: CoSBBI

Background: Overfitting occurs when a machine learning or deep learning model fits a specific data set perfectly, resulting in weakened generalization, and ultimately affecting accuracy when predicting future data. The effect of overfitting on prediction performance of deep learning using non-image medical data has not yet been fully studied based on the relatively small number of related published papers on Google scholar. This study begins with training deep learning prediction models using Keras based on non-image EHR (electronic health records) datasets concerning five year breast cancer metastases, and focuses on identifying the most relevant factors for mitigating overfitting to improve deep learning prediction performance.

Methods: This study uses a unique type of grid search - a process to select the best values for hyperparameters - to study how each of the eleven hyperparameters influences model overfitting and prediction performance when assuming various values. For each of the hyperparameters, grid search is repeated thirty times and the average of those is used as the best value. To evaluate model performance with these hyperparameter values, five-fold cross validation is used to compute ROC (receiver operator characteristic) and in turn AUC (area under ROC curve).

Results: The eleven different hyperparameters used are Activation Function, Weight Initializers, Network Structure, Learning Rate, Momentum Beta, Iteration-based decay, Dropout Rate, Training Epochs, Batch Size, L1, and L2. The study's results show that the top five hyperparameters of a deep learning model that impact overfitting performance are: iteration-based decay, learning rate, batch size, L2, and L1.

Conclusion: The results illustrate that different hyperparameters will cause different impacts on the overfitting performance of the model. Therefore, hyperparameter tuning based on grid search will help to improve accuracy of the model in predicting future observations. Future studies could look at other ways to combat overfitting, or potentially examine its counterpart, underfitting.

Iron Metabolism in Ovarian Clear Cell Carcinoma: Determining the role CD10- enMSCs plays in promoting OCCC by altering iron regulation

Scholar: Michelle Orioha

College: Case Western Reserve University, Cleveland Ohio

Lab: Lan Coffman, MD, PhD

Mentor: Huda Atiya, PhD

Site: Women's Cancer

Ovarian Clear Cell Carcinoma (OCCC) is a rare, aggressive, and chemo-resistant subtype of Epithelial Ovarian Cancer with a strong link to endometriosis. Endometriosis is an inflammatory condition characterized by the present of the endometrium outside the uterus cavity. The endometriotic microenvironment is uniquely hypoxic with high levels of iron due to recurrent menstrual cycling, and this iron-rich microenvironment has been linked to promoting ovarian carcinogenesis through iron-induced oxidative stress. However, the mechanism by which endometriosis is increasing the risk of OCCC is still unknown. Our lab identified a subset of endometriosis-derived mesenchymal stem cells (enMSCs) that are characterized by loss of CD10 expression, a known endometrial stromal marker. CD10-negative enMSCs enhance OCCC growth through increasing intracellular iron. Here, I investigate if increasing iron uptake using Ferric Ammonium Citrate (FAC) has the same impact on OCCC co-cultured with CD10-negative enMSCs. OCCC tumor cells were treated with different concentrations of FAC to promote iron uptake in the cells. OCCC proliferation rate was measured. Quantitative PCR was used to determine the expression of FTL, FTH, RRM2, and 4KR1C2 as FAC concentration increased. Western blot was used to look at the protein levels of FTL, FTH, and the transferrin receptor changed with FAC treatment. Our result showed that increase FAC negatively effect OCCC proliferation. Our result also showed there was no significant change in expression of FTL, FTH, and RRM2 with FAC treatment. Protein levels of both FTL and FTH increased as FAC treatment increased while protein levels of the transferrin receptor decreased with increased FAC treatment. Our study shows that tumor cells alone are unable to handle an increased amount of iron. These results indicate that adding iron to the microenvironment does not influence OCCC in a similar way to enMSCs. Further studies will look at how enMSCs helps OCCC handle iron increasing.

Age-associated chromatin accessibility in primary human breast and prostate carcinomas

Scholar: Yash Patel

College: Vassar College, Poughkeepsie, New York

PI of group/lab: Hatice Ulku Osmanbeyoglu, PhD

Mentor: Sanghoon Lee, PhD

DDCF Undergraduate Intern at University of Pittsburgh Department of Biomedical Informatics

Background: Aging is associated with a decline in physiological function and increased risk of mortality and incidence of cancers. Old age is a strong risk factor for cancer. Researching the differences in cancer biology between young and old patients is necessary to develop more specific and effective cancer treatment strategies. While genomic and transcriptomic features of young and old cancer patients have been characterized, genome-wide chromatin accessibility differences between young and old patients remain largely unexplored.

Methods: We characterized tumor-intrinsic chromatin accessibility differences between young and old patients of breast (n=75) and prostate cancers (n=26) using primary tumors from The Cancer Genome Atlas (TCGA) assay for transposase-accessible chromatin with sequencing (ATAC-seq) dataset. Age ranges for younger and older patients varied by tumor type, we defined the young group as the youngest 20% and the old group as the oldest 20% for each cancer type.

Results: We identified distinct patterns of genome-wide chromatin accessibility in young and old patients of breast and prostate cancers. Inferred patient transcription factor (TF) motif activities revealed regulatory differences between and within young and old tumors. GRHL2 and the FOX family were higher in older patients, while the SOX family, JUN family, FOS family, GRHL2, BATF, FRA2, ATF3, AP-1, and EHF were higher in younger patients. We identified immune cell activation, Notch signaling, and oxidative stress response to be commonly enriched in young patients of breast and prostate cancers. In addition, we confirmed that differential peak accessibility and differential gene expression between young and old patients are associated.

Conclusions: This study reveals the distinct epigenomic features of young and old patients in breast and prostate cancers as well as the active TFs driving cancer progression. This provides valuable information for patient prognosis and ultimately effective cancer treatment strategies based on age.

SEMOARS: The Symptom Experience, Management, and Outcomes of Breast Cancer According to Race and Social Determinants

Scholar: Sofi Adams

College: College of Wooster, Wooster, Ohio

PI of group/lab: Margaret Rosenzweig

Mentor(s): Margaret Rosenzweig

Site: Women's Cancer Research Center (WCRC)

Background: There is a persistent racial disparity in breast cancer (BC) survival. Patient-provider communication could be part of solving the puzzle, particularly in the reporting of toxicity during BC treatment.

Aim: To quantify the provider's skill in communication during medical interviews prior to cyclic chemotherapy for early-stage BC patients and compare the results by race.

Methods: Symptom Experience, Management, and Outcomes According to Race and Social Determinants (SEMOARS) is a multi-site, repeated measures, multi-method study comparing the symptom experience of Black and White women with BC during treatment. The study focuses on females, Black or White race, 18 years or older, prescribed chemotherapy for stages 1-3 BC. Medical oncology clinic visits in Pittsburgh and Cleveland were audiotaped via recorders in exam rooms with all participants' permission. The interviews were later transcribed and analyzed using the 4 Habits Coding System (4HCS), a standardized clinician communication assessment tool. 4HCS includes four subscales measuring communication habits that are derived from the Four Habits Model. Habits are scored through 23 items on a 1–5-point scale by two reviewers. In this study, a 22-item version of the 4HCS was used, one item measuring nonverbal behaviors could not be assessed, for a total score of 22-110. T-tests were used to compare the mean scores between Black and White women.

Results: For this analysis, a subsample of 40 interviews was used. The sample demographics were 50% black. Black patient interviews had significantly lower scores ($t(38) = -1.78$, $p = .042$) for Habit 2: Eliciting Patient Perspective ($M = 7.1$, $SD = 3.6$). Mean scores were lower for Black interviews for Habits 3, 4, and the total Habit scores, but not significantly so. Eliciting patient perspectives may be particularly important for racially discordant patient-provider interviews.

N^6-Methyladenosine RNA Post Transcriptional Modification (PTM) Profiling in HBV-Infected Primary Human Hepatocytes (PHH)

Mohammed Ali Al-Nagash

School: Science and Technology Academy, Pittsburgh, Pa

PI: Prof. Haitao Guo, Ph.D.

Mentor: Elena Kim, Ph.D.

Site: Cancer Biology

Introduction: Hepatitis B Virus (HBV) is an exceptionally large-scale infection; around 300 million people live with chronic hepatitis B, the main disease that causes around million deaths per year. The virus is transmitted sexually and other horizontal transmissions, such as contaminated blood transfusions and needles, and vertical transmission. HBV infection can progress into liver fibrosis, cirrhosis, and hepatocellular carcinoma. N6-methyladenosine (m6A) is one of the most prevalent modifications of mRNA, which affects transcription stability and function of the methylated RNA, including viral mRNAs. Our objective is to model HBV infection in primary human hepatocytes (PHH) by m6A RNA PTM profiling in HBV-infected cells.

Methods: PHHs were infected with *wt*HBV at 500MOI. Total RNA was extracted from the hepatocytes, and Nanodrop2000 was used to detect RNA concentration, and Agilent Bioanalyzer - for distinguishing RNA integrity number (RIN). The RNA was then fragmented to optimal size. M6A RNA molecules were immunoprecipitated using anti-m6A antibodies. Pulled-down RNA concentration was assessed using Quant-it RiboGreen RNA Assay. RT-qPCR was used to quantify marker genes. Purified RNA was treated with DNase to reduce DNA contamination. The RNA inputs and IP-fractions underwent M6A-seq using HiSeq 2000.

Results: There was a significant drop in sequence reads for m6A modification of RNA in both the infected and uninfected cells. The comparative m6A RNA profiling demonstrated differential methylation and differential expression of the following hits: metastasis associated lung adenocarcinoma transcript 1(MALAT1), Calreticulin (CALR), Apolipoprotein B(APOB), Complement component 1(C1S) and Collagen alpha-3(VI) (COL6A3).

Conclusion: These hits could be potential prognostic markers for HBV infection, and may play a significant role in HBV-associated pathogenesis. Biological and technical replicates of this experiment will be done to confirm this result. Epitranscriptomic analysis of HBV and host cells will shed new light on virus-host interaction in the development of chronic HBV infection and hepatocellular carcinoma.

Novel Drug Combinations For The Treatment of Small Cell Lung Cancer

Scholar: Donovan Allen

High School: Central Catholic High School, Pittsburgh, PA

PI: Dr. Taofeek Owonikoko

Mentor: Dr. John Schmitz

Site: Cancer Biology

Small cell lung cancer (SCLC) is an aggressive form of lung cancer that accounts for 15% of all lung cancer cases. Heavily associated with smoking, small cell lung cancer generally has a poor prognosis and usually only detected in the later stages when it has already metastasized, making it difficult to treat effectively. While the initial treatments are often effective, the cancer almost always returns and becomes resistant to previous treatment. Single drug treatments are rarely effective, and the testing of new drug treatments and combinations are critical in the search of effective treatments. Our project focused on identifying possible drug combinations for the treatment of SCLC, using small cell DMS273 lung cancer cells. Our preliminary data demonstrated that SCLCs are sensitive to Polo-like kinase 1 (PLK1) inhibitors. Following IC50 determination of onvansertib (PLK1i) and four standard chemotherapeutic agents (AZD6738, BAY1895344, lurbinectedin, paclitaxel), the agents were combined and potential synergies were identified using Compusyn. The combination of onvansertib and paclitaxel showed the most synergy. To investigate the mechanism of action of onvansertib and paclitaxel, cells were exposed to the agents for 24 hr and then processed for immunoblot analysis. We observed rapid inhibition of PLK1 followed by stalling of the cell cycle at the G2/M phase. The combination resulted in enhanced PARP cleavage indicated that the cells underwent apoptosis. Onvansertib and paclitaxel are synergistic and the combination treatment was able to induce apoptosis in SCLC cells. Future studies will evaluate this combination in our in vivo animal models.

Effects of Methionine on Osteoblast Differentiation

Scholar: Franco Alvarez

High School/College/City/State: Greensburg Central Catholic High School, Greensburg, PA

PI of group/lab: Matthew Steinhauser, M.D.

Mentor(s): Tânia Amorim, Ph.D.

Site: Technology Drive X

Background: Research has shown that fasting results in beneficial physiological adaptations. For instance, studies have linked fasting to positive effects on chronic conditions such as obesity, diabetes, and cancer. However, fasting can also lead to negative health consequences, such as bone loss. A recent study investigating the effects of fasting on bone health in healthy adults revealed that P1NP circulating levels (bone formation marker) significantly decreased as fasting progressed. Interestingly, as P1NP levels decreased, methionine levels significantly increased, suggesting a potential relationship. But how methionine impacts bone formation is not fully understood. The aim of this study was to test the hypothesis that excess methionine impairs osteoblast (bone-forming cells) differentiation.

Methods: A human pre-osteoblast cell line (hFOB1.19) was used. Cells were incubated at 39.5˚C to intiate differentiation with exposure to 4 different levels of methionine during 16 days of differentiation: 1) no methionine; 2) 20 µmol of methionine (control); 3) 100 µmol of methionine; and 4) 500 µmol of methionine. Media was changed every 3 days, with treatment remaining constant. Following 16 days, mineralization levels were assessed using Alizarin Red.

Results: No methionine treatment resulted in significantly less mineralization compared to normal levels of methionine (20 µmol) (no methionine: 0.0141 ± 0.00182 mM; 20 µmol methionine: 0.0762 ± 0.00477 mM, $p < 0.01$). High doses of methionine (100 and 500 µmol) induced less mineralization than the 20 µmol dose (methionine 100 µmol: 0.0572 ± 0.00297 mM; methionine 500 µmol: 0.0474 ± 0.00545 mM, $p < 0.01$).

Conclusion: Methionine seems to play a significant role in osteoblast differentiation; for osteoblasts to differentiate, optimal levels of methionine are needed. It seems that osteoblasts do not differentiate in the absence of methionine, but excess methionine may also impair mineralization. Additional studies will be necessary to confirm this effect and to determine the mechanism of how methionine levels regulate bone formation.

Studying the Effects of Mesothelial to Mesenchymal Transition on High-Grade Serous Ovarian Carcinoma Metastasis

Scholar: Sophia Alvarez

High School: Norwin High School, North Huntingdon, PA

PI of Lab: Ioannis Zervantonakis

Mentor: Dorota Jazwinska

Site: Center for Biotechnology and Bioengineering

Background: High-grade serous ovarian cancer is the most common and deadliest type of ovarian cancer. This disease accounts for about 90% of all ovarian cancer diagnoses each year. Ovarian cancer originates in the fallopian tubes and once the tumors break off from the original tumor, it can metastasize through the peritoneum. The peritoneum is made up of a single layer of mesothelial cells, which the cancer invades through in order to metastasize. However, it is unclear exactly how the cells invade through the mesothelial monolayers. We hypothesize that the cancer cells induce mesothelial to mesenchymal transition (MMT) in the mesothelial cells in order to make them more motile.

Methods: To investigate this, we used microfluidics to observe the interaction of cancer cells and mesothelial cells and the effect of MMT inducing treatment. To create the devices, we poured PDMS into SU8 or 3D printed molds and bound them to glass slides creating the channels. The device has a center channel filled with collagen type I that simulates the stroma and allows for observation of the invasion of cellsd. To investigate the interactions between the mesothelial cells and cancer cells, we seeded mesothelial cells in one channel with cancer cells in the opposite channel, and both mesothelial cells and cancer cells in the same channel. In addition, we treated mesothelial cells with 2 ng/mL and 10 ng/mL TGFβ treatments to induce MMT.

Results: Preliminary images suggest that TGFβ treatments have an effect on the mesothelial cells which causes a more mesenchymal phenotype. When the cells were in the same channel, the cancer spheroids invaded through the mesothelial cells, making holes within the monolayers. When cells were in the opposite channel, preliminary data showed that the mesothelial cells began to invade towards the cancer cells.

References:

https://www.cancer.net/cancer-types/ovarian-fallopian-tube-and-peritoneal-cancer/statistics#:~:text=This%20year%2C%20an%20estimated%2019%2C880,with%20ovarian%20cancer%20in%202020.

Cyclin E amplification or overexpression in High Grade Serous Ovarian Carcinoma (HGSOC) increases DNA damage

Scholar: Joi Anthony-Gray

School: The Neighborhood Academy, Stanton Heights Pennsylvania

Lab: Katherine Aird, PhD

Mentor: Apoorva Uboveja

Site: Women's Cancer Research center

Background: Epithelial Ovarian cancer is the most lethal gynecologic malignancy. High Grade Serous Ovarian Carcinoma (HGSOC) is the most prevalent histo-subtype of epithelial ovarian cancer. Approximately 20% of HGSOCs have amplification or overexpression of *CCNE1* (encoding cyclin E). Cyclin E is an oncogene that induces replication stress and subsequent DNA damage. Previous studies have demonstrated that Cyclin E-high cells upregulate DNA repair genes to overcome replication stress, but the molecular mechanism remains unknown. Patients suffering from HGSOC have a worse prognosis in part due to their intrinsic resistance to standard-of-care poly (ADP-ribose) polymerase inhibitor (PARPi) therapies. PARP is an enzyme that plays an important role in the DNA repair process. PARP is required for single strand break repair. If it is inhibited, single strand breaks will be converted into double strand breaks, which are then repaired by the error-free homologous recombination (HR) pathway. In HR-deficient cells, neither pathway is available for DNA repair, leading to accumulation of DNA damage and cell death. As a result, PARP inhibitors have shown great promise for HGSOC patients with HR-deficient tumors. However, cyclin E-high tumors are generally HR-proficient. Therefore, identifying strategies to overcome HR-proficiency and sensitize cyclin E- high HGSOCs to PARPi is urgently needed.

Methods: I used cell pairs with low and high cyclin E expression (Ovcar8/Ovcar8-CCNE1 and FT282/FT282-CCNE1). Importantly, overexpressing of cyclin E in isogenic pairs (the same genetic background) allows for direct comparison of phenotypes. Ovcar8 cells are an HGSOC cell line while FT282 cells are derived from the fallopian tube. I performed immunofluorescence to detect the expression of DNA damage markers (53BP1 and yH2AX) in the cell lines mentioned above.

Results: Cyclin E-high (Ovcar8-CCNE1 and FT282-CCNE1) cells demonstrated a substantial increase in both 53BP1 and yH2AX DNA damage foci as compared to their Cyclin E-low counterparts. 53BP1 DNA damage foci were increased by about 23% and yH2AX foci were increased by about 8% in FT282-CCNE1(Cyclin E-high) cells as compared to FT282 (Cyclin E-

low) cells. In Ovcar8-CCNE1 (Cyclin E-high) cells, 53BP1 DNA damage foci increased by about 5% and yH2AX foci increased by about 7% as compared to Ovcar8 (Cyclin E-low) cells.

Conclusion: My results conclude that Cyclin E-high cells have increased DNA damage because of Cyclin E overexpression as is evident by the increased expression of DNA damage markers (53BP1 and yH2AX) as compared to Cyclin E-low cells.

Studies are currently ongoing in the lab to delineate the pathway by which Cyclin E-high cells overcome the replication stress caused by Cyclin E overexpression. Simultaneously, studies are being conducted to see how Cyclin E-high cells can overcome HR-proficiency so that they respond better to PARP inhibitors.

Effects of ATP-citrate lyase inhibitor on Phenotypic and Functional $CD8^+$ T cell Exhaustion

Scholar: Alessandra Azure

High School/College/City/State: Newport High School, Bellevue, Washington

PI of group/lab: Greg Delgoffe, PhD

Mentor(s): Kellie Spahr

Site: Immunology and Cancer Immunotherapy (ICI)

Background: T cell exhaustion is a hypofunctional fate induced by chronic infection or cancer that carries distinct metabolic characteristics. Preventing T cell exhaustion could sustain the immune system's anti-tumor response. Exhausted T cells lose full mitochondrial function, causing them to perform less oxidative phosphorylation (OXPHOS). We have previously observed an accumulation of lipid droplets in exhausted T cells, suggesting that metabolic insufficiency results in alternative carbon utilization. This raises the question of how lipid synthesis might be related to the progression of T cells towards exhaustion. We sought to investigate the impact of limiting intracellular Acetyl-CoA production on the development of T cell exhaustion by targeting ATP-citrate lyase (ACLY), which converts citrate to Acetyl-CoA.

Methods: $CD8^+$ T cells from C57Bl/6 mice were activated for 24 hours through the TCR using aCD3/aCD28 dynabeads. Cells either received no additional stimulation (acute stimulation - AS) or continuous TCR stimulation for 6 days (chronic stimulation - CS). Within each AS/CS group, cells were treated with ACLY inhibitor concentrations of 0μM, 10μM, 20μM, or 40μM per subgroup. Cells were analyzed by flow cytometry for markers of exhaustion.

Results: In both AS and CS conditions, a greater number of cytokines were produced by cells treated with 40μM ACLYi than those treated with lower concentrations. CS cells were most impacted: 5.39% of cells without ACLYi were $IFN\gamma^{hi}$ $TNF\text{-}\alpha^{hi}$, compared to 51.0% with 40μM ACLYi. No significant difference in PD-1 or TIM-3 expression was observed in any cell group.

Conclusion: These data suggest that ACLY inhibition preserves T cell effector function under chronic stimulation conditions. The optimal dosage of ACLYi may lie around 30μM - high enough to impact cytokine production, but low enough not to hinder cell proliferation. Future steps include repeat testing under hypoxia and in vivo experimentation with mice tumors.

Generating Summaries of Oxygen Therapy Decisions from Transcribed Oral Presentations of ICU Patients

Elizabeth Bair[1], Jeremy M Kahn MD, Andrew J King PhD

[1]Hempfield Area High School, Greensburg, PA; [2]Department of Critical Care Medicine, University of Pittsburgh, Pittsburgh, PA

Abstract

Automatically generated summaries of oxygen therapy decisions would improve the decision-making efficiency of physicians, when needing to understand past treatment. Using annotated transcriptions of 135 *orally presented cases, we developed a system to scan for keywords indicating that an oxygen therapy decision is past or current. We found that including temporal status of decisions produces a more accurate summary than not including it (95% confidence interval of accuracy of our system minus baseline: 0.33, 0.47).*

Introduction

Patients in the intensive care unit (ICU) are the most critically ill, often experiencing multiple organ failure and requiring intensive monitoring and treatment. ICU patients often receive oxygen therapies, such as invasive mechanical ventilation, to help support their breathing. A physician who is monitoring a busy ICU may make dozens of oxygen therapy decisions each day, which makes keeping track of all the decisions difficult. If the oxygen therapy decisions could be automatically summarized, then it may help physicians quickly understand each patient's trajectory on oxygen therapy, which could improve care. Our objective was to develop an expert system for classifying utterances (i.e., spoken sentences) relating to oxygen therapy as being related to a past or current decision. We hypothesized that an automatically generated summary of oxygen therapy decisions that includes temporal status will be more accurate than one that does not.

Methods

In a prior study, de-identified electronic health record data for 135 ICU patient cases were reviewed and orally presented by ICU physicians [1]. Transcriptions of the presentations were annotated for mentions of past and current decisions about oxygen therapy. In total, 327 utterances were found to include oxygen therapy decisions and were used for this study. We manually developed a set of rules (i.e., keywords that indicate a past or current decision) using a training group of 116 utterances, which was further split into five batches (i.e., subsets) to progressively update and evaluate the rules based on accuracy. The final rules were applied to a test group containing the remaining 211 utterances to classify each as being either a current or past decision about oxygen therapy. We evaluated the classifications against the annotated classes and calculated accuracy, sensitivity, and specificity. Each rule is an if-then statement that uses regular expressions to scan for keywords within each utterance. We also created a baseline classifier that randomly assigns an oxygen therapy decision as being past or current. We call the two methods "expert system" and "random assignment," respectively. All experiments were conducted in Python using a Jupyter Notebook.

Results

Figure 1 shows the 95% confidence intervals of accuracy, sensitivity, and specificity for the expert system and random assignment classifiers. The confidence interval of the difference in accuracy (expert system – random assignment) is (0.33, 0.47). The interval does not include 0 so we can reject the null hypothesis that there is no difference between the two methods and accept the alternative hypothesis that our expert system performs significantly better.

Discussion

This research shows that using keywords to extract temporal status can improve the accuracy of summarizing oxygen therapy decisions. Beyond temporal status, other types of contextual information may be valuable additions to this work. For example, the ConText algorithm developed by Harkema et. al. also annotates contextual

information such as negation and experience [2]. Additionally, we plan to apply a similar process to classify utterances relating to other therapeutic decisions.

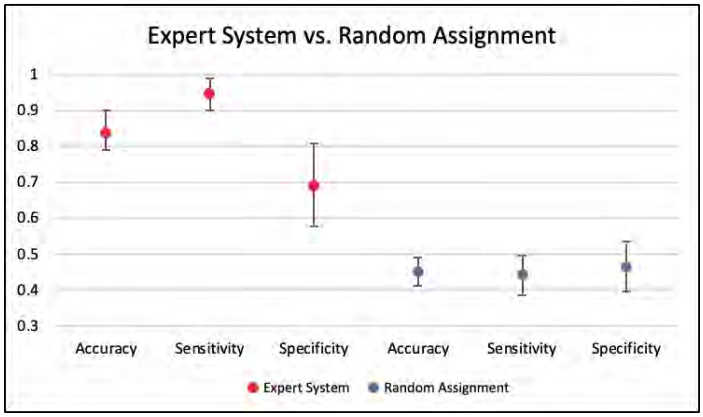

Figure 1: Performance of two methods (expert system and random assignment) when classifying the temporality of utterances about oxygen therapy decisions. Accuracy is out of all decisions (past and current) what percent did the method correctly classify. Sensitivity is out of the past decisions what percent did the method correctly classify. Specificity is out of the current decisions what percent did the method correctly classify. 95% confidence intervals were estimated using bootstrapping.

References

[1]: King AJ, Cooper GF, Clermont G, Hochheiser H, Hauskrecht M, Sittig DF, Visweswaran S. Using Machine Learning to Selectively Highlight Patient Information. *J Biomed Inform.* 2019 Dec;100:103327.

[2]: Harkema H, Dowling JN, Thornblade T, Chapman WW. ConText: an algorithm for determining negation, experiencer, and temporal status from clinical reports. *J Biomed Inform.* 2009 Oct 1;42(5):839-51.

What Is The Right Number Of Conformers for Pharmacophore Virtual Drug Screening (and How Should They be Generated)?

Scholars: Sophia Song[1], Ananya Vyas[2], Fatimah Bisiriyu[3]
Schools: [1]Upper St. Clair High School (Pittsburgh, PA); [2]Taylor Allderdice High School (Pittsburgh, PA); and [3]The Neighborhood Academy, (Pittsburgh, PA)
Mentor: Dr. David Ryan Koes, PhD, Department of Computational and Systems Biology

Summary: We used computational methods to generate different numbers of conformations of 102 different proteins. These were used to determine the "right" number of conformers to generate for specific proteins. This was accomplished through pharmacophore based virtual screening through pharmit. Pharmit is a vast library of many conformations of numerous molecules.

Introduction: Using computational methods, our research aims to discover new drugs that could aid in improving cancer treatment. A vital part of drug discovery is identifying inhibitors that could bind to harmful proteins in our bodies and prevent them from functioning. The shape of an inhibitor is key to our research. In order to prevent a specific protein from functioning, the inhibitor has to be able to fit the shape of the binding pocket in the protein. Conformers (the 3D make-up of atoms in a molecule) are generated using computational methods to see which molecular conformations best fit with the protein. We specifically looked at how many conformers are the optimal amount to generate in a timely and efficient manner. Generating too few conformers could cause molecules that should match a pharmacophore query not to match. If too many are generated, it will take longer to perform the query, and the molecules that shouldn't match the query could end up matching by accident.

Methods: We used computational methods to generate the conformers. We utilized pharmit (pharmit.csb.pitt.edu) to download all possible conformations of a specific molecule. We created databases of 1, 5, 10, 20, 30, 40, 50, and 100 conformations of each protein. Then, we used different Python scripts to generate the F1 numbers of each conformation. The databases with higher F1 values have a more favorable amount of conformers generated.

Results: Our results came in the form of F1 numbers (also referred to as the f1-score or the F-score). The F1 score is the harmonic mean of precision and recall. The precision is the number of correct results over the number of returned results. The recall is the number of results returned over the number of results that should have been returned. We made graphs with x-axis being the number of conformers and y-axis being the F1 value to find out the trend. We categorized the 100 targets into different categories based on their individual trendline: 1. The f1 performance

does not change overall; 2. with more conformers, the f1 performance is doing significantly better; 3. with generating more conformers, the f1 performance is doing worse. The average number of conformers that has the best f1 value is ____.

Discussion: Our results show that the performance is best when the average number of conformers is __. However, each individual protein has a different trend. Overall speaking, there are three types of trends: 1. The f1 performance does not change overall; 2. with more conformers, the f1 performance is doing significantly better; 3. with generating more conformers, the f1 performance is doing worse. For the first category, since the line is pretty flat, generating more or less conformers does not matter. The less conformers we generate, the less time it takes. For the second category, the f1 value increases when there are a larger number of conformers. With that stated, generating more conformers will improve the accuracy. For the third category, with the more conformers generated, the f1 value decreases. Hence, the less conformers we generate, the better performance it is. In conclusion, the best average number of conformers is ___. Nevertheless, specific proteins do have different trends. Our findings can potentially improve the efficiency of virtual screening performance in drug discovery industry since it recommends a certain number of conformers to be generated in a swift and efficient manner.

References

- *Pharmit: interactive exploration of chemical space.(https://pharmit.csb.pitt.edu)*

Sunseri, Jocelyn, and David Ryan Koes. "Pharmit: Interactive Exploration of Chemical Space." OUP Academic, Oxford University Press, 19 Apr. 2016, https://academic.oup.com/nar/article/44/W1/W442/2499312.

- *Rdkit*

Improving Conformer Generation for Small Rings and Macrocycles Based on Distance Geometry and Experimental Torsional-Angle Preferences

(https://pubs.acs.org/doi/full/10.1021/acs.jcim.0c00025)

Shuzhe Wang, Jagna Witek, Gregory A. Landrum, and Sereina Riniker

Journal of Chemical Information and Modeling 2020 60 (4), 2044-2058

Application of SPaRTAN to Breast Cancer Datasets

Hillary B. Boyzo Magno[1], April Sagan[2], Hatice U. Osmanbeyolgu[2]

[1]Pittsburgh Science and Technology Academy, Pittsburgh, Pennsylvania, USA

[2]Hillman Cancer Center, Pittsburgh, Pennsylvania, USA

The assigning specialized cell types originates from signaling and transcriptional programs. The activation or suppression of genes by signaling-regulated transcription factors (TFs) drive transcriptional programs and assigns cellular characteristics and functions. Alteration of transcriptions factor could lead to diseases like cancer. Multi-omics single cell technology can evaluate the expression of target genes and surface proteins in single cells. By adapting the technology into a framework like SPaRTAN, we can computationally model gene regulation. Configuring this technology to cancer dataset would allow new information to be obtain from CITE-seq dataset.

Sequencing technologies like scRNA-seq and CITE-seq allowed scientists to characterize cell types and genomic relationship with diseases. Computational predictions of gene regulation based on single cell genomics is a modern field of study. SPaRTAN (Single-cell Proteomic and RNA based Transcription factor Activity Network) is a computational framework that uses single-cell proteomic and transcriptomic data with cis-regulatory information to predict the coupling of transcription factor and cell-surface signaling receptors with gene expression. By applying SPaRTAN to breast cancer data, we hope to understand the role of protein signaling pathways and gene regulation in different types of breast cancer.

SPaRTAN is implemented in Python and builds on existing tool to analyze CITE-seq, like Scan.py (Ma, 2021). Before inserting the dataset into SPaRTAN, we must ensure that it is viable and in the right format. We use our methodology to analyze publicly available breast cancer data (Wu, 2021)

We use our methodology to analyze publicly available breast cancer data (Ma, 2021). The dataset contains CITE-seq data for four tumor samples (two TNBC, one ER+, and one HER2+.

By applying SPaRTAN to CITE-seq data from breast cancer tumors, we can identify signaling pathways relevant in cell type specific gene regulatory programs for different breast subtypes.

References

Ma Xiaojun “Spartan, a Computational Framework for Linking Cell-Surface Receptors to Transcriptional Regulators.” *Nucleic Acids Research*, U.S. National Library of Medicine, 27 Sept. 2021, https://pubmed.ncbi.nlm.nih.gov/34500467/.

Wu, Sunny Z., et al. “A Single-Cell and Spatially Resolved Atlas of Human Breast Cancers.” *Nature News*, Nature Publishing Group, 6 Sept. 2021, https://www.nature.com/articles/s41588-021-00911-1.

Title: FANCD2 Interacts in a Complex with PRMT5 and CtIP in Response to DNA Damage

Scholar: Jason Chen

High School: Seneca Valley High School, Harmony, PA

PI: Dr. Wei Du, PhD

Mentors: Dr. Limei Wu, PhD

Site: Cancer Biology

Fanconi Anemia (FA) is a genetic disorder associated with bone marrow failure and susceptibility to malignancies. FA is genetically heterogynous with 22 genes, and among them, FANCD2 links upstream to a FA core complex and downstream to recruited DNA damage repair proteins. The FA proteins are essential for the DNA repair process especially in homologous recombination. CtIP is an interacting partner of the Mre11/Rad50/Nbs1 DNA damage sensor protein complex which recognizes DNA double-strand breaks and promotes the resection of 5' strands to generate 3' single-stranded intermediates that are necessary for homologous recombination. Protein arginine methyltransferase (PRMTs), particularly PRMT5 is involved in oncogenic responses in hematopoietic stem and progenitor cells in the absence of two of the FA core complex proteins, FANCA and FANCC. A previous proteomic study has demonstrated that FANCD2 interacted with PRMT5 and CtIP using the Fancd2$^{3XFLAg/HA}$ (FANCD2-KI) mice model. Therefore, it was hypothesized that FANCD2 interacts in a complex with PRMT5 and CtIP in response to DNA damage. To test this, the FLAG-HA tagged human FANCD2 cDNA was overexpressed in HEK293 cells to establish a stable FANCD2 overexpressed human cell line. As a control, pcDNA3-FLAG-HA-FANCD2 KR mutant was overexpressed, resulting in the presence of non-ubiquitinated FANCD2. Immunoprecipitation will be conducted to detect the IR-induced FANCD2-CtIP-PRMT5 complex formation.

Title: Evaluation of how *SNORD67* promotes distant metastases

Scholar: Nancy Chen

High School/College/City/State: Seneca Valley Senior High School, Harmony, Pennsylvania

PI of group/lab: Dr. Yvonne Chao, MD, PhD

Mentor(s): Dr. Haizhou Liu, PhD & Dr. Dixcy Jaba Sheeba John Mary, PhD

Site: Cancer Biology

Small nucleolar RNAs (snoRNAs) are a class of non-coding RNAs that lead to RNA modification. There is increasing evidence that snoRNAs have roles in promoting cancer. Using a mouse model of breast cancer, previous work in the lab demonstrated that the snoRNA *SNORD67* may be important for cancer metastasis to lymph nodes. A *SNORD67* knockout was generated using CRISPR/Cas9 gene editing in 4T1 mouse breast cancer cells. Knockdown of *SNORD67* decreased cancer cell proliferation and tumorigenesis *in vitro*. 4T1 wild-type and *SNORD67* knockout cells were injected into the mammary fat pad of mice to form breast tumors. We then quantified metastasis to lymph nodes and to the lung. Metastasis to the lung was quantified using two different methods, quantitative RT-PCR (qPCR) and immunohistochemistry (IHC). While there was a statistically significant decrease in lung metastases in both *SNORD67* knockout cell lines when measured by IHC, only one knockout cell line showed a statistically significant decrease in lung metastases when measured by qPCR. These results show that qPCR is a more sensitive method to detect lung metastasis than immunohistochemistry. Because the known function of SNORD67 is to facilitate the methylation of the RNA U6, future directions include determining whether methylation is necessary for the cancer phenotype of *SNORD67* knockouts. We will measure proliferation and tumorigenesis in wild-type, *SNORD67* knockout, and *SNORD67* knockout cells that overexpress mutant *SNORD67* that cannot methylate U6. We will measure methylation of U6 using a method called reverse transcription at low deoxy-ribonucleoside phosphate followed by PCR (RTL-P). These experiments will help us to understand the mechanisms of how *SNORD67* promotes metastasis.

Using the Ubiquitin System to Reduce Replication of the Coronavirus

Scholar: Elise Chu

High School/College/City/State: Taylor Allderdice High School, Pittsburgh, PA

PI of group/lab: Dr. Bill Chen

Mentor(s): Dr. Travis Lear, Áine Boudreau

Site: Tech Drive X

COVID-19 is the leading infectious cause of death worldwide. Coronavirus replicates by using its spike proteins to attach to host lung cells and hijacks ribosomes to replicate a chain of the viral genomic RNA. Then a protease (3CLPro) cuts that chain and each portion becomes a virus. This protease is critical to efficient coronavirus replication.

One strategy to curtail viral replication is to utilize the ubiquitin system. Ubiquitin is a protein that tags other proteins that require degradation. It finds proteins that have completed their function or are damaged and attaches to them via an amino acid peptide bond. A polyubiquitin chain is formed to attract a proteasome, which then degrades the attached protein back into amino acids. The Chen Lab is exploring methods to use ubiquitin to degrade the coronavirus protease and prevent its replication, thereby limiting the spread of coronavirus.

Since SARS-CoV2, the cause of COVID-19, is too dangerous to handle, we use a very similar coronavirus, OC43, that has the same protease used for replication (NSP5). The main ubiquitin protein used to combat the OC43 virus is ZBTB25. Cycloheximide (CHX) was used to clog ribosomes, stopping production of new protein. Clofazimine (CFZ), a proteasomal inhibitor, was used to monitor the amount of accumulated ZBTB25. The Beas 2-B (bronchial) (B2B) cells, both wild type (untampered)(WT) and ZBTB25 knock-out (KO) were infected with varied doses of OC43 and/or incubated in CHX and/or CFZ for varied periods. We were able to identify the effects of ZBTB25 and prove that it is critical in degrading NSP5.

The OC43 dose courses of ZBTB25 KO B2B with CHX treatment showed that OC43 levels were constant or increased. In contrast, the OC43 dose courses of WT B2B with CHX treatment expressed that OC43 and NSP5 levels consistently decreased. In the CFZ time courses, as OC43 dose increased, the amount of ZBTB25 increased (because they were attached and CFZ prevented full degradation) further proving the utilization of ubiquitin.

The next step is finding the site(s) where ubiquitin (ZBTB25) binds to the NSP5. Since ubiquitin binds to proteins via peptide bond, we will mutate amino acids at potential binding sites in NSP5. The mutants will be run through the same experimental design as described above. If a mutated NSP5 does not degrade (or degrades less than our initial experiments), then the spot of the mutation is a critical ubiquitination site.

Comparing Healthcare Experiences Between Deaf and Hard of Hearing vs Hearing patients During the COVID-19 Pandemic

Scholar: Valerie DeVos

College: Rochester Institute of Technology

Mentors: Richard Boyce, Olga Kravchenko, and Jonathan Maeir

Site: CoSBBI

Introduction: Persons who identify as deaf, Deaf, or Hard of Hearing (d/DHH) have a greater burden with respect to healthcare due to barriers in communication and discrimation/bias. Of particular concern is that d/DHH and hearing patients might have different experiences of treatment for COVID-19. Also, healthcare offices might not let sign language interpreters enter the building due to concerns about the spread of the COVID-19 virus.

Objective: This project seeks to identify differences in the perception of healthcare experiences during the COVID-19 pandemic between persons in the d/DHH community compared to the hearing community. The project uses data from a database called All of Us (AoU). AoU is a national cohort study currently seeking to enroll 1 million patients who are highly diverse that includes d/DHH people.

Methods: Using the AoU workbench, cohort definitions were created to identify d/DHH and hearing participants who completed a survey about their experiences during the COVID-19 pandemic. Summary statistics were used to compare perceptions about their experience between the participants in each cohort.

Results: 18294 AoU participants were identified as d/DHH and 310776 as hearing. Of the participants, 8239 (45.0%) of d/DHH and 91474 (29.4%) of hearing completed the COVID-19 survey. Differences in the answers we examined tended to be small when comparing the d/DHH and hearing participant responses. The largest difference was that, compared to hearing survey completers, d/DHH reported attending fewer social gatherings of < 10 people (39.4% vs 30.1%).

Conclusions: The AoU dataset allowed for comparison of perceptions about COVID-19 pandemic experience between d/DHH and hearing participants. Further research is ongoing to compare healthcare and outcomes using the same dataset.

Objective Analysis of Mindfulness for Youth with Autism

Aiden Dorneich, Dr. Murat Akcakaya, PhD, Busra Tugce Susam, Nathan T. Riek
Fox Chapel Area High School, Pittsburgh, PA; University of Pittsburgh Hillman Cancer Center Academy, Pittsburgh, PA

Abstract

Although much speculation has been done on the effectiveness of mindfulness exercises on mood stabilization in youth with Autism Spectrum Disorder, little objective support has been produced. The use of machine learning algorithms on electroencephalography produced before and after short mindfulness activities in youth with ASD may produce quantifiable evidence to the effectiveness of such exercises.

Introduction

Electroencephalography (EEG) has successfully been used in previous studies to show the effects of mindfulness exercises on brain activity [1]. Mindfulness activities (MF) such as breathing exercises have also been shown to be especially effective for youth diagnosed with Autism Spectrum Disorder (ASD), but little objective analysis of brain activity has been done on this subject. Given the promising work using EEG methods to measure the impact of MF meditation in neurotypical populations, this study sought to apply EEG methods to measure the effect of MF among youth with ASD.

Methods

A total of 40 subjects participated in the experiment, with 5 excluded due to technical issues. All subjects were 12–21 years old, with a clinical diagnosis of ASD and an Emotion Dysregulation Inventory raw score of no less than 7. Each subject completed 10 phases: Task 1, Task 2, Task Rest 1, Task 3, Pre-MF, MF, Post-MF, Task 4, Task Rest 2, and Task 5 (Figure. 1). Tasks consisted of an Affective Posner Task, in which subjects were shown two cards (white squares) and asked to pick the card with a star on its back (Figure. 2). A blue rectangle was placed over one of the cards signifying a 75% chance of having the star. If an answer was not given within the time limit, "too slow" was given as feedback. As a deception component in Tasks 3 and 4, there was a 60% chance of getting "too slow" as feedback after selecting the correct card, regardless of speed. Tasks 1 and 2 were used as practice rounds. EEG scans were run during Pre-MF and Post-MF (each 1 minute). The MF activity was a 2 minute pre-recorded breathing exercise, assisted by a MF-based stress reduction teacher with clinical expertise in ASD. This study aims to analyze differences in EEG features before and after this MF activity using machine learning, and to show that certain patterns can be generalized across subjects despite differences between subjects [4, 5].

A total of 133 spectral features were calculated using Welch's periodogram method for each channel [2, 3]. All analysis was done using Python 3.10, using SciKit-Learn and PyTorch libraries. The data was normalized with a standard scaler. The normalized data was used to train a Support Vector Machine (SVM) using a Radial Basis Function (RBF) kernel. We used leave-one-participant cross validation to prevent overfitting. We then applied feature reduction and selection methods such as Principal Component Analysis (PCA) and Sequential Forward Selection (SFS) on the normalized data. When we applied PCA, we kept 32 features and about 95% variance. After each feature selection method, we applied an RBF SVM classifier to differentiate the Pre-MF vs Post-MF resting state.

Results

The results show no clear sign of a difference between Pre-MF and Post-MF. Average accuracy, sensitivity, and specificity were 0.54, 0.66, and 0.42 respectively, with SFS (metrics were averaged from the 35 metrics produced when each subject was used as the test set). Results were nearly the same with SFS and with PCA. This does not rule out the possibility of a difference, however, and more analysis should be done using other algorithms.

Discussion

Although the results do not show any difference, it is still possible that another model may fit better than an SVM with an RBF kernel, such as deep neural networks to uncover potentially more complex relationships. In particular, an Artificial Neural Network may be capable of learning more complex differences and relationships in the data than a model such as SVM. Additionally, more data should be collected, as the models currently have very little.

Figure 1. Phases of data collection, in chronological order. Tasks were Affective Posner Tasks as shown in figure 2.

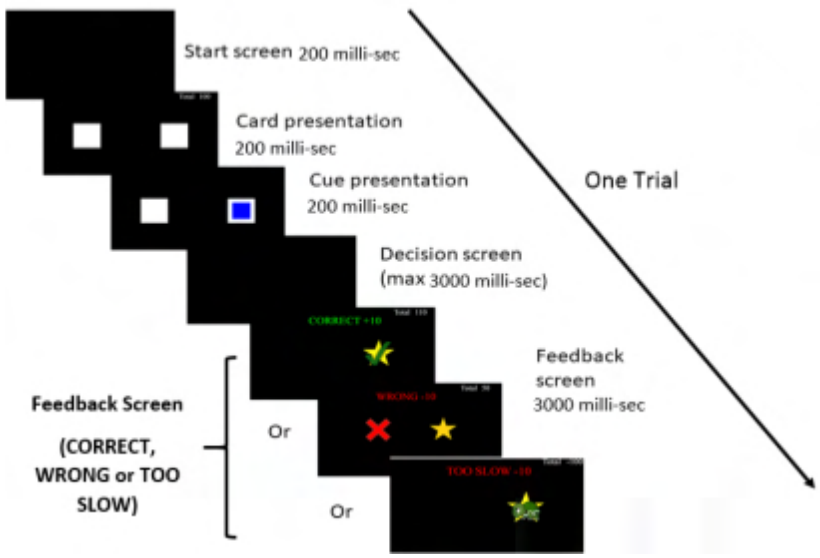

Figure 2. Phases of the Affective Posner Task, in chronological order from top left to bottom right. Two cards are presented, then a blue square appears on one. The blue square has a 75% chance of being on the same side as the star. "Too slow" will be given as feedback 60% of the time on tasks 3, and 4 only, with no real relationship with the subject's decision speed.

References

1. Lomas, Tim, Itai Ivtzan, and Cynthia HY Fu. "A systematic review of the neurophysiology of mindfulness on EEG oscillations." Neuroscience & Biobehavioral Reviews 57 (2015): 401-410.
2. Welch, Peter. "The use of fast Fourier transform for the estimation of power spectra: a method based on time averaging over short, modified periodograms." IEEE Transactions on audio and electroacoustics 15.2 (1967): 70-73.
3. Murias, Michael, et al. "Resting state cortical connectivity reflected in EEG coherence in individuals with autism." Biological psychiatry 62.3 (2007): 270-273.
4. Gevins, Alan, et al. "Monitoring working memory load during computer-based tasks with EEG pattern recognition methods." Human factors 40.1 (1998): 79-91.
5. Hefron, Ryan, et al. "Cross-participant EEG-based assessment of cognitive workload using multi-path convolutional recurrent neural networks." Sensors 18.5 (2018): 1339.

Constructing a machine learning regression model that predicts levels of chromatin accessibility in uniform open chromatin regions across different cell types

Scholar: Orion Douglas

School: Ossining High School, Ossining, New York

Principal Investigator: Dr. Maria Chikina

Mentors: Dr. Maria Chikina, Ali Tugrul Balci

Site: Computational Biology

DDCF Undergraduate Intern at University of Pittsburgh Department of Computational and Systems Biology

Abstract: Sequence motifs possess functional features in biological processes, but little is known about them in the context of cell diversity. Thus, we created a machine learning model, paired with elastic net regularization, that selects motifs from uniform open chromatin regions from different cell types that display the most robust signals; we believe these motifs may provide information on biological processes occurring in various cell types.

Background: Sequence motifs are short, recurring patterns of nucleotides that possess integral, functional features in biological processes, most notably as transcription factor binding sites. However, little is known about sequence motifs in the context of cell diversity and cell differentiation. Thus, it is important to address how sequence motifs govern cell type identity.

Methods: To address this question, we trained a machine learning regression model with features from ATAC-seq data, in tandem with elastic net regularization, and used it to predict signals that indicate levels of chromatin accessibility from uniform open chromatin regions from a number of cell types. We hypothesized that these signals exhibit variance across different cell types. Subsequently, we selected motifs that displayed the most robust signals. We believe these specific motifs might be informative about biological processes in a variety of cell types.

Results: - - -

Discussion: Through our model, we hope to provide insight into the implication of sequence motifs in different cellular processes in diverse cell types.

When Minutes Matter: Utilization and Time-Saved by Air Medical Transport of Trauma Patients

Scholar: Rae'Nell Durham
High School: Pittsburgh Science and Technology Academy
PI of group: Joshua Brown, MD, MSc
Mentor(s): Joshua Brown & Jamison Beiriger
Site: UPMC Presbyterian

Background: The use of helicopter transport (HT) for trauma patients originated from the military and is now an important way to transport civilians to trauma centers. HT saves vital time and subsequently lives. Several concerns regarding HT such as cost and safety despite survival advantages of HT over ground transport (GT) in trauma patients make selecting the right patients crucial. Faster transport times, as seen with HT, are associated with improved outcomes in trauma. Our objective was to map areas in Pennsylvania to see where HT is overutilized or underutilized based on time-saved.

Methods: We performed a secondary analysis of patient-level data from the Pennsylvania Trauma Outcomes Study (PTOS) collected from 2000 to 2017. Patients transported by HT or GT from the incident location to a trauma center were included. HT and GT transport time from incident location to trauma center were calculated by network analysis for each patient. The average time-saved by HT and proportion of trauma patients undergoing HT was calculated for each zip code. Our outcomes were under-utilization (high potential time-saved, low utilization) and over-utilization (low potential time-saved, high utilization) and were mapped across Pennsylvania.

Results: A total of 273,212 patients over 1542 zip codes were included for analysis. Average potential time saved via helicopter use and percent of patients flown were aggregated by zip code and mapped. Bivariate choropleth mapping of percent flown vs time saved identified 214 high-low and 70 low-high zip codes (Figure 1).

Conclusion: We identified specific geographic areas of under- and over-utilization of HT. This allows us to target educational quality improvement programs to specific areas to teach EMS personnel to identify the optimal transport modality for their patients. This may reduce healthcare system costs and transport risks while saving more lives after injury.

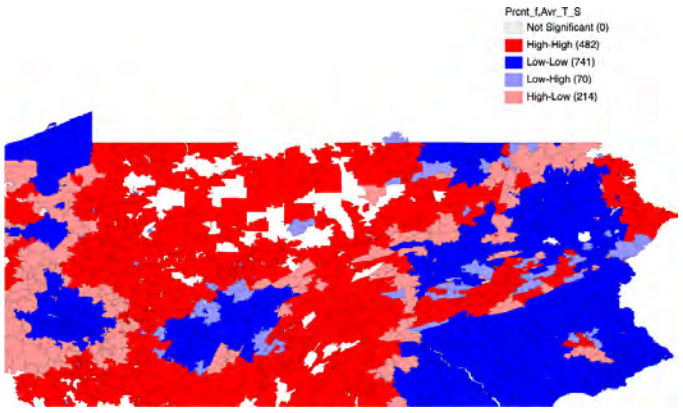

Figure 1. Bivariate Choropleth map of helicopter transport utilization (proportion of trauma patients) and time-saved over ground ambulance transport. Light blue areas denote zip codes with low helicopter utilization but high potential time-saved (under-utilization). Pink areas denote zip codes with high helicopter utilization but low potential time-saved (over-utilization).

A Machine Learning Approach to Predict Changes in Psychological Stress Levels Based on Experimental and Demographic Factors

Shaun Fernando[1], Dr. Dana Bovbjerg, PhD[2], Jessica Manculich[3]
[1]PA Leadership Cyber Charter School, Pittsburgh, PA; [2]University of Pittsburgh Hillman Cancer Center Academy, Pittsburgh, PA

Abstract

Possible effects of acute psychological stress including increased DNA damage and the use of demographic and experimental factors as moderators have received little attention in the field of biomedicine. Increased DNA mutations and lesser DNA repair mechanisms could be a result of this DNA damage, which could lead to a development of cancer. Statistical analysis and a machine learning approach will be used to identify the use of these factors as moderators of stress.

Introduction

Worsened DNA repaid mechanisms and DNA mutations caused by increased DNA damage leading to cancer development as possible effects of acute psychological stress have widely received little attention. The use of demographic and experimental factors as potential moderators of these effects and of psychological stress have also been given little attention in the biomedical field. To determine if the above statements are true, a well-validated stress test and a series of stress-measuring tools will be utilized. To analyze, interpret, and predict psychological stress data based on demographic and experimental factors, a statistical analysis and machine learning approach will be used.

Methods

The stressor data was collected from 200 healthy patients arranged by race, sex, and age (The data collected is part of a larger study researching the effects of demographic and experimental factors on DNA damage and DNA repair capacity in isolated Peripheral Blood Mononuclear Cells (PBMCs)). The subjects were also randomly split into a Placebo Group and Propranolol Group, where the role of propranolol in reducing psychological stress is being tested. Finally, the subjects were randomly split by session order, where roughly half of the subjects had their stress visit first and half had their control visit first. To test the hypothesized effects of psychological stress, each patient acted as their own control (within subjects design). Each patient was exposed to a highly validated and accepted social stress test called the Trier Social Stress Test (TSST) to measure stress levels under a controlled environment. Three stress-measuring tools were utilized: A Visual Analogous Score (VAS) which is a self-reported stress score, Total Mood Disturbance (TMD) which is calculated based on a series of mood sub scores, and percentage lymphocytes (Lymph) which is taken by an IV line and measures the percentage of lymphocytes in white blood cells. The VAS scores were taken pre-task, mid-task, and post-task. The Lymph blood samples were taken pre-task, post-task, and post-recovery. The TMD scores were taken upon arrival, pre-task, post-task, and post-recovery. After all the data was collected, the change in each of the stress scores for each patient from pre-task to post-task were calculated and stratified based on race, age, gender, medication group, and session order to determine if these factors moderate induced stress. The means of this data were calculated to graphically represent the variation between factors. After the factors with the most variation were identified, a K-Nearest Neighbors (KNN) model was run on those factors (as well as all factors to compare) to predict stress levels based on combinations of certain demographic and experimental factors that influence psychological stress.

Results

Based on the statistical analysis of the change in stress levels from pre-task to post-task, there were six factors and their corresponding stress-measuring tools that showed significant variation between groups: change in VAS and TMD for gender, change in VAS and TMD for age, change in TMD for race, and change in VAS and Lymph for the medication group. No stress-measure values were found to have significant variance in the session order factor. The KNN results showed that the accuracy of the model prediction increased when only the factors with variation were used in contrast to using all of the factors.

Discussion

The results from the statistical analysis and KNN model prediction show promising results: there are certain demographic and experimental factors that do affect the change in acute psychological stress, and therefore we can to a certain degree predict if a significant amount of stress will be induced by a person based on certain factors.

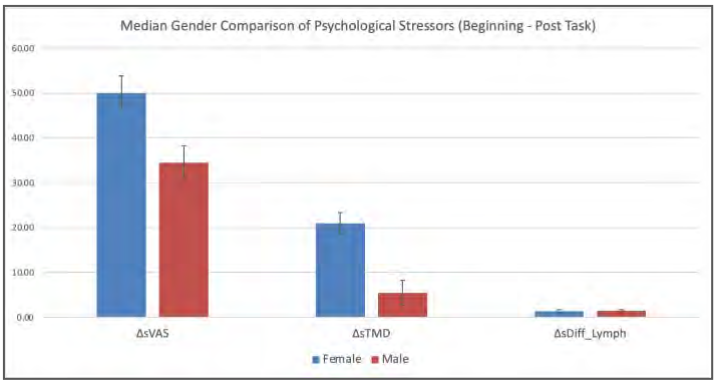

Figure 1. Median Comparison of Stressors for Gender

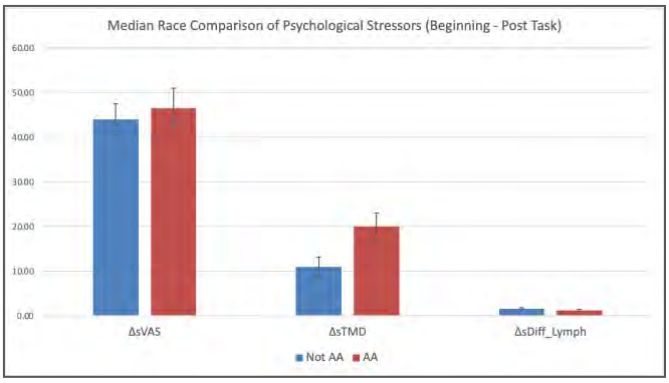

Figure 2. Median Comparison of Stressors for Race

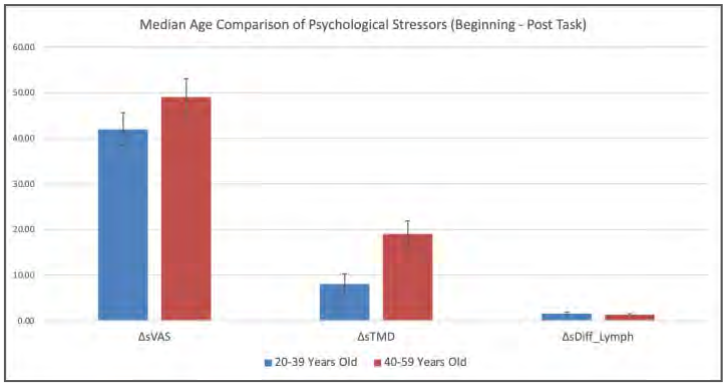

Figure 3. Median Comparison of Stressors for Gender

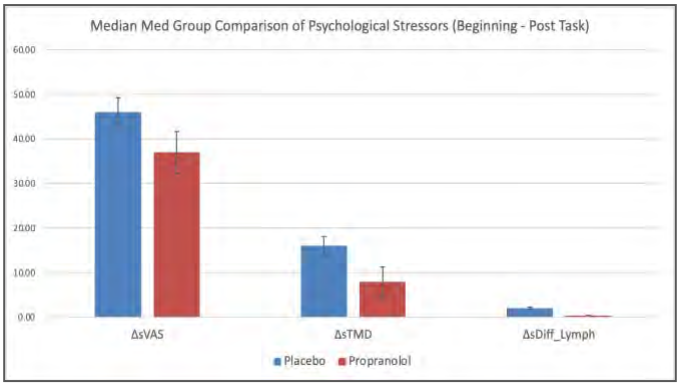

Figure 4. Median Comparison of Stressors for Med Group

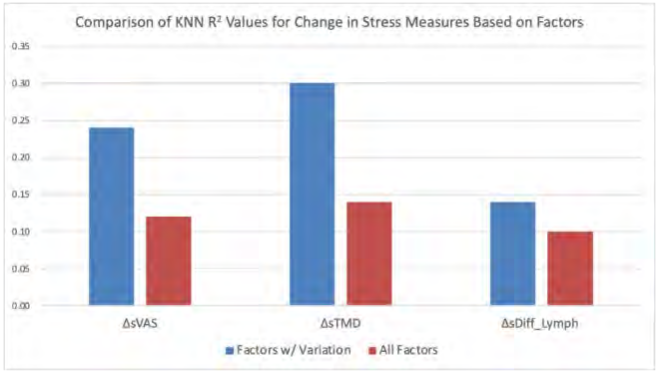

Figure 5. KNN Accuracy Comparison Based on Factors

References

1. Jenkins FJ, Van Houten B, Bovbjerg DH. Effects on DNA Damage and/or Repair Processes as Biological Mechanisms Linking Psychological Stress to Cancer Risk. J Appl Biobehav Res. 2014 Feb 1;19(1):3-23. doi: 10.1111/jabr.12019. PMID: 24891812; PMCID: PMC4039216.

ADMET Exploration of PLK1 Inhibitor Drug Candidates

Zivia Gale, Highschool Senior[1]; Samantha Fernsebner, Highschool Senior[2]; Dr. Daniel Lundberg, Ph.D[3]; Dr. Adebowale Ogunjirin, Ph.D[3]; Dr. Tugba Kucukkal, Ph.D[3]

Maryland School For the Deaf, Fredrick, Maryland[1]; Marie Philip School, Framingham, Massachusetts[2]; Gallaudet University, Washington, DC[3]

Abstract: In recent years, virtual screening methods in drug discovery are now widely used for their advantages such as speed and cost-effectiveness. This virtual screening research is used to identify the ten most promising anticancer (Polo-like Kinase 1 inhibitor) candidates from forty-six molecules. We explored the Absorption, Distribution, Metabolism, Excretion, and Toxicity (ADMET) of these drug candidates to determine their druggability. Future studies will include more in-depth simulations for these top 10 compounds.

Introduction: Previous research indicated that PLK1 is overexpressed in cancer cells, and it has a key role in cell division making it an excellent target to prevent cancer proliferation. A consideration in developing drugs that selectively target PLK1 is the pharmacokinetics (absorption, distribution, metabolism, excretion) and toxicity (ADMET) of the drug. Based on the prior virtual screening of 6 million small molecules, we were given forty-six (46) top hit drug compounds that needed to be studied further with more in-depth molecular simulations. The goal of our research was to narrow them down to ten (10) drug compounds to be further studied in the laboratory or through Molecular Dynamics simulations. The top drug candidates must present the best binding affinity along with the optimal ADMET properties that will have a high potential of being a safe drug that can target PLK1 to stop cancer cell proliferation.

Methods: 46 compounds were provided to us as Simplified Input-Entry Line System (SMILES) codes. First, Open Babel was used to converting from SMILES into Tripos structure (Mol2) files. Then, each compound was subjected to Molecular Docking utilizing CB-Dock2. Each molecule with five bound ligand-receptor conformations was further used to calculate their binding affinity utilizing molecular mechanics-based methods CSM-Lig and PRODIGY. Based on these simulations, the compounds that have the strongest binding affinity for PLK1 were identified. After screening for binding affinity, we chose the top 20 that have the strongest binding in their pose out of all compounds. After that, ADMETlab was used to evaluate 87 pharmaceutical properties for medicinal chemistry, absorption, distribution, metabolism, excretion, toxicity, and environmental toxicity. Additionally, SwissADME was used to obtain such drug-likeness properties. Multidimensional plots provided by the two ADME exploration programs were embedded in a color-coding system (green = excellent, yellow = medium, red = poor) in our spreadsheets to complete the screening based on ADME properties. Finally, Toxtree was utilized to obtain toxicity profiles for all 46 compounds with Cramer's rules (Class I as non-toxic, Class II as moderately toxic, and Class III as high toxicity.). Once all the calculations are completed, the top 20 compounds in each program (except ToxTree) were identified. The compounds' ADMETlab profiles in these lists of top 20 were then compared to determine the final top 10 drug candidates.

Results and Discussion: These 46 compounds were initially identified through virtual screening which requires more in-depth studies to confirm their binding profile and pharmacokinetic properties. Each compound had its own five curvature-based cavity detection poses of the same cavity size with a variety of binding values, which was straightforward in screening the drug candidates. During the ADMET exploration simulations, finding a protocol to compare the drug candidates' 87 pharmaceutical properties to obtain the top 20 drug candidates was challenging. Toxicity was not a useful measure to screen the compounds because we discovered that all of the 46 drug compounds were classified to have Class III toxicity. With further research, we found out that many drugs that are currently in use are also classified the same, however; they can still be utilized with a tolerable dosage and a suitable delivery method. In conclusion, we learned that drug discovery is a complicated process that consists of the evaluation of numerous pharmacokinetic parameters as well as structural properties and that computational chemistry is an invaluable method in drug discovery.

References

Adelusi, T. I., Oyedele, A.-Q. K., Boyenle, I. D., Ogunlana, A. T., Adeyemi, R. O., Ukachi, C. D., Idris, M. O., Olaoba, O. T., Adedotun, I. O., Kolawole, O. E., Xiaoxing, Y., & Abdul-Hammed, M. (2022, February 12). Molecular modeling in Drug Discovery. Informatics in Medicine Unlocked. Retrieved June 22, 2022, from https://www.sciencedirect.com/science/article/pii/S235291482200034X

Lee, K. S., Burke, T. R., Park, J.-E., Bang, J. K., & Lee, E. (2015, December). Recent advances and new strategies in targeting PLK1 for anticancer therapy. Trends in pharmacological sciences. Retrieved June 27, 2022, from https://www.ncbi.nlm.nih.gov/pmc/articles/PMC4684765/

Yang Liu, et al. CB-Dock2: improved protein-ligand blind docking by integrating cavity detection, docking and homologous template fitting. Nucleic Acids Research, 2022. Retrieved June 29, 2022, from https://cadd.labshare.cn/cb-dock2/php/index.php

Dong, J., Wang, N.-N., Yao, Z.-J., Zhang, L., Cheng, Y., Ouyang, D., Lu, A.-P., & Cao, D.-S. (2018, June 26). ADMETlab: A platform for systematic ADMET evaluation based on a comprehensively collected ADMET database - journal of Cheminformatics. BioMed Central. Retrieved July 5, 2022, from https://jcheminf.biomedcentral.com/articles/10.1186/s13321-018-0283-x

Exploring The Effects of Congenital Heart Disease on Functional Connectivity

Ansh Goyal[1], William Reynolds[2], Joy Roy[2], Rafael Ceschin, PhD[2], Ashok Panigrahy, MD[3]
[1]Upper St. Clair High School, Pittsburgh, PA; [2]Department of Biomedical Informatics, University of Pittsburgh, Pittsburgh, PA; [3]Department of Radiology, Children's Hospital of Pittsburgh, Pittsburgh, PA

Abstract
Congenital Heart Disease (CHD) patients have known neurocognitive deficits. To examine possible correlations with brain function, we examined resting-state functional imaging for differences in connectivity associated with CHD. Our study found patients with CHD have alterations in key connectome metrics. We observed increased local efficiency in specific brain regions in CHD patients, and more broadly decreased clustering coefficient in patients with CHD.

Introduction
Functional connectivity is defined as the correlation in measured activity within anatomically separated brain regions[1]. An increasing number of studies in recent years have explored correlations between functional connectivity and a plethora of diseases[2]. Congenital Heart Disease (CHD), which manifests as defects in the heart present before birth, has been shown to impair cognitive development in patients from a young age[3]. This study aims to identify changes in functional connectivity between patients with CHD and age-matched healthy controls by analyzing blood oxygenation level-dependent (BOLD) images. BOLD images measure the changes in concentration of deoxygenated hemoglobin as a proxy for brain activity. We believe that leveraging these trends could help predict the severity of neurocognitive deficits in children with CHD, and better our understanding of impaired neurodevelopment associated with CHD.

Methods
Images were first processed for manual quality assessment prior to any image processing. Each image was corrected for motion using FSL's MCFLIRT algorithm, and skull stripped using FSL's Brain Extraction Tool. The standard AAL3 brain atlas[4] was then registered to each BOLD image using FSL's FLIRT and FNIRT algorithms to allow for segmentation. Each BOLD image was sent through a custom preprocessing pipeline that included bandpass filtering to remove extraneous frequencies, bias correction, smoothing, and an artifact detection algorithm that removed unusable frames from the image. After preprocessing, the intensity values from each voxel were extracted and averaged per region per time point, resulting in correlates of regional activity. Pearson correlation coefficient between all regions was calculated and arranged in a 2D matrix, where each row and column represented a region from the AAL template. The Brain Connectivity Toolbox was used to calculate each subject's global efficiency, local efficiency, and clustering coefficients from the similarity matrix. Finally, we tested for statistically significant differences between CHD and controls using t-tests using the SciPy package.

Results
The initial dataset contained a total of 142 BOLD images. 17 patients were excluded during the manual QA, and an additional 33 were excluded due to artifact detection, resulting in 37 CHD patients and 55 controls in the final analysis. The difference in global efficiency between CHD and control patients was statistically negligible. However, statistically significant differences in local efficiency and clustering coefficients in specific brain regions were observed. The thalamus, lingual gyrus, and the superior temporal gyrus saw substantial changes in local efficiency between CHD and control patients, while the thalamus, the superior and medial frontal gyrus, the hippocampus, postcentral gyrus, insula, pallidum, precuneus, vermis, superior temporal gyrus, and superior parietal gyrus saw significant changes in clustering coefficient. While the clustering coefficient of these brain regions was decreased in patients with CHD, the local efficiency of the structures was found to have increased in patients with CHD.

Discussion
While these are preliminary results and will require further testing and analysis with a larger dataset for further validation, the results offer an insight into the effects of CHD on functional connectivity. The increase in local efficiency in certain brain regions indicates isolated neural activity within these regions[5], while the decreased clustering coefficient indicates lower connectivity between neighboring brain regions.

Figures

Metric	Structure Name	P-Value	Control Average	CHD Average	Greater
Local Efficiency	Thalamus, Anteroventral nucleus, Right	0.047	-0.016	-0.010	CHD
	Thalamus, Lateral geniculate, RIght	0.046	-0.017	-0.012	CHD
	Thalamus, Ventral anterior, Left	0.045	-0.016	-0.011	CHD
	Thalamus, Ventral posterolateral, Left	0.044	-0.015	-0.010	CHD
	Superior temporal gyrus, Right	0.044	-0.015	-0.009	CHD
	Lingual gyrus, Left	0.029	-0.013	-0.008	CHD
	Lingual gyrus, Right	0.025	-0.014	-0.009	CHD
Clustering Coefficient	Vermis, Lobule 7	0.020	0.342	0.271	Control
	Mediodorsal medial magnocellular, Left	0.018	0.368	0.280	Control
	Superior temporal gyrus, Right	0.017	0.364	0.270	Control
	Thalamus, Intralaminar, Right	0.015	0.379	0.291	Control
	Superior frontal gyrus, Medial, Left	0.015	0.340	0.262	Control
	Superior frontal gyrus, dorsolateral, Left	0.011	0.368	0.280	Control
	Middle frontal gyrus, Left	0.007	0.353	0.265	Control

Table 1: A list of the 7 most statistically significant results from each metric, including (from left to right) the graph metric calculated, the structure, the p-value from the T-Test, the average value for controls, the average value for CHD patients, and the group with the higher average.

References

1. Van Den Heuvel, Martijn P., and Hilleke E. Hulshoff Pol. "Exploring the brain network: a review on resting-state fMRI functional connectivity." European neuropsychopharmacology 20.8 (2010): 519-534.
2. Gaudet I, Hüsser A, Vannasing P, Gallagher A. Functional Brain Connectivity of Language Functions in Children Revealed by EEG and MEG: A Systematic Review. Front Hum Neurosci. 2020 Mar 12;14:62. doi: 10.3389/fnhum.2020.00062. PMID: 32226367; PMCID: PMC7080982.
3. McQuillen PS, Goff DA, Licht DJ. Effects of congenital heart disease on brain development. Prog Pediatr Cardiol. 2010 Aug 1;29(2):79-85. doi: 10.1016/j.ppedcard.2010.06.011. PMID: 20802830; PMCID: PMC2927012.
4. Rolls ET, Huang CC, Lin CP, Feng J, Joliot M. Automated anatomical labelling atlas 3. Neuroimage. 2020 Feb 1;206:116189. doi: 10.1016/j.neuroimage.2019.116189. Epub 2019 Sep 12. PMID: 31521825.
5. Rubinov M, Sporns O. Complex network measures of brain connectivity: uses and interpretations. Neuroimage. 2010 Sep;52(3):1059-69. doi: 10.1016/j.neuroimage.2009.10.003. Epub 2009 Oct 9. PMID: 19819337.

DRP1 Splice Variants May Differentially Regulate Ovarian Cancer Cell Viability and Survival

Scholar: Donise Griffin

High School: Carnegie Mellon University, Pittsburgh, PA

PI of group/lab: Dr.Nadine Hempel

Mentor: Dr.Sierra White

Site: Women's Cancer Research Center

Background: High-grade serous epithelial ovarian carcinoma is the most common and most lethal gynecologic cancer. Mitochondrial fission is essential for mitochondrial regulation and, thus, impacts pathways such as cell proliferation and survival. The effects of mitochondrial fission and fusion dynamics remain heavily under-researched in epithelial ovarian cancer (EOC), however. DRP1, a protein necessary for mitochondrial fission to occur, has splice variants that may differentially regulate mitochondrial fission and exhibit altered expression patterns in ovarian cancer. Using a Human Epithelial ovarian carcinoma cell line (OVCA433) that overexpresses *Drp1* (Dynamin-related protein 1) variants 001 and 011 (001 lacks exons 3 and 16 but has exon 17, while 011 is lacking exon 3 but has exons 16 and 17) in comparison to cells that overexpress only GFP, this study aims to investigate the effects overexpression of splice variants have on cell viability and survival in baseline OEC cells.

Methods: OVCA433 OEC cells overexpressing variants 001 and 011 were subjected to western immunoblotting to determine DRP1 protein expression. A clonogenicity assay assessed the cell's capability to clone itself and form colonies. A Caspase assay to determine the activity of Caspases 3 and 7 was utilized to examine apoptosis following variant overexpression.

Results: Western blots exhibited successful overexpression of DRP1. Clonogenicity assays demonstrated decreased cell viability in variant 001 when compared to GFP controls and 011. Finally, the caspase assay may indicate a slight increase in cell death via apoptosis in variant 001 compared to GFP controls and 011, though not significant.

Conclusions: Based on this data, DRP1 splice variant 001 may differentially impact cell viability and survival. This could prove important in the context of drug response by ovarian cancer cells.

Future directions: Drug studies using chemotherapies can be done to examine these splice variants' individual effects on EOC cell stress response and survival.

N^6-methyladenosine (m^6A) Modification and Chromatin Remodeling Regulate Kaposi's Sarcoma-associated Herpesvirus (KSHV) Lytic Replication

Scholar: Daniel Guo

High School/College/City/State: North Allegheny Senior High School, Wexford, PA

PI of group/lab: Shou-Jiang Gao, PhD

Mentor(s): Wen Meng, PhD

Site: Cancer Biology

Kaposi's sarcoma-associated herpesvirus (KSHV) causes various malignancies including Kaposi's sarcoma (KS). Currently, the FDA has not approved any therapy for KSHV infection. Development of treatments against KHSV is in high priority. KSHV has both latent and lytic phases in its life cycle. During the latent stage, minimal viral genes are expressed, which helps the virus hide from the surveillance of the immune system. During lytic replication, KSHV expresses almost all lytic, produces infectious virions, which facilitate the spread of the virus and induce cell proliferation in an autocrine and paracrine mechanism. N^6-Methyladenosine (m^6A) is the most prevalent RNA modification. The cellular machinery driving m^6A modification includes "writer" methyltransferases, "reader" m6A binding proteins, and "eraser" methylases. The SWI/SNF complex remodels the nucleosome, increasing the binding affinity of DNA and transcription factors. In this study, inhibitors of m^6A writer METTL3 (UZH1, STM2457) and SWI/SNF complex (ACBi) were tested using a KSHV-infection system iSLK-RGB-BAC16 cells, which express RFP, GFP and BFP proteins to track the expression of viral latent, early lytic and late lytic protein, respectively. Sodium butyrate (NaB) was used to induce KSHV lytic replication from latency, which is indicated by GFP signal. Fluorescent microscopy was used to examine GFP-positive cell number change during reactivation with different inhibitor treatment. All three inhibitors could upregulate the number of GFP-positive cells during NaB reactivation, indicating UZH1, STM2457, and ACBi treatment can enhance KSHV lytic replication. Hence, m^6A writer METTL3 and SWI/SNF complex likely function to maintain KSHV latency by repressing viral lytic replication.

Outcome measures regarding procedural approaches for ruptured abdominal aortic aneurysms

Aniya Hall, Dr. Nathan Liang

Louisiana State University, Baton Rouge, Louisiana; University of Pittsburgh Hillman Academy, Pittsburgh, PA

Abstract Patients that received repairs for ruptured abdominal aortic were compared by procedural repair type, patient's mortality, and length of stay. The end goal was to evaluate and provide evidence to determine which procedural repair had the most favorable outcomes for a patient post-procedure and hospital stay.

Introduction Abdominal aortic aneurysms (AAAs) are enlargements of the aorta, located in the abdomen, that are caused by the weakening of the aortic wall over a vast period. Symptoms of AAAs can be easily overlooked, which is why some patients are not diagnosis until the AAA ruptures. Ruptured AAAs (rAAAs) can be life threatening because they cause major internal bleeding. Currently, there are two types of procedures used to repair rAAAs: open and minimally invasive endovascular repair (EVAR).

Methods Using the Agency of Healthcare Research and Quality's Florida State impatient dataset from 2004-2014, we evaluated various variables and outcomes in 4,143 patients that had rAAA's by open and EVAR. The frequency of each procedure was measured over time. The primary variables we compared were age, gender, race, and previous medical history that could indicate causes of the AAA and its rupture. The primary outcomes were 30-day mortality and length of stay.

Results Out of the 4,143 patients, 2,175(52.5%) underwent open repairs and 1,007(24.3%) underwent EVAR repairs; the remaining 961(23.2) patients died before they could undergo surgery. On average, the rAAA patients treated with EVAR repairs spent 6 days in the hospital, whereas open repair patients spent 9. 44.18% of open repair patients and 26.32% of EVAR patients died within 30 days after their procedure. In addition, 264(12.15%) open repair patients were readmitted within 30 days compared to 196(19.46%) EVAR patients (Figure 2 shows more details). Over the length of the study period, open surgeries decreased while EVAR increased.

Conclusion EVAR patients are readmitted more within 30 days than open patients; but those undergoing open repair had higher mortality than EVAR. From 2004-2004, EVAR operations have increased steadily while open repair has decreased. Overall, the data supports that outcomes for EVAR repairs are more favorable for rAAA patients.

Table 1.

	Open	EVAR	Total	p Value
Weighted size	2,175	961	3,136	
Variables				
Age, Mean[	73.37(9.52)	74.37(9.73)		0.0065
Age, categorized				0.285
<65	390(17.93%)	165(16.39%)	555(17.44%)	
>=65	1,785(82.07%)	842(83.61%)	2,627(82.56%)	
Sex				
Male	1,685(77.47%)	824(81.83%)	2,509(78.85%)	
Female	490(22.53%)	183(18.17%)	673(21.15%)	
Race				0.016
White	1,895(87.13%)	849(84.31%)	2,744 (86.24%)	
Black	89(4.09%)	62(6.16%)	151(4.75%)	
Hispanic	123(5.66%)	66(6.55%)	189(5.94%)	
Asian/Pl	10(0.46%)	10(0.99%)	20(0.63%)	
Native American/Other	58(2.67%)	20(1.99%)	78 (2.45%)	
Year of Admission				0
2004	299(13.75%)	41(4.07%)	340(10.69%)	
2005	317(14.57%)	38(3.77%)	355(11.16%)	
2006	259(11.91%)	55(5.46%)	314(9.87%)	
2007	205(9.43%)	55(5.46%)	260(8.17%)	
2008	228(10.48%)	78(7.75%)	306(9.62%)	
2009	213(9.79%)	88(8.74%)	301(9.46%)	
2010	169(7.77%)	104(10.45%)	274(8.61%)	
2011	149(6.85%)	109(10.82%)	258(8.11%)	
2012	133(6.11%)	147 (14.60%)	280(8.80%)	
2013	110(5.06%)	137 (13.60%)	247(7.76%)	
2014	93 {4.28%)	154 (15.29%)	247(7.76%)	
Payer				0.008
Medicare/caid	1,741(80.05%)	840(83.42%)	2,581(81.11%)	
Private p	306(14.07%)	102(10.13%)	408(12.82%)	
Self/None/Other	128(5.89%)	65(6.45%)	193(6.07%)	

Figure 1.

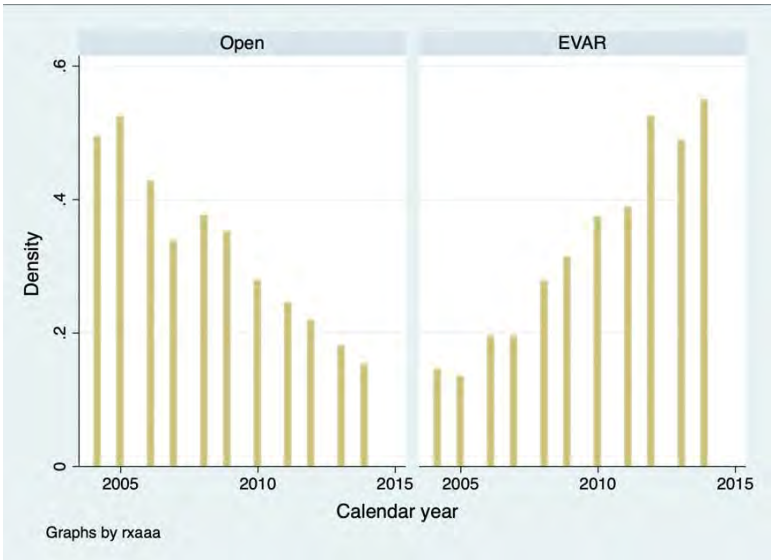

Figure 2.

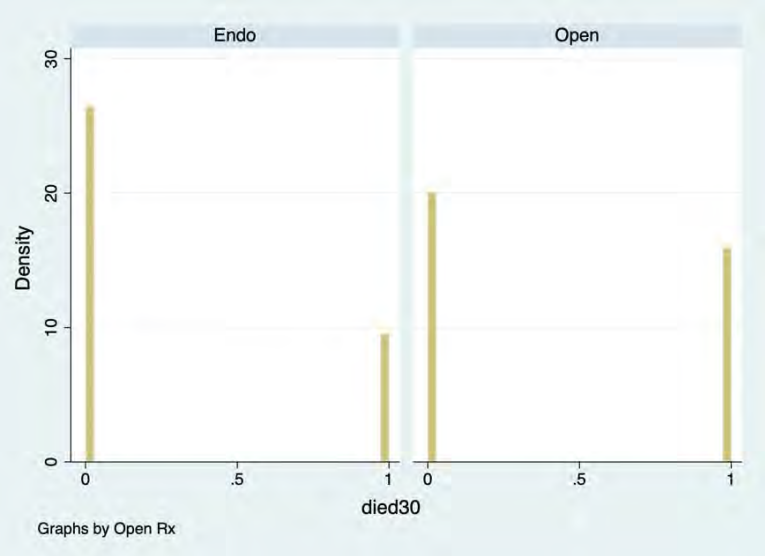

Table 2.

Readmissions		Open	EVAR	Total
	0	1,911 (87.86%)	811 (80.54%)	2,722 (85.54%)
	1	237 (10.90%)	166 (16.48%)	403 (12.66%)
	2	23 (1.06%)	24 (2.38%)	47 (1.48%)
	3	3 (0.14%)	5 (0.50%)	8 (0.25%)
	4	1 (0.05%)	1 (0.10%)	2 (0.06%)
Total		2,175	1,007	3,182

Title: Investigating Mesothelial to Mesenchymal Transition in Invasive Lobular Cancer Metastasis

Scholar: Isaiah Hooks

High School/College/City/State: Obama Academy, Pittsburgh, PA

PI of group/lab: Adrian Lee, PhD and Steffi Oesterreich, PhD

Mentor(s): Olivia McGinn, PhD, Lauren Brown

Site: Women's Cancer Research Center

Intro: We want to investigate why ILC, characterized by a lack of E-cadherin, has a unique metastatic pattern. The unique pattern of ILC is that it tends to metastasize to the ovaries, leptomeninges, GI organs, and peritoneum. Mesothelial cells originate from the mesoderm but show characteristics analogous to both mesenchymal and epithelial cells. Studies suggest that mesothelial cells can undergo phenotypic changes following activation of an epithelial state to a more mesenchymal morphology. This process has been coined as Mesothelial-Mesenchymal Transition (MMT). MMT is a dynamic cellular process that occurs during development, tissue repair, fibrosis, and metastasis. MMT is characterized by the gradual loss of cell-cell adhesion networks through the expression of adherence and tight junctional proteins; E-cadherin (Cdh1) and ZO1 respectively. We want to see if ILC or IDC cells induce MMT; MMT has been reported to promote ovarian cancer metastasis. We hypothesize that MMT promotes ILC metastasis and IDC cells to exert no reaction.

Methods: To study this, we will treat mesothelial cells with conditioned media from ILC cells and IDC cells lines. We will look at morphology of the cells and perform western blots for MMT markers such as E-cadherin, mesothelin, vimentin, WT-1, N-cadherin, alpha-SMA, and beta-actin.

Results: All the breast cancer conditioned media increased E-cadherin and A-SMA. There are no major differences among mesenchymal or mesothelial markers between ILC and IDC cell lines; it is unclear whether MMT is occurring more from ILC or IDC conditioned media. We also performed a trans-well migration assay which showed that ILC cells had more migration towards mesothelial cells than IDC cells.

Conclusions: It is unclear whether MMT occurs more with ILC or IDC cell lines, however ILC cells show more migration toward mesothelial cells.

Future Directions: Future directions include testing additional mesenchymal markers such as fibronectin, MMP2, and TGFB-1.

Tracking Eye Movements in Excitebike

Scholar: Jasmine Horton

Highschool: Winchester Thurston, Pittsburgh, Pennsylvania

Lab: Yuanyuan Chen, Ph.D

Mentor: Dr. Patrick Mayo

Site: Opthalmology

Experience is familiarity with an event or a task. Generally speaking, the more experience one has with a task, the better they will perform. Vision is considered the most important of the senses when it comes to taking in and processing surrounding information. This research looks at how experience impacts sight patterns. It is crucial to understand how gained experience impacts visual eye movement patterns because the majority of learning occurs through visual observation. We specifically asked if eye movement variability decreases as experience increases. If we could figure out how to train desired eye movement patterns early on in the learning process, it could make that process more efficient. A deeper understanding of how eye movement patterns change as a function of learning and expertise may therefore reveal avenues for treatments and rehabilitation. Using a Tobii Glasses 3 portable eye tracker, we recorded eye movement patterns during the game Excitebike on the Nintendo 64 video game console. To measure how the pattern changes, we plotted the 2D gaze data (horizontal and vertical eye position) from the Tobii Glasses, then compared the data across rounds of Excitebike played. As the lap time during the game decreased, the eye movements tended to become more concentrated in a smaller area relative to the slower lap times. This study suggests that eye movements become more attuned as task completion time increased. Further studies could be done to determine if requiring or training for specific eye movement patterns would make the learning process for a given task more efficient.

Using Machine Learning to Analyze the Correlation Between Cancer-Driving Alterations and Sensitivity to Certain Drugs

Katherine Y. Hu[1], Dr. Lu Xinghua[2], MD[2], PhD[2], MS[2], Shuangxia Ren[3]
, [1]North Allegheny Senior High School, Wexford, PA; [2] University of Pittsburgh Hillman Cancer Center Academy, Pittsburgh, PA

Abstract

In this project, machine learning is used to investigate driving genomic alterations of cancers as possible predictors of variations in drug sensitivity across 1,001 cancer cell lines screened with 265 anti-cancer compounds. Using genomic alteration data and drug response of cell lines as input, we first performed linear regression on the genomic features to predict the IC50 values for the gene-drug interactions. Secondly, we performed logistic regression using the genomic data and discretized drug-response values. The results show that the performance of regression using IC50 values was unsatisfactory, whereas predicting discretized drug response using logistic regression had encouraging results.

Introduction

Large-scale, pre-clinical pharmacogenomic studies provide an opportunity to develop methods for predicting cancer cell responses to different anticancer drugs and translate such insight to clinical settings. Clinical trials can be expensive and time-consuming, whereas the inclusion of this data can help during this process. The occurrence of genomic alterations in certain genes, such that the protein they produce behaves aberrantly, can lead to cancer. Some of these cancer-driving alterations are used as determinants of treatment response in the clinic. Collecting data from patients' tumor DNA to identify the driver alterations of their cancers helps determine the treatment that best targets the mutations. This form of medicine, commonly known as precision medicine or personalized medicine, helps match each patient with the most effective treatment for them. By using models that look at clinically relevant oncogenic alterations and correlation with drug sensitivity, gene-drug interactions are effectively encapsulated and help guide the future treatment of patients. For this project, the purpose is to use machine learning models to determine the relevance of molecular data type in influencing drug response.

Methods

Using an inventory of clinically relevant cancer gene mutations (CGs), focal recurrently aberrant copy number segments (RACSs), and hypermethylated informative 5'C-phosphate-G-3' sites in gene promoters (iCpGs), clinically relevant matrixes for each data type were curated[1]. The CGs feature matrix has 1,001 cell lines each with 468 CGs; the RACSs feature matrix has 539 cell lines each with 558 RACSs; the iCpGs feature matrix has 789 cell lines each with 338 iCpGs. When combined, a concatenated complete feature matrix of 1,001 cell lines by 1,364 of the unique pan-cancer CFEs (cancer functional events: CGs, RACSs, iCpGs) is created. Using an IC50 dataset of the screenings of 265 drugs across 990 cell lines and the complete feature matrix[1], the data was split into a training set (70%) and a testing set (30%). A linear regression model was then run for the training set. After creating the model we ran a correlation analysis between the predicted IC50 values and the observed IC50 values. Once completing linear regression, using the complete feature matrix and discretized AUC values, we split the data into a training (70%) and testing (30%) set. We then ran a logistic regression model on the data. Using the predicted and observed y values, we calculated the accuracy, sensitivity, and positive predictive value (PPV).

Results

By observing the results of our correlation analysis, we found that using cancer-driving alterations in genes cannot effectively predict drug sensitivity measured using IC50 values. In Figure 1 we can see that the correlation coefficient when using genomics as the identifier is most populated around 0, showing little correlation between the

predicted IC50 values and so forth for the observed ones. Analyzing the results from the logistic regression model, we saw much more promising indicators of drug sensitivity in the gene-drug interactions. Figure 2 shows that the accuracy of our model was on the higher end, and the sensitivity and PPV values also had clusters at around 0.6.

Discussion

This study serves as a baseline for future studies in developing computational models that transform the current input features in the study into more informative features for predicting drug sensitivity. We believe that by combining gene expression data and genomics, better predictions of drug sensitivity can potentially be made. Furthermore, we want to investigate performing linear regression and logistic regression using deep learning and neural networks to predict drug response with the data, which can possibly produce more significant results.

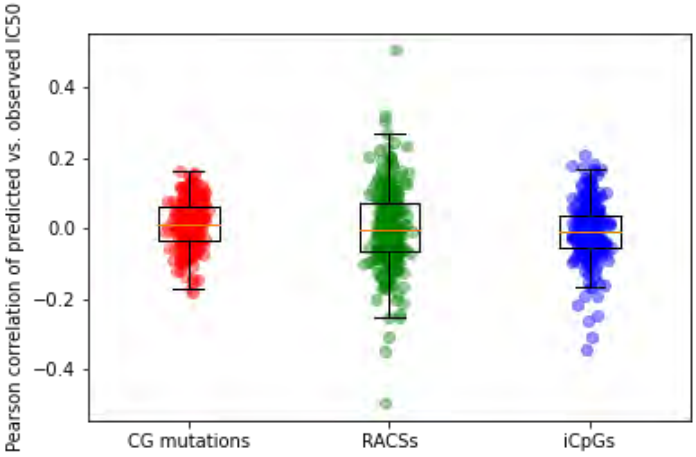

Figure 1. Pearson correlation of predicted vs. observed IC50 for each cancer-driving alteration molecular data type

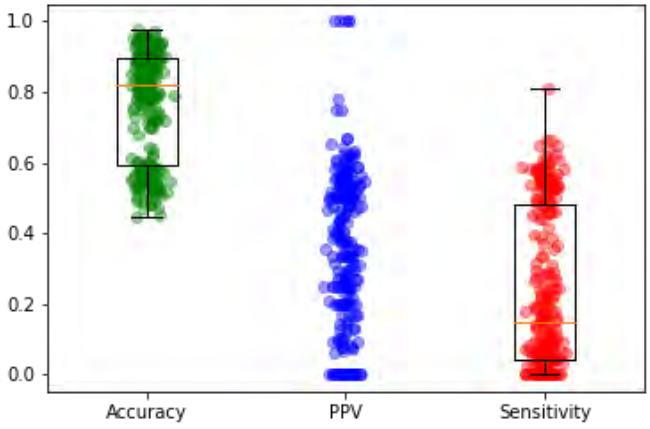

Figure 2. Accuracy, PPV, and sensitivity using logistic regression

References

1. Iorio F, Knijnenburg TA, Vis DJ, Bignell GR, Menden MP, Schubert M, et al. A Landscape of Pharmacogenomic Interactions in Cancer. Cell. 2016 Jul;166(3):740–54.

Spatial Analysis of Fibroblast-Mediated Drug Resistance in HER2$^+$ Breast Cancer

Griffin J. Hurt[1], Matthew D. Poskus[2], Ioannis K. Zervantonakis[2]
[1]University of Pittsburgh, Pittsburgh, PA; [2]Department of Bioengineering, Swanson School of Engineering, University of Pittsburgh, Pittsburgh, PA

Abstract

Fibroblasts contribute to disease progression and drug resistance in HER2+ breast cancer. Establishing the spatial relationship between tumor cells and fibroblasts on proliferation may help elucidate fibroblast-mediated drug resistance. Here, we show that an individual tumor cell's distance from the closest fibroblast is positively correlated with proliferation, despite the opposite trend previously being observed for proliferating cell density. Furthermore, we observed a negative correlation between a tumor cell's fibroblast Voronoi neighbor frequency and its proliferation.

Introduction

Modeling interactions in the tumor microenvironment (TME) is important for developing effective cancer treatment strategies but creating such models proves to be difficult in some circumstances. For instance, while it has been shown that fibroblasts reduce lapatinib sensitivity in some HER2$^+$ breast cancer subtypes, an exact model of their interaction has yet to be developed[1]. One factor in the interplay may be the spatial relationship between tumor cells and fibroblasts. For instance, the density of proliferating HER2$^+$ tumor cells has been shown to be greater when the clusters are closer to cancer-associated fibroblasts[2]. Moreover, we have seen in mice injected with HER2$^+$ breast cancer cells to form tumors in vivo that a greater number of proliferating tumor cells exist within 100 microns of the fibroblast-rich stroma than the center of the tumor. Based on these findings, we believe that an image analysis pipeline quantifying spatial relationships could help unveil other connections not previously seen. Similar cellular models have demonstrated a spatial correlation between lung cancer recurrence and T cells by analyzing neighbor frequencies in a Voronoi diagram, indicating the possible utility of the metric[3]. Here, we investigate how Voronoi neighbor frequencies and tumor cell to fibroblast distance affects proliferation of individual tumor cells. In order to measure cell proliferation, we stained for Ki67, as it is widely utilized as a cell proliferation marker that degrades during quiescence[4].

Methods

In a 96-well plate, EFM-192 tumor cells expressing GFP in coculture with AR22 fibroblasts were treated with increasing amounts of lapatinib and imaged after 96 hours for Hoechst and Ki67. The subsequent images were loaded into the CellProfiler computer program[5] and run through an analysis pipeline to segment the image by Hoechst, measure the intensity of the markers for each cell, and classify identified objects as tumor cells or fibroblasts based on their GFP intensity. Detected objects and their associated intensity data were then loaded into the MATLAB program for further analysis. Cells were classified as proliferating or not proliferating depending upon whether their Ki67 intensity was above or below the mean respectively. Voronoi neighbor frequencies were found using the "voronoin" function in MATLAB, and closest fibroblast and average fibroblast distances were computed using the "pdist" function in the "Statistics and Machine Learning Toolbox". To test for significance, 500 Monte Carlo simulations for distance and 100 Monte Carlo simulations for Voronoi neighbors similar to the methodology in Enfield et al. were performed by assigning each cell a uniformly distributed random location in the microscope field and each tumor cell a random Ki67 intensity from an exponential distribution fit to the measured intensities. An exponential distribution was chosen for Ki67 intensity, as this better reflected the experimental data.

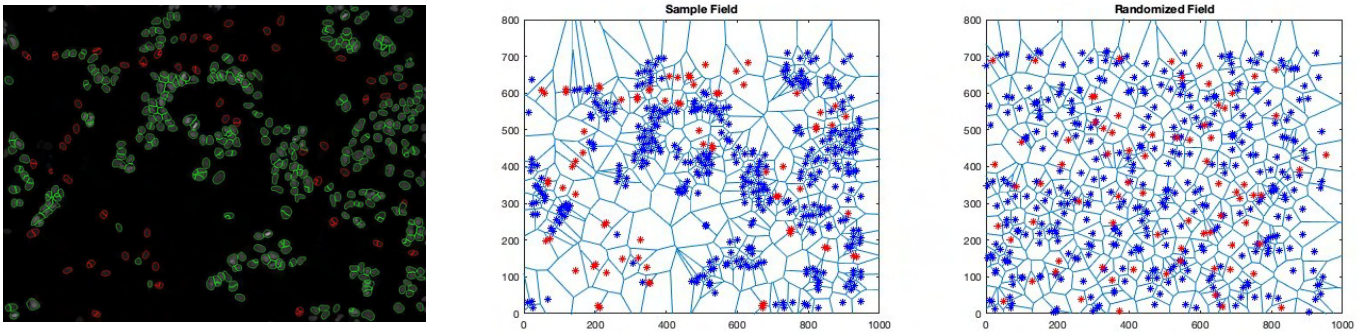

Figure 1. A microscope field with tumor cells marked in green and fibroblasts marked in red (left), its representative Voronoi diagram with tumor cells marked in blue and fibroblasts marked in red (center), and the same field after being randomized during Monte Carlo simulation (right).

Distance to closest fibroblast, average distance to fibroblast, and fibroblast Voronoi neighbor intensities were plotted against Ki67 intensity and analyzed.

Results

The correlation between distance to the closest fibroblast and Ki67 intensity was found to be positive and significant against the simulation ($p < 0.001$) for both non-drug-treated and drug-treated (lapatinib doses of 0.01μM, 0.03μM, 0.1μM, 1.0μM, and 3.0μM) tumor cells, indicating that tumor cells further away from fibroblasts tended to proliferate more. The correlation coefficient between minimum fibroblast distance and Ki67 intensity for drug-treated tumor cells was found to be 0.0730, roughly 1.64 times greater than the correlation coefficient of 0.0446 for non-drug-treated tumor cells, indicating a stronger spatial relationship between tumor cells and fibroblasts when being treated with lapatinib. The correlation between fibroblast Voronoi neighbors and Ki67 intensity was also found to be significant against the simulation ($p < 0.001$) and negative, indicating that cells proliferated less when surrounded by a greater number of fibroblasts than tumor cells. The correlation coefficient between neighbor frequency and Ki67 intensity was found to be -0.0765 for drug-treated cells, roughly 1.19 times greater than the correlation coefficient for non-drug-treated cells, -0.0641. There is insufficient evidence to support a correlation between average tumor cell to fibroblast distance and Ki67 intensity, as the correlation coefficient was not found to be significant against the simulation.

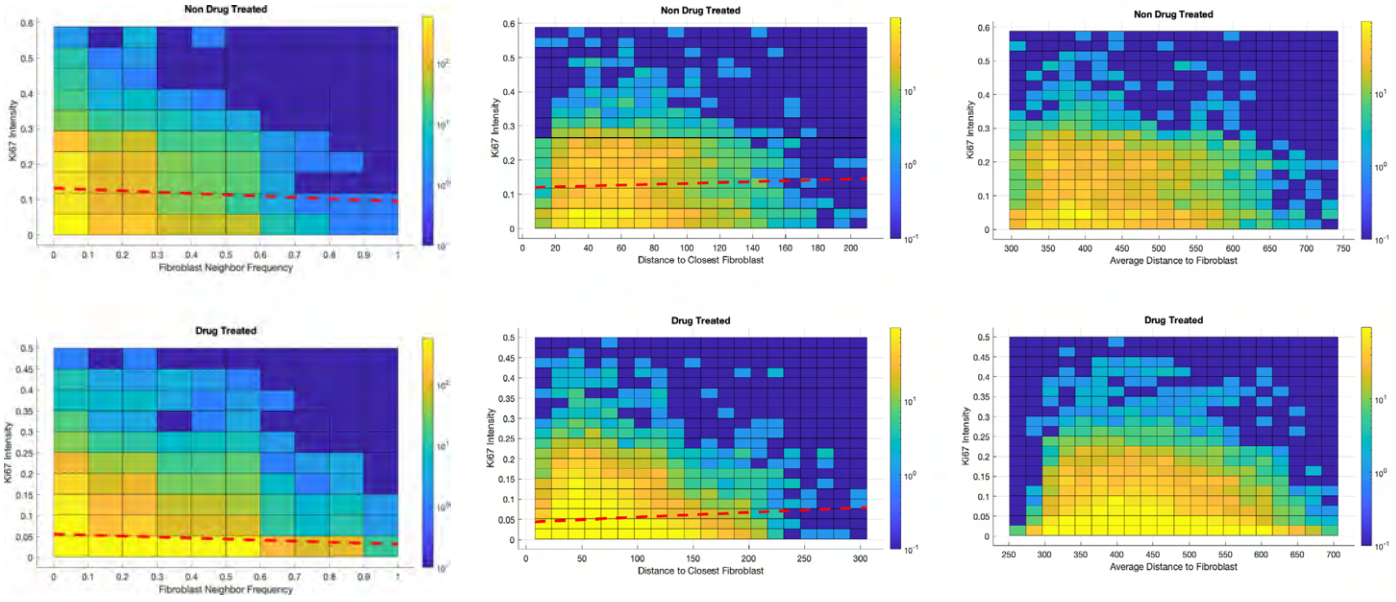

Fibroblast Neighbor Frequency | Closest Fibroblast Distance | Average Fibroblast Distance

Figure 2. Ki67 intensity as a function of fibroblast neighbor frequency, closest fibroblast distance, and average fibroblast distance. Lines of best fit are included for significant correlations.

Discussion

While density of proliferating cells appears to be positively impacted by proximity to fibroblasts, on an individual cell basis the opposite trend appears to be true. One possible explanation for this inconsistency is the adjacency of newly spawned cells during proliferation. When a cell undergoes mitosis, the daughter cell is formed directly next to the parent, which limits how close a fibroblast can be to proliferating cells. This fact also contributes to the lack of fibroblast Voronoi neighbors surrounding proliferating cells, as daughter cells generally occupy that space. Furthermore, the trends seen in vitro may not match the true tumor microenvironment, as fibroblast-secreted growth factors and cytokines diffuse quickly in the medium, as opposed to their slower diffusion through the extracellular matrix in vivo. Further studies are needed to establish the effects of fibroblasts on individual tumor cells in vivo. Based on the significance of fibroblast neighbor frequencies, the construction of Voronoi diagrams will most likely prove to be useful in the wdevelopment of an image analysis pipeline focused on spatial properties.

References

1. Zervantonakis, Ioannis K., et al. "Fibroblast–Tumor Cell Signaling Limits HER2 Kinase Therapy Response via Activation of MTOR and Antiapoptotic Pathways." *Proceedings of the National Academy of Sciences*, vol. 117, no. 28, 2020, pp. 16500–16508., https://doi.org/10.1073/pnas.2000648117.
2. Marusyk, Andriy, et al. "Spatial Proximity to Fibroblasts Impacts Molecular Features and Therapeutic Sensitivity of Breast Cancer Cells Influencing Clinical Outcomes." *Cancer Research*, vol. 76, no. 22, 2016, pp. 6495–6506., https://doi.org/10.1158/0008-5472.can-16-1457.
3. Enfield, Katey S., et al. "Hyperspectral Cell Sociology Reveals Spatial Tumor-Immune Cell Interactions Associated with Lung Cancer Recurrence." *Journal for ImmunoTherapy of Cancer*, vol. 7, no. 1, 2019, https://doi.org/10.1186/s40425-018-0488-6.
4. Miller, Iain, et al. "KI67 Is a Graded Rather than a Binary Marker of Proliferation versus Quiescence." *Cell Reports*, vol. 24, no. 5, 2018, https://doi.org/10.1016/j.celrep.2018.06.110.
5. Stirling, David R., et al. "Cellprofiler 4: Improvements in Speed, Utility and Usability." *BMC Bioinformatics*, vol. 22, no. 1, 2021, https://doi.org/10.1186/s12859-021-04344-9.

Cellular and Tissue Level Analysis of Endometriosis Angiogenesis

Scholar: Priyasha Itani, Upper St. Clair High School, Upper St. Clair, PA

Lab: Vascular Bioengineering Laboratory, David A. Vorp, PhD. (Director), Justin Weinbaum, PhD. (Associate Director)

Mentor: Isabelle Chickanosky (Ph.D. Student)

Site: Tech Drive X

Introduction: Endometriosis is an unusually high prevalence gynecological disease affecting 10% of premenopausal women (~190 million) worldwide. Defined as the proliferation of endometrial like tissue outside the internal uterine wall, the disease is associated with symptoms such as chronic pelvic pain, excessive bleeding, and infertility. Sampson's Theory of Retrograde Menstruation is the field's main theory of pathogenesis, however, 90% of premenopausal women experience retrograde menstruation, i.e., more than the 10% that develop endometriosis. Therefore, there is at least one or more additional mechanisms at play. For example, increased levels of estrogen (E2) are present within endometriotic patients compared to non-suffering patients and could point to another possible mechanism; previous literature also alludes to E2 as a pro-angiogenic factor. For this study, we hypothesized that E2 would increase endothelial cell (EC) proliferation and thus angiogenesis, allowing for the further development of endometriosis; and higher density of blood vessels would be found in endometriosis tissue.

Methods: A proliferation assay was performed to quantify the effect of varying amounts of E2 (1 ng/mL, 1.5 ng/mL, 2 ng/mL, and 4 ng/mL) and the negative and positive control, Dulbecco's Modified Eagle Media (DMEM) and Supplemented DMEM, respectively, on the growth of Human Coronary Artery ECs on tissue culture plastic. ECs were also seeded on top of collagen gel, treated with such experimental groups, and quantified using ImageJ cell counter software after 3 days of incubation. Healthy and endometriotic tissue samples were studied using hematoxylin and eosin staining to identify and quantify vascular formation.

Results and Discussion: The proliferation assay displayed a general trend towards a peak of increased proliferation for the middle concentration of E2 tested, in line with previous literature. Furthermore, the collagen gel displayed that ECs cultured in 1.5 ng/mL E2 significantly increased in cell count compared to the negative control. Histological analysis indicated varied results in vascular formation for different patients, indicating the complexities of endometriosis presentation. One limitation of this work is that phenol red present in the culture can mimic E2 signaling so future work should be done in phenol red-free media. Another limitation is the use of coronary artery ECs, which are not directly involved in endometriosis – human endometrial microvascular ECs could be used to increase the clinical relevance.

Conclusion: This study has displayed encouraging results on the effect E2 has on ECs proliferation and angiogenesis, suggesting an impact in accelerating endometriosis development. Additionally, this study identified collagen gel as a potentially effective substrate for further exploration of EC angiogenesis in endometriotic conditions.

3D Printing Components for an OCT prototype

Scholar: Marcus Jones

High School: Central Catholic High School

Lab: Optical Coherence Tomography Laboratory

Mentor: Shaohua Pi

Site: Ophthalmology

Background: Optical Coherence Tomography (OCT) is used to produce micron-resolution, non-invasive, 3-D retinal images in humans to assist diagnosis of various ocular diseases. A next-generation OCT prototype, called visible-light OCT is being built in the lab, which involves customizing supporting components using a 3-D printer.

Methods: The dimensions of the desired components were measured either from reality or online resources. A 3-D modeling software called *SOLIDWORKS* was used to design the components. It includes sketch tools such as lines, circles, and fillets to build the panels, holes, and barriers with adjustable geometry properties including length, diameters and depth to depict the 3D structure. After saving as .STL file, the structure was transported into the printing software to designate printing material, slice layers, determine infill density and pattern, and pick the printing speed and cooling options to generate the GCODE, which is the filetype that can be processed directly by the 3D printer.

Results: Two components were designed, printed, and successfully integrated into the OCT system. One part was an adapter for a lens (mounted in a 60 mm cage plate) to be connected to a breadboard with one M4 hole and two M6 holes. The second structure was designed to align light beams from a collimator (mounted in a 16 mm to 30 mm cage adapter) to a grating (mounted in a precision 30 mm rotation cage). It has a rectangular base, with custom extrusions on top of the base and multiple M6 and M4 holes.

Conclusion: The skills for 3D printing have been learned and mastered to create components for OCT, which will eventually lead to helping diagnose retinal diseases in patients.

Fully Unsupervised DDU-Net for the Task of Pediatric Bone Age Assessment

Preetam S. Jukalkar, Xiyao Fu, Dr. Liang Zhan[2]
South Fayette High School, McDonald, PA; University of Pittsburgh Hillman Cancer Center Academy, Pittsburgh, PA

Abstract *Currently, radiologists require up to 7 minutes to assign scores to 20 individual bones[1] to perform bone age assessment, the practice of identifying bone age from left hand-wrist x-rays. This study implements a Dense Dense U-Net, a convolutional neural network, to segment hand x-rays using K-Means clusters as ground truths. A Support Vector Regression model utilizes produced segmentations to predict bone age with greater speed and precision than a radiologist without sacrificing accuracy.*

Introduction Bone age assessment (BAA) is the practice of using one of two methods (TW2 or GP) to identify the relative maturity of a left hand-wrist x-ray[1], which is independent from chronological age. TW2 requires 7 minutes to perform on average, while GP requires 1 minute but sacrifices accuracy and precision[1]. Furthermore, radiologists often suffer from INTRA-OBSERVER BIAS and have no choice but to use valuable time assessing bone age[1]. New approaches harness the power of deep learning, streamlining pediatric care and developing a more efficient process.

To perform BAA, x-ray images must first be segmented to reduce noise and complexity; semantic (supervised) segmentation has delivered promising results[2] in predicting bone age. However, current approaches to BAA often utilize supervised convolutional neural networks[2,3,4] (CNNs) which, while capable of outperforming radiologists (CITATION), are limited by data concerns. CNNs require annotated segmentations, labeled by hand pixel-by-pixel as 0 or 1 based on relevance[2]. To combat this problem of "expensive" and at times unavailable data, our proposed architecture aims to utilize a small yet varied dataset without any need for perfectly annotated segmentations. The proposed architecture is able to use existing x-ray datasets in unique ways, automatically creating data in the form of rough, flawed segmentations from which the neural network can learn to achieve desirable results. By utilizing existing data in unique ways and capitalizing on available resources, the horizons of biomedical imaging can be expanded to include unsupervised learning, which has been largely ignored in favor of semantic segmentation.

Methods The dataset utilized consists of 100 randomly chosen training images, each of a left hand-wrist x-ray with different brightnesses, positions, and sizes, and 50 testing images, again with different brightnesses and positions to test the robustness of the proposed model. Another dataset, consisting of x-rays and corresponding bone ages, contains 625 images which are used to train the SVR; this dataset is split 51.68% male and 48.32% female, and the ages are skewed toward 10 years old and above (Fig. 1). Pre-processing is required to standardize the images; CLAHE normalization is used and the images are then resized to 256x256 grayscale images. K-Means clustering is applied to all training images to produce rough ground truths; the algorithm performs poorly on many of the more variable x-rays (Fig. 2). A Dense Dense U-Net[3] (Fig. 3) is then implemented, with inputs of processed x-rays and outputs of the K-Means clustered images. The segmented images produced by the proposed model are then used in a SVR model trained on 625 images, inputs being the segmented image and outputs being the predicted bone age.

Results The DDU-Net performs with an accuracy of 86% on training set and 91% on testing set, with a binary cross entropy loss of 0.2945. The model was stopped early (14 epochs out of 25) to avoid overfitting to the same problems and noise faced by the K-Means clusters used as ground truths. Training took 238 minutes on a MacBook Air (M1 chip), and producing a prediction for one x-ray takes 3 seconds, a far cry from the 7 minutes it can take a radiologist. The SVR model produced a mean absolute error (MAE) of 28.3 months, which drastically decreased to 12.1 months for bone ages above 10 years old. For comparison, radiologists produced MAEs ranging from 14.6 to 16 months, and current state-of-the-art models produced a MAE of 7.35 months[4] (Fig. 4).

Discussion While performing BAA through deep learning has been accomplished with great accuracy, data has hindered the ability of machine learning in bioinformatics; models usually require exorbitant amounts of "perfect" data to learn, numbering in the thousands of images that is simply implausible in many cases. The proposed model is able to break many of these barriers to entry, working with only 100 images and no true labels outside of flawed ground truths created unsupervised. The promising results of the model hint at a widening image segmentation field that now shows promise for tasks in which large datasets may not be achievable.

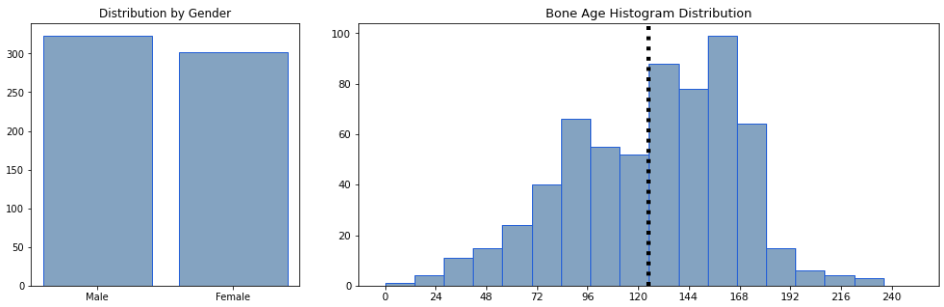

Figure 1. Distribution of 625 images. Equally divided by gender, skewed toward bone ages above 120 months, or 10 years.

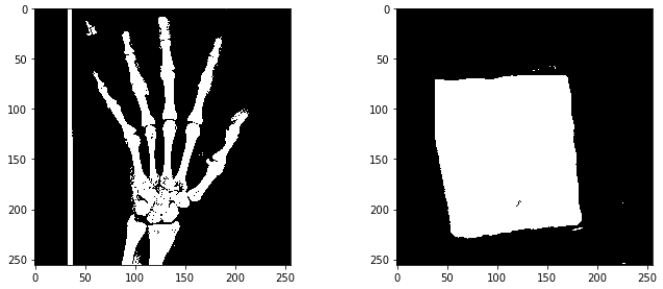

Figure 2. Images produced by K-Means clustering (5 clusters, 3 selected as foreground). Algorithm produces noisy results that commonly suffer in producing detail and removing background. At times, can produce desired results.

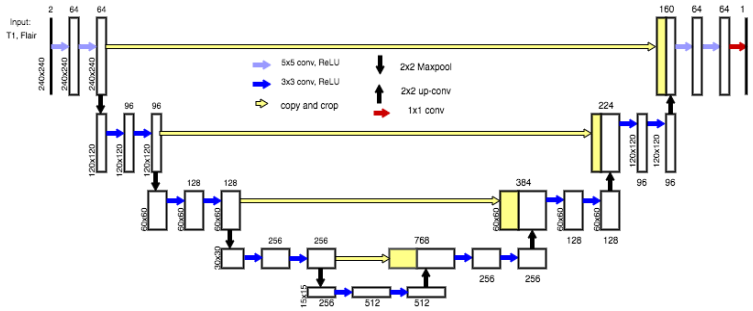

Figure 3. Architecture of Dense Dense U-Net, as proposed in [3].

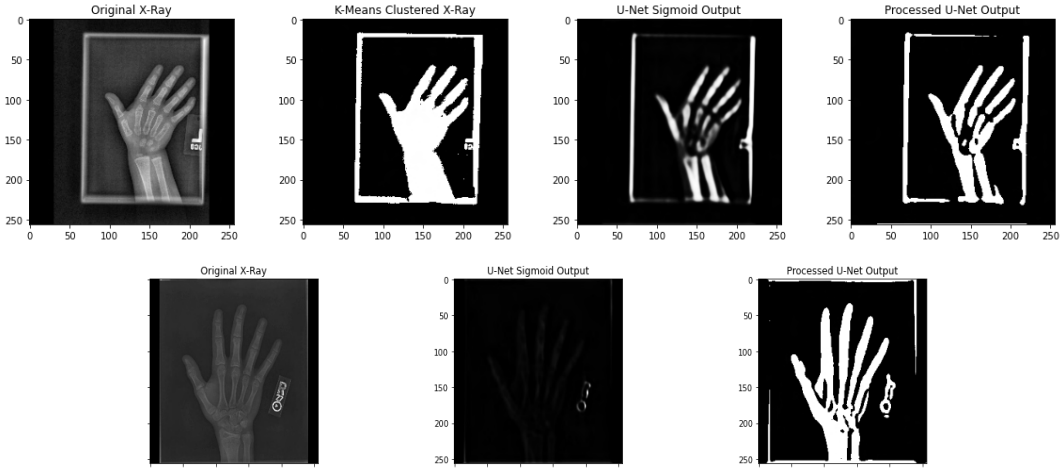

Figure 4. Predictions of U-Net on training set compared to original x-ray and K-Means clustered image. Sigmoid output represents confidence of each pixel, confidences above mean value for image selected as foreground. Consistently able to produce detail and find signal in low brightness, noisy images in which K-Means fails.

References

1. Satoh M. Bone age: assessment methods and clinical applications. Clin Pediatr Endocrinol. 2015;143-152 doi:10.1297/cpe.24.143
2. Xiaoying P, Yizhe Z, Hao C , De W, Chen Z , and Zhi W. Fully Automated Bone Age Assessment on Large-Scale Hand X-Ray Dataset. International Journal of Biomedical Imaging; 2020
3. Fan J, Wing W, and Tieyong Z. DDUNet: Dense Dense U-Net with Applications in Image Denoising. Department of Mathematics, The Chinese University of Hong Kong; 2021
4. Ian P, Grayson B, Simukayi M, Derek M, Carrie R, David S, and Rama A. Rethinking Greulich and Pyle: A Deep Learning Approach to Pediatric Bone Age Assessment Using Pediatric Trauma Hand Radiographs. Radiology: Artificial Intelligence 2020 2:4

Targeting PUMA to Enhance Intestinal Regeneration

Scholar: Anthony Kalvi

High School/College/City/State: Upper st. Clair High school, Pittsburgh, PA

PI of group/lab: Dr. Jain Yu

Mentor(s): Dr. Brian Leibowitz

Site: Cancer Biology

Chemotherapy and Ionizing radiation are common methods of cancer treatment and are used to target rapidly dividing tumor cells. The small intestine (SI) is the most rapidly proliferating tissue in adult mammals and is maintained by a pool of tissue stem cells. The SI is extremely sensitive to injury caused by chemo and radiation, which can be a limiting factor for cancer patients and their treatment. PUMA, a protein downstream of p53, is primarily responsible for inducing apoptosis following radiation-induced DNA damage, and is a potential target to reduce intestinal injury. Using a mouse model, as well as a small molecule PUMA Inhibitor (PUMAi), we assessed the benefits of PUMAi for intestinal recovery from 9.1 Gy of radiation. Intestinal tissue was collected 12 days after irradiation. One group of mice was treated with PUMAi, and the other group was vehicle control. Hematoxylin and eosin staining was performed along with immunofluorescence. We found that PUMAi treatment led to dramatic improvements in intestinal recovery, as measured by crypt numbers and villus height. The structural integrity of the PUMAi mice's SI was better due to the increased organization of terminally differentiated cells in their crypts. Treatment with PUMAi also improved DNA damage clearance and proliferation. Having previously found that PUMAi treatment blocks intestinal stem cell apoptosis in the first few hours after radiation, the present data suggests that targeting PUMA also has long term benefits for intestinal recovery. This finding is supported by a concurrent survival study, which found that irradiated mice given three doses of PUMAi have significantly improved long term survival compared to irradiated mice receiving vehicle control treatments.

Sex-Based Differences in Environmental Regulation of Macrophage Mediated Cancer Immunity

Scholar: Sulwe Kauffmann-Okoko

High School: Winchester Thurston School, Pittsburgh, PA

PI of group: Dr. Adam Soloff

Mentors: Adam Soloff, Amy Powers, Seth Eisenberg, Kamili Wiley, Rajeev Dhupar

Site: Immunology and Cancer Immunotherapy (ICI)

Introduction: We are looking at how environmental factors such as pollution and contamination regulate cancer immunity. We are also looking at whether or not there is a difference in this regulation depending on sex-based differences such as male and female responses and the levels of estrogen and testosterone present in a phenotype.

Methods: We extracted bone marrow from female and male C57BL/6 mice. After this bone marrow was collected, we put it into macrophage stimulated cell culture made with media without exogenous estrogen. We put the cells into separate plates; one for female, and one for male. The plate sizes were chosen based on how much fluid was able to fit in each well equally. The cells in the plate had added estrogen, testosterone, as well as toxins. The toxins we used were diesel exhaust particulate (DEP), a particle released from diesel fuel combustion, and malathion, a type of pesticide. We also performed a histone extraction to measure the protein production in the cells. Additionally, we were interested in cytokine production differences to inform us about pro versus anti-tumor effects. To figure this out, we collected the supernatant from our wells and used a cytometric bead array kit.

Results: ---

Conclusion: ---

Future Directions: Future directions include incorporating healthy habits into our daily lives. Healthy habits include wearing masks and using eco-friendly vehicles to limit the amount of toxins we are releasing and breathing in around us. Washing organic fruits and vegetables, and eating a variety of these will reduce the risk of pesticide exposure, especially to a particular type of pesticide. Overall, since we do not currently have any specific results, future directions also include conducting further research on this topic of sex-based differences in environmental regulation of macrophage-mediated cancer immunity.

Interrogating B Cell Function in the Ascites of Patients with High Grade Serous Ovarian Cancer

Grace M. Ketler, Dr. Ian MacFawn, Dr. Tullia Bruno, Sheryl Kunning, Hye Mi Kim, Asia Williams, Dr. Ayana Ruffin, Noor Nader
Norwin High School, Irwin, PA, Hillman Cancer Center, Pittsburgh, PA

Abstract

With 21,000 women in the United States a year being diagnosed with ovarian cancer, a typically aggressive one, immunotherapy is a large focus in the field of cancer research for this cancer. Immunotherapy harnesses the body's own immune response to combat cancer. While T cells have been the main focus of current immunotherapies, B cells demonstrate promise as new targets as they correlate with improved patient survival and response to immune checkpoint inhibition (ICI).

Introduction

Ovarian cancer is a typically aggressive cancer that starts in the fallopian tubes and spreads to the ovaries. With the United States five year survival rate being 47.4%, there is a need for more targeted immunotherapies as the only standard of care is currently surgical removal and chemotherapy. Ovarian cancer can spread to the abdomen in late stage disease and create ascites fluid, which is typically composed of tumor, immune, and stromal cells. There is a need to assess the function of B cells in ascites fluid to understand if this unique microenvironment impacts B cell phenotype and function. My central hypothesis was that ascites fluid from ovarian cancer patients would promote memory B cell differentiation because since the immune composition of ascites fluid is relatively unknown, it would force the B cells to take on new antigens for the first time and would then differentiate into memory B cells after some time in the ascites fluid.

Methods

We cultured B cells in vitro to simulate B cell differentiation in the presence of acellular ascites fluid. First, we isolated leukocytes from the healthy donor blood using a Ficoll gradient. We then used a magnetic kit to isolate naive or memory B cells for culture with the ascites fluid from patients with high grade serous ovarian cancer. We utilized a 50% media and 50% ascites culture mix, and we utilized media alone as a comparative control. We also utilized a master mix to promote differentiation of B cells into plasmablasts. At days 0, 4, and 7, we stained the cells for flow cytometry to analyze their differentiation into plasmablasts.

Results

We found that differentiation and growth of B cells occurred faster in ascites fluid compared to media alone. There was a 10% increase in viability of naive B cells in ascites compared to the media and the cells doubled in number. There was a 14% increase in viability for memory B cells and the cells tripled in number. The speed of differentiation was faster for both naive and memory B cells. Specifically, there were more plasma blasts at day 4 in the ascites fluid compared to media alone.

Discussion

We saw from these experiments that B cells in ascites fluid have improved numbers, increased viability, and faster differentiation. From these results, I conclude that there is something in the ascites fluid that is forcing and promoting the B cells to become activated quicker and produce antibodies to fight off antigens. In the future, studies such as large- scale staining can be conducted to better understand what it is in ascites fluid that makes the B cells differentiate faster. The fluid is generally unknown, but while we know there are immune cells, tumor cells, and stromal cells, we also now know that there is something else in the ascites fluid that needs to be discovered and investigated. Additionally, I would like to study the differences in B cell differentiation between ascites fluid from ovarian cancer, and ascites fluid from other diseases such as liver disease.

References

1. *Ascites*. Johns Hopkins Medicine. (2022, April 11). Retrieved July 29, 2022, from https://www.hopkinsmedicine.org/health/conditions-and-diseases/ascites#:~:text=Ascites%20is%20a%20condition%20in,chest%20and%20surround%20your%20lungs

2. Dutta, D. S. S. (2018, December 20). *Types of antibodies*. News. Retrieved July 29, 2022, from https://www.news-medical.net/life-sciences/Types-of-Antibodies.aspx

3. GE;, S. K. A. M. L. A. N. R. (n.d.). *Multicellular spheroids in ovarian cancer metastases: Biology and pathology*. Gynecologic oncology. Retrieved July 29, 2022, from https://pubmed.ncbi.nlm.nih.gov/19135710/

4. *Ovarian cancer statistics: How common is ovarian cancer*. American Cancer Society. (n.d.). Retrieved July 29, 2022, from https://www.cancer.org/cancer/ovarian-cancer/about/key-statistics.html#:~:text=Ovarian%20cancer%20ranks%20fifth%20in,is%20about%201%20in%20108.

5. Team, H. J., & Team, H. J. (2017, December 14). *Thymus function, locations and role in immune system*. Health Jade. Retrieved July 29, 2022, from https://healthjade.com/what-is-thymus/

Title: Testing effectiveness of novel GFP amino acid tag
Scholar: Daniel R. Komlosi
High School/College/City/State: Pittsburgh Science and Technology Academy, Pittsburgh, PA
PI of group/lab: Dr. Robert Shanks
Mentor(s): Dr. Robert Shanks, Nicholas Stella, and Rachel Calvario
Site: Department of Ophthalmology

Introduction: Green fluorescent protein (GFP), originally isolated from the jellyfish Aqueora victoria, is a ubiquitous molecular engineering tool used in biological research. GFP is used as a marker protein, important for tracking processes within cells. Therefore it is important to advance GFP effectiveness for a variety of research applications because improving GFP fluorescent intensity would increase the sensitivity of GFP-based assays.
The goal of this study was to test if a 20 amino acid N–terminal tag (580N) would increase the fluorescence intensity of a fluorescent protein in Saccharomyces cerevisiae compared to GFP without the tag. This unpublished 580N tag has shown to increase the fluorescence intensity of fluorescent proteins in several bacterial species, but has never been tested in a eukaryote. Therefore, we evaluated whether 580N could improve GFP function in an important yeast Species.

Method: Yeast in vivo homologous recombination was used with a plasmid and synthetic DNA to generate two plasmids. One had the mUkG1 gene and the other with mUkG1 fused to the 580N tag. Each expressed mUkG1 under the control of the strong ADH1 promoter. A vector control without mUkG1 was used as a negative control. These plasmids were moved into S. cerevisiae strain InvSc1. MUkG1 was picked for this project because it is one the brightest GFP's tested in yeast. Yeast plates without uracil were used to select for yeast colonies with the plasmid. Fluorescence was first measured with a fluorescent dissecting scope and a fluorometer and normalized by the optical density value (OD 600). Data was analyzed with Prism software.
Results: Based on both quantification methods, the plasmid with the 580N tag conferred less fluorescence than the plasmid with mUkG1 only.

Conclusion: The 580N tag showed no increase in mUkG1 fluorescence intensity in S. cerevisiae; therefore, the null hypothesis is accepted.

Use of an event-driven data release in the care of individuals suffering from symptomatic genetic diseases.

Scholar: Ryan Krishna

High School: Winchester High School, Massachusetts

Lab: School of Computing and Information

Mentor: Balaji Palanisamy, PhD

Site: CoSBBI

Background: Oftentimes, individuals with a genetic/hereditary condition make the choice to remain oblivious to their condition until it is imperative to their health. During this process, failure to "mark down" symptoms at their earliest onset, can lead to an untimely, perhaps too late, diagnosis. This could lead to patients suffering from Alzheimer's not receiving the appropriate care to learn about and work with their condition correctly. To prevent this, a python application featuring an event-driven data release would be beneficial. Adding an intermediary such as a computer application to the patient's lifestyle is an effective method of ensuring properly timed disease discovery. Therefore, this application has a purpose of determining the symptoms a patient is suffering from for a specific disease and reporting if those symptoms indicate that the patient should take further steps in their healthcare.

Methods: The most efficient way of creating a application to serve this purpose was in python. Using the panda's library a sample Alzheimer's questionnaire was implemented with user input. The user is asked to input either a 1, or a 0, depending on if their answer to the questions is yes, or no, respectively. The application then adds up the total number of "yes" answers and categorizes them into the "normal cognition" or the "you may be at risk for Huntington's Disease" category.

Results: There were successful trials of the Alzheimer's questionnaire. Upon a user selecting the appropriate responses to the questions, the application was able to deduce a response about their brain function according to standardized questionnaire answers.

Conclusion: Our results show that in a situation where a patient may not wish to know their diagnosis until necessary, a application such as this featuring an event-driven release could be applicable. Further questionnaires will be created to confirm the effectiveness of this intermediary in a patient's healthcare journey.

This material is based upon work supported by the National Science Foundation under Grant #2020071. Any opinions, findings, and conclusions or recommendations expressed in this material are those of the author(s) and do not necessarily reflect the views of the National Science Foundation

Genotyping PCR for Animal Model of Retinitis Pigmentosa

Jonathan Li[1], Yuanyuan Chen[2]
[1], Fox Chapel Area High School, Pittsburgh, PA, USA 15238; [2], Department of Ophthalmology, University of Pittsburgh School of Medicine, Pittsburgh, PA, USA 15213

Abstract

RHODOPSIN (RHO) associated autosomal dominant retinitis pigmentosa (adRP) is a retinal hereditary disease that currently lacks efficacious treatment. This project focuses on pharmacological studies of the RHO^{P23H} knock-in mouse model to develop effective and safe drug candidates to treat RHO-associated adRP. Therefore, consolidating the genotype of these animals is the essential step before they are tested for drug efficacy. PCR is used to identify the genotypes of Rho$^{P23H/+}$, Rho$^{P23H/+}$, or Rho$^{P23H/+}$ in mice.

Introduction

Mutations in over 60 genes are found to cause retinitis pigmentosa (RP) (1). Mutations in the *RHO* gene account for 25-30% of all adRP cases, and the Proline to Histidine mutation at codon 23 (P23H) of the *RHO* gene alone is found in about 10-12% of all adRP patients in the U.S. Rhodopsin is the most abundant protein in rod photoreceptors. The *RHO* mutation causes rhodopsin protein to misfold, eventually leading to rod cell death and vision loss. No effective treatment is currently available for any type of RP, demonstrating an urgent medical need.

Resembling the adRP inheritance pattern in human patients, the heterozygous Rho$^{P23H/+}$ mice were used for efficacy tests. These heterozygous animals are obtained by cross-breeding a Rho$^{P23H/P23H}$ mouse with a wild-type (WT) mouse (Rho$^{WT/WT}$). To identify the mice carrying the genotypes we need, we use genotyping Polymerase Chain Reaction (PCR) by determining the size of specific PCR products in each genotype.

Methods

A small piece of tissue of either tail tip or ear punch is collected from each animal and put in a tube containing tissue lysis buffer and DNA release additive to be incubated at room temperature for 5 min before heating at 98 ^{o}C for 2 min. This step is to release genome DNA from the tissue sample. The tube is centrifuged at 12,000 rpm in a tabletop centrifuge for 1 min to pellet the insoluble tissue pieces and supernatant which contain genome DNA for the PCR reaction. Each PCR reaction system contains a total of 10 µL of solution: 2 µL of nuclease-free water, 2 µL of genome DNA from mice, 1 µL of primer mix (0.5 µM in final solution), and 5 µL of master mix containing the Taq DNA polymerase, DNA dye, Deoxynucleoside triphosphate (dNTP) building blocks and buffer (ThermoFisher, Cat#F170L). Primers used are: GenoRhoL 2163, 5′-TGGAAGGTCAATGAGGCTCT-3′; and GenoRhoR 2561, 5′-GACCCCACAGAGACAAGCTC-3′. The PCR reaction mixes were put into PCR tubes and then into a PCR cycler (Eppendorf). The reaction was set as 95 ^{o}C for 5 min; 35 cycles of 98 ^{o}C for 20 sec, 60 ^{o}C for 30 sec and 72 ^{o}C for 1 min; and 72 ^{o}C for 7 min. The PCR products were taken out and loaded on a 1.5% agarose gel prestained with SYBR Safe DNA Gel Stain (Thermo). DNA electrophoresis was performed in the tris base, acetic acid, and ethylenediaminetetraacetic acid(TAE) buffer at 100 V for 30 min until the blue dye gets to the end of the gel. The gel was then imaged under UV illumination using the iBright imager.

Results

Due to the genetic manipulation in the knock-in mice, the PCR products from WT and Rho^{P23H} gene alleles are 399 and 573 bp, respectively. We did two sets of experiments.
In the first experiment (**Figure 1**), all PCR products showed ~400 bp DNA bands, suggesting they are from WT (Rho$^{+/+}$) animals, which is coherent to our expectations. In experiment 2 (**Figure 2**), sample 4 showed ~400 bp PCR product, samples 8-10 showed ~600 bp DNA bands and samples 5-7 showed no bands.

Discussion

The results of this project show that genotyping PCR is a reliable method for consolidating the animals' genotypes. I have successfully performed genotyping of Rho^{P23H} vs. WT animals and obtained most of the results as expected. The failed two samples without any PCR products may be due to the genome DNA being degraded. In the future, fresh tissue samples will be taken from these animals again to obtain fresh genome DNA for genotyping PCR. The confirmed Rho$^{P23H/+}$ mice will be used for efficacy tests of compounds developed by the Chen Lab. The Rho$^{P23H/P23H}$ and WT mice will be used as breeders.

Figure 1. Frist genotyping PCR reaction.

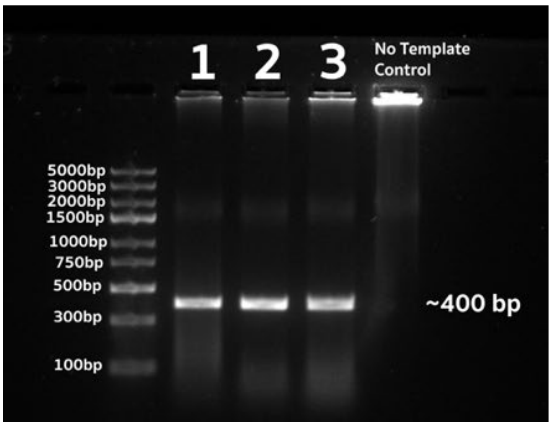

Figure 2. Second genotyping PCR reaction.

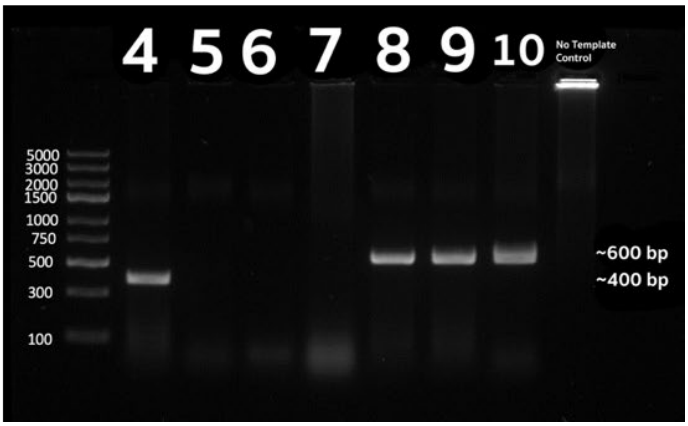

Table 1. Genotyping PCR result summary from Figures 1 and 2.

Samples	Results	Genotype
1	~400 bp band	*Rho*$^{+/+}$
2	~400 bp band	*Rho*$^{+/+}$
3	~400 bp band	*Rho*$^{+/+}$
4	~400 bp band	*Rho*$^{+/+}$
5	No bands	Need to repeat
6	No bands	Need to repeat
7	No bands	Need to repeat
8	~600 bp band	*Rho*$^{P23H/P23H}$
9	~600 bp band	*Rho*$^{P23H/P23H}$
10	~600 bp band	*Rho*$^{P23H/P23H}$

Note: Samples 5-7 do not have shown any bands, maybe due to genome DNA being degraded.

References

1. Hartong DT, Berson EL, Dryja TP. Retinitis pigmentosa. Lancet. 2006 Nov 18;368(9549):1795-809. doi: 10.1016/S0140-6736(06)69740-7. PMID: 17113430.
2. Sakami S, Maeda T, Bereta G, Okano K, Golczak M, Sumaroka A, Roman AJ, Cideciyan AV, Jacobson SG, Palczewski K. Probing mechanisms of photoreceptor degeneration in a new mouse model of the common form of autosomal dominant retinitis pigmentosa due to P23H opsin mutations. J Biol Chem. 2011 Mar 25;286(12):10551-67. doi: 10.1074/jbc.M110.209759. Epub 2011 Jan 11. PMID: 21224384; PMCID: PMC3060508.
3. Canene-Adams K. General PCR. Methods Enzymol. 2013;529:291-8. doi: 10.1016/B978-0-12-418687-3.00024-0. PMID: 24011055.

Analyzing CD4 T-cells in the tumor microenvironment

Kevin Lu, Dr. Xinghua Lu, MD, PhD
Williamsville North High School, Buffalo, NY; Dept of Biomedical Informatics in University of Pittsburgh, Pittsburgh, PA

Synopsis
Tumors of certain types of cancers contain different amounts and types of white blood cells(T-cells), leading to different tumor microenvironments. Single-cell RNA sequencing (scRNAseq) is a specific process to determine the gene expression for each T-cell, which reflects the cellular state of cells. By mining scRNA data, we find subtypes of CD4 T-cells that are shared among multiple cancers.

Introduction
Immunotherapy is a widely used method to combat tumor cells within cancers. Analyzing scRNA data can distinguish each cell's gene expression and the amount of cells present in each tumor. Therefore, distinguished efficacies of immunotherapy of different cancers can lead to discovering important genes that advance cancer treatment. CD4 T-cells are the primary focus of this study because they play an important role in the tumor microenvironment. The purpose of this study is to investigate the presence of certain subsets of CD4 T-cells in different cancers.

Methods
The programming platform Jupyter notebook and the package pandas were used to manipulate and organize large amounts of data. The data of this task consists of T-cells scRNAseq data derived from lung, colon, and liver cancers, including metadata and cell-by-gene count matrices. The metadata is concatenated and the count matrices are merged through inner join. Then, principal component analysis(PCA) was applied to the count matrices for dimensional reduction, cells were clustered using the Leiden algorithm, and UMAP of cells were plotted. Genes enriched in each cell cluster were identified and were used to characterize the cell clusters.

Results
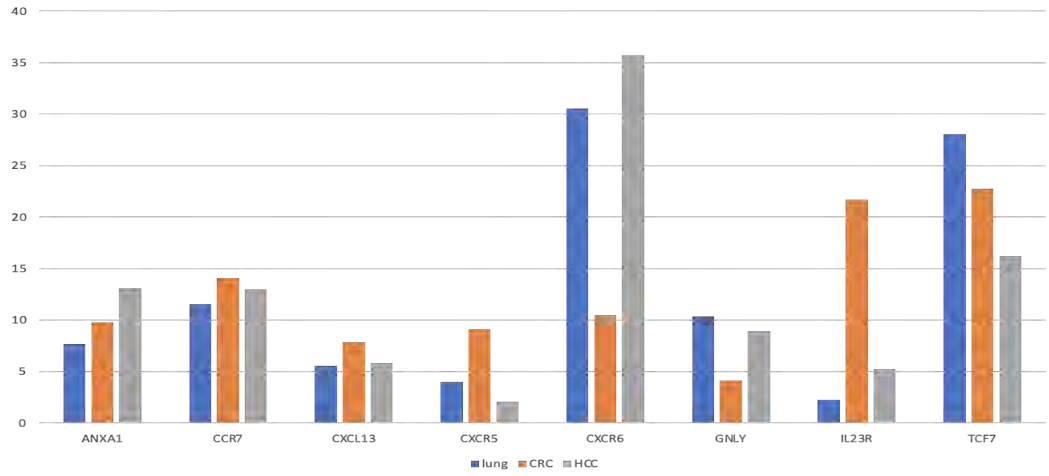

We identified 8 subtypes of CD4 T-cells from this study among 3 cancer types. Each subtype is present in all three types of cancers, but their percentages in different cancers are distinct. The resulting data shows that in lung and liver(HCC) cancers, the CXCR6 subtype of CD4 T-cells showed the highest presence percentage, and colon cancer (CRC) had the highest presence percentage of TCF7 CD4 T-cells.

Discussion

In order to determine the efficacy of immunotherapy and specifically CD4 T-cell subsets, we mainly want to discover the percentages of CD4 T-cell subset presence in each type of cancer. This way we have a better understanding of immunotherapy treatment of cancer and how to battle it.

N^6-methyladenosine (m^6A) Modification Regulates Kaposi's Sarcoma-associated Herpesvirus (KSHV) Lytic Replication

Scholar: Catherine M. Maldia

High School/College/City/State: North Allegheny High School, Wexford, Pennsylvania

PI of group/lab: Dr. Shou-Jiang Gao, PhD

Mentor(s): Dr. Wen Meng, PhD

Site: Cancer Biology

Background: Kaposi's Sarcoma-Associated Herpesvirus (KSHV) is an oncogenic virus that causes various malignancies. Like other members of the gamma herpesvirus family, KSHV life cycle has two distinct phases. The latent phase is characterized by persistent infection, restricted viral gene expression and no production of infectious virions while the lytic phase is marked by the expression of viral lytic genes in a cascade fashion and the production of infectious virions. KSHV lytic replication promotes tumorigenesis by spreading infection into other cells and stimulating cell proliferation by autocrine and paracrine effect. KSHV transcripts contain abundant m^6A modifications during latent and lytic replication. Cellular machinery of m^6A includes "writer" methyltransferases, "reader" m^6A binding proteins, and "eraser" methylases. m^6A is involved in all stages of mRNA biogenesis and functions, including pre-mRNA splicing, pri-miRNA processing, mRNA export, mRNA stability, translation modulation and mRNA degradation. The objective of this study is to evaluate the effects of m^6A "eraser" FTO or ALKBH5 inhibitors on KSHV lytic replication.

Methods: iSLK-BAC16-RGB cells, which express RFP, GFP and BFP proteins tracking the expression of viral latent, early lytic and late lytic protein, respectively, were treated with various doses of m^6A "eraser" FTO or ALKBH5 inhibitors (FB23-2, IOX1, C6, C3) under sodium butyrate (NaB) induction of lytic replication. Fluorescent microscopy was used to quantify the number of GFP-positive cells to track KSHV lytic replication.

Results: Cells treated with FTO inhibitor FB23-2 or ALKBH5 inhibitor C6 decreased the number of GFP-positive cells in a dose dependent manner compared to control cells without any inhibitor. The highest concentration of inhibitors used in experiment caused minimal cell toxicity.

Conclusion: FTO inhibition by FB23-2 and ALKBH5 inhibition by C6 could reduce KSHV lytic replication. FTO and ALKBH5 are likely essential for optimal KSHV lytic replication, and FB23-2 and C6 are potential inhibitors for KSHV replication.

Targeting *MET*-altered NSCLC through Inhibiting TWIST1

Scholar: Leviticus McGraw-Sapp

High School/College/City/State: Woodland Hills High School, Churchill, PA

PI of group/lab: Timothy F. Burns, M.D./Ph.D

Mentor(s): Timothy F Burns, M.D./Ph.D., Vinod Kumar, Ph.D.

Site: Cancer Biology

Background: Non-small-cell lung cancer (NSCLC) is the leading cause of cancer-related deaths in the US and worldwide. Patients diagnosed with *MET* amplified (*METamp*) or *MET* exon 14 skipping (*METexΔ14*) mutant NSCLC can be treated with targeting therapy via MET tyrosine kinase inhibitors (TKIs); however, such treatments are eventually rendered ineffective due to *de novo* or acquired resistance induced by the presence of the epithelial-mesenchymal transition (EMT) transcription factor, TWIST1. We previously discovered that TWIST1 is required for oncogene-driven NSCLC, including *MET*-altered NSCLC. Moreover, targeting TWIST1 via genetic silencing or treatment with the TWIST1 inhibitor, harmine, can elicit increased sensitivity to EGFR TKIs and possibly MET TKIs.

Hypothesis: Inhibiting TWIST1 will sensitize MET TKI insensitive *MET*-altered NSCLC to MET TKIs by inducing cellular senescence and/or apoptosis.

Method: The *METexΔ14* mutant NSCLC cell lines, H596 and H1437, and *METamp* cell lines, H1648 and H1993, were treated with increasing concentrations of harmine. MTS assays were conducted to measure cell viability and cytotoxicity at early and late time points. Colony formation assays were used to determine if harmine deprived cancer of its colony-forming property. SA-β-galactosidase staining was performed utilizing the Senescence β-Galactosidase Staining Kit from Cell Signaling Technology.

Results: Harmine had increased cytotoxicity with time after treatment with a significant leftward shift in the half maximal inhibitory concentration (IC50) at later time points. This increased sensitivity was accompanied by evidence of senescence at later time points.

Conclusion: Pharmacologic inhibition of TWIST1 was effective in *MET*-altered NSCLC cell lines with reduced sensitivity to MET TKIs. In addition, the enhanced-delayed cytotoxicity observed may be mediated by reactivation of oncogene-induced senescence. Our current and future directions include determining 1) whether senescence is required for the enhanced-delayed response across cell lines, 2) the contribution of apoptosis, 3) whether harmine sensitizes MET TKIs, and 4) if we can develop more potent harmine derivatives.

Title: Development of annotated brain MRI dataset to develop machine learning algorithms for neuroimaging quality control

Scholar: Arya Mehta

High School/College/City/State: North Allegheny Intermediate High School, Pittsburgh, PA

PI of group/lab: Dr. Pradeep Reddy Raamana/Open Minds Lab

Mentor(s): Dr. Pradeep Reddy Raamana

Site: CoSBBI

Abstract: MRI scans are a non-invasive tool to detect brain abnormalities, but their utility is affected by unwanted artefacts. Accurately identifying artefacts is complex, especially for machine learning (ML) algorithms. In this project, I learnt to recognize different MRI artefacts and carefully generated an annotated brain MRI dataset to train ML algorithms.

Introduction: MRI artefacts transpire from different discrepancies. Experimental errors contain objects that are beyond the confines of an image. During the scan, patient movement inside the machine causes subject motion errors. The interference of [foreign] radio waves result in noise and other hardware issues. Reconstruction errors result from parcellation mistakes during physical analyses. Patterns categorizing the specificity of the artefact through manual ratings can be detected computationally following the development of ML algorithms.

Methods: Manual rating using the program VisualQC grants raters three dimensional cross sections of axial, sagittal, and coronal views of neuroanatomy. Raters adjust the illumination of each individual scan to better review regions of interest. Comparing slices within orientations of alike or differing views highlights the appearance of artefacts, should one be present.

Results: We reviewed a dataset of 216 MRIs from the Amsterdam Open MRI Collection, and found that 90 images were blurry, 29 with ghosting, 2 had motion errors, 169 had a discrepant orientation or field of view, and 42 had ringing artefacts. Only 8 scans appeared to be free of any noticeable artefacts.

Discussion: Accurate rating of these complex artefacts requires further training and practice, but our project has already contributed to improving VisualQC and the guidelines for rating by high-school students like me. On estimate, the first 100 scans were used to become familiarized with the patterns of each artefact for categorization. The completion of this set evaluated the tell-tale signs of each artefact for future analyses, and eventually, an automatic algorithm to detect artefacts.

Title: CtIP Deletion Affects DNA Damage Repair & Hematopoietic Stem Cell Function in Mice

Scholar: Ethan Minzer

High School: Montour High School, McKees Rocks, PA

PI of group/lab: Dr. Wei Du, MD, PhD

Mentors: Neha Atale, PhD & Limei Wu, PhD

Site: Cancer Biology

CtIP is a partner of the MRN DNA damage sensor protein complex, which recognizes double-strand breaks and assists with homologous recombination (HR). Yet the exact function of CtIP, especially in the hematopoietic system, remains contentious. By crossing conditional CtIP knockout (KO) mice with hematopoietic lineage-specific deleter strain Vav1Cre mice, we attempted to obtain hematopoietic-specific CtIP KO mice. However, deletion of CtIP in the hematopoietic system is embryonically lethal. This experiment planned to investigate the impact of CtIP loss in the blood system by using an inducible CtIP knockout model (KO: CtIPco/co CreER) and a "knock-in" CtIP R861K mutant knock-in model (KI: *CtIPKI/KI;Vav1Cre*). Immunofluorescent staining will be used to determine the levels of DNA damage and the efficiency of error-free homologous recombination versus error-prone nonhomologous end joining (NHEJ) in CtIP KO and KI cells. A functional colony forming unit (CFU) assay will be conducted to determine the progenitor activity of the KO and KI cells. Consistent with our observation that hematopoietic CtIP deletion is embryonically lethal, our preliminary studies showed that a standard 5 doses of tamoxifen injections led to substantial death of the KO mice due to pancytopenia. This data suggests that CtIP plays a critical role in hematopoiesis. We are now in the process of optimizing the tamoxifen injection protocol to establish a partial CtIP deletion in the mouse blood system. We will also isolate bone marrow cells from CtIP KI mice for CFU and immunofluorescence analysis.

Reconfigurable Convolutional Neural Networks with Dynamic Channel Depth for Battery Powered Biomedical Devices

Tejas Mitra , Yuyang Li, and Dr. Inhee Lee
Sewickley Academy, Sewickley , PA; University of Pittsburgh Hillman Cancer Center Academy, Pittsburgh, Pennsylvania

Abstract

Biomedical devices have small battery capacity and storage. To implement convolutional neural networks in a biomedical device, we must minimize the amount of mac operations by reducing the amount channels in the network but still trying to maintain accuracy. We found that the lower the performance value, or the FOM, the better the neural network is for the device.

Introduction

Convolution neural networks are a part of deep learning and are used for facial recognition, object detection for self-driving cars, and tumor detection. CNNs apply channels, or filters, to the image and look for certain patterns and features. Biomedical devices have a low amount of storage and battery capacity and if a CNN with a high amount of mac operations is implemented, the device would die in a matter of days and not be useful for the patient. The objective of this study was to improve the original CNN of a biomedical device and minimizing mac operations and maximizing accuracy. Another objective of this study was to also see how the performance score, or FOM, changes with different simulations.

Methods

We used University of Pittsburgh's CRC and VPN to work on the convolutional neural network. The original neural network for this biomedical device had an input of 3 channels and the first layer had 5 channels, the second layer had 10, and the third layer had 20. We would change the amount of channels of the output in one layer and then train and test the model on a CIFAR-10 data set. We would record the best accuracy of the model and calculate the mac operations by calculating the mac operations for each individual layer and then adding the values together. The formula for calculating the mac operations for each layer was: output height * output width * kernel height * kernel width * input # channels * output # channels. The kernel size was always 5 by 5 and the output width and height were always the same. To calculate the performance values we used 2 different formulas:

1. FOM = (alpha * accuracy percentage change)/ mac operations percentage change
2. FOM =(accuracy percentage change^{alpha}) / mac operations percentage change

The mac operations percentage change and the accuracy percentage change were calculated using the accuracy and mac operations for the original neural network, 72.51% and 1,260,070 respectively. For calculating the FOM in the first formula, we used an alpha of 10 and for the second formula, the alphas were 1, 3, and 5.

Results

We saw that the lower the FOM was of the neural network, the better the neural network was for the biomedical device. The 3 lowest FOMs with the formula were 0.3058, 0.1146, and -0.8768. The accuracies for these 3 neural networks were 72.17% , 72.04% , and 72.9% respectively. The mac operations of these neural networks decreased with the FOMs. The last one was negative because it was better than the original neural network with an accuracy better than 72.51% and less mac operations than 1, 260, 070.

Discussion

These results show that we can decrease the amount of channels in the Conv 2 and Conv 3 layers while not losing a substantial amount from accuracy but still decreasing the mac operations for the proposed device. In the future, an adaptive CNN can be created using these neural networks that were found throughout the study. The adaptive CNN can calculate the battery capacity left on the device and pick a neural network to use to save battery.

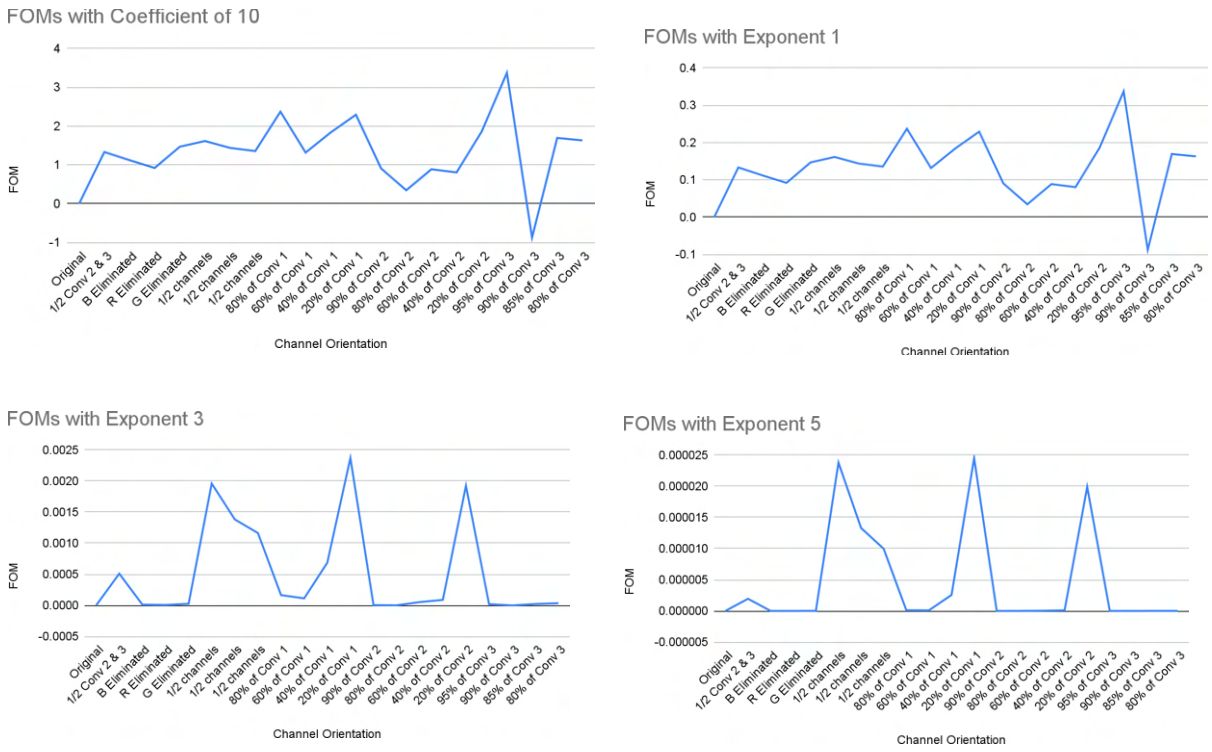

Figure 1 Graphs for all the FOMs with FOMs for the y axis and orientation of the channels for x axis

Tracking the Development of Menopause-Induced Sarcopenia during Female Muscle Aging

Scholar: Tabo Mkandawire

High School: North Allegheny Senior High School, Wexford, PA

PI of Lab: Dr. Fabrisia Ambrosio

Mentors: Dr. Zachary Hettinger, Gabrielle Gilmer

Site: Tech Drive X

Background: Aging and the coinciding decline of physiological functions affect several body systems. In the muscular system, this manifests as sarcopenia, the age-related deterioration of skeletal muscle. Nearly three-quarters of postmenopausal women report muscle aches and pains; however, the most commonly utilized animal models (i.e., rodents) do not display a menopausal phenotype. Consequently, little is known about the mechanisms underlying menopausal effects on muscle nor the time course upon which this happens. **Purpose:** This study tracks metrics of sarcopenia, as defined by muscle fiber size, connective tissue infiltration, and fat content, throughout perimenopause and menopause. **Methods:** Menopause was chemically induced via vinylcyclohexene diepoxide (VCD) intraperitoneal injections. Middle-aged (14-16 mo.) female C57/BL6 mice were injected with either VCD (160 mg/kg/day) in sesame oil (menopause) or sesame oil (non-menopause) for 10 days. Muscles were collected at five timepoints: start and middle of perimenopause, end of perimenopause/start of menopause, and middle and late menopause. Tibialis anterior and gastrocnemius muscles were cryopreserved and sectioned for immunohistochemistry. Sections were either immunoreacted with anti-laminin and anti-collagen I antibodies or stained with Oil Red O (ORO). **Anticipated Results:** We hypothesize that the onset of menopause will bring about a decrease in cross-sectional area (CSA) and a corresponding increase in connective tissue and fat infiltration. To test this hypothesis, automated image analysis software will be used. Muscle size will be quantified via area within laminin-outlined muscle cells. Connective tissue and fat infiltration will be quantified via area of collagen I and ORO per muscle cell, respectively. **Impact:** By defining the onset of menopause-induced sarcopenia, the timing of intervention, such as hormone therapy, can be determined. These results could ultimately extend postmenopausal women's healthspan and promote a higher quality of life.

Effects of Regorafenib and BETd-260 on Colorectal Cancer Cells

Audrey Monro-Neely

Avonworth High School, Pittsburgh, PA

PI: Lin Zhang

Mentor: Suisui Hao, Ermine Kaylee

Site: Hillman Cancer Center

Abstract

Colorectal cancer (CRC) is the second leading cause of cancer-related deaths among men and women in the United States. Bromodomain and extra-terminal domain (BET) proteins are epigenetic readers that regulate gene expression and are involved in cancer pathogenesis. Over the last several years, BET inhibitors have been developed and clinically tested, but showed limited effects in solid tumors. Besides, the molecular mechanisms by which cancer cells respond to BET inhibition are not fully understood. In this study, we found that a combination of BET degrader-260, a compound designed and synthesized by conjugating a BET inhibitor to an E3 ubiquitin ligase binder through a flexible linker, and regorafenib, a multi-kinase inhibitor that is used in the therapy of refractory metastatic colorectal cancer, could suppress the growth of HCT116 colon cancer cells efficiently, compared to regorafenib or BETd-260 alone. Flow cytometry analysis of Annexin V/PI staining showed that Annexin V and Annexin V/PI double positive cells increased almost 2 fold in combination group in comparison to BETd-260 or regorafenib treatment group. Western blot analysis revealed that BETd-260 combined with regorafenib transcriptionally activates p53/PUMA/caspase3 pathway to trigger apoptosis in HCT116 cells. Knockdown of PUMA by siRNA could significantly block apoptosis, especially in the combination group. Furthermore, caspase inhibition by z-VAD-fmk (Z-VAD) could markedly rescue apoptosis in the combination treatment group, although this was also observed in BETd-260 or regorafenib treatment group. These results provide a rationale, mechanistic insights, and potential biomarkers for developing a precision CRC therapy by inducing BET protein degradation.

Understanding the effects of COVID-19 on Scientific Collaboration Networks

Iliyan Nazarali, Swapnil Keshari, and Dr. Jishnu Das
Chestatee High School, Gainesville, Ga; University of Pittsburgh, Pittsburgh, PA

Abstract

To understand the impact of COVID-19 pandemic on the scientific community, I analyzed the changes in authorship and publications between three phases: pre-pandemic year 2019, pandemic year 2020, and post-pandemic year 2021. Each author and collaboration is represented as a node and edge in a network. Using python pandas and networkx, I was able to find important findings: various centralities measures, consortiums, and many high population inter-continent collaborations decreased.

Introduction

As a result of COVID-19, there was limited access to in-person interaction while communication across virtual platforms increased. It is unknown how the scientific community and publications were affected. We wanted to understand how collaborations in the scientific community were impacted by COVID-19 through three years or phases by applying network science. Network science is a mechanism through which we can represent and understand real-world interactions[1]. Modeling the relationship between authors and publications as a network provides insight into the changes in collaboration or connectivity in the network. This is accomplished by measuring node's authority and hub score, betweenness centrality, and degree centrality for the authors in our data for each of the three years. We are able to discern the number of authors in each of the author's collaboration circles using hub and authority score. Authors that bring together a multitude of other authors increase the connectivity of a network and have a high betweenness centrality. Authors that have a high number of collaborations have a high degree centrality[2]. In order to understand how consortiums and standalone, high-publication authors were affected, we visualized the relationship between degree and publication count, characterized authors in these two categories, and observed changes over the three years. We also wanted to understand the impact of COVID-19 on collaborations through a geographic lense. Thus, we calculated inter and intra wise continent collaborations to understand changes for each continent across the three years.

Methods

To understand the changes in authorship and collaboration between pre-pandemic, pandemic, and post-pandemic years, we collected the author and author's collaborators' information for 2019, 2020, and 2021.This data consisted of scientific publications between each pair of authors who collaborated together from a list ~16000 papers from ~100 journals including all major Nature (NPG), Science (AAAS), Cell Press (Elsevier), and PLOS journals, generating an co-authorship network for each of the years 2019, 2020, and 2021. To analyze the changes in connectivity in the network, we calculated hub centrality using the hyperlink-induced topic search (HITS) function as well as degree centrality and betweenness centrality using networkx for 2019, 2020, and 2021. To examine geographic changes in collaborations, I mapped each country to its continent and calculated inter and intra wise counts for each continent for 2019, 2020, and 2021.

Results

Throughout the course of the pandemic, the betweenness, hub, and degree centralities had decreased, indicating connectivity between authors have decreased. The 2020 publication co-author scatterplot, in comparison to 2019 and 2021 scatterplots, has decreased numbers of high co-author low publication papers, or consortiums (Figure 4). Inter-continent collaborations of Asia, North America, Europe, and Africa decreased across all three years. Inter-continent collaborations of South America increased in 2019-2020 and decreased in 2021. Inter-continent collaborations of Oceania decreased in 2019-2020 but increased after 2021 (Figure 2).

Discussion

The centralities decreased most likely due to the unexpected nature of the pandemic, resulting in decreased collaborations and connectivity. All the inter-wise continent collaborations decreased in 2020 except for South America, which may have resulted due to more ease in moving to virtual platforms. Further research for 2022 could be conducted to see whether these findings are consistent as well as repeating the analysis with journals in other fields other than biology-related research.

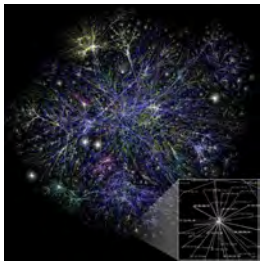

Figure 1: Partial map of the Internet based on the January 15, 2005 modeling a real world network[3]

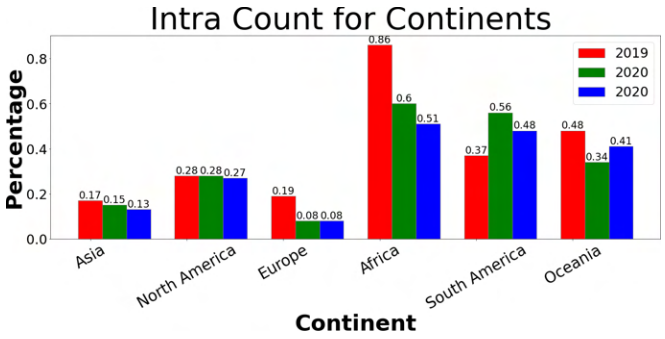

Figure 2: Percentage of edges of a network developed by our data that took part in inter-continent collaborations for each continent for 2019, 2020, and 2021

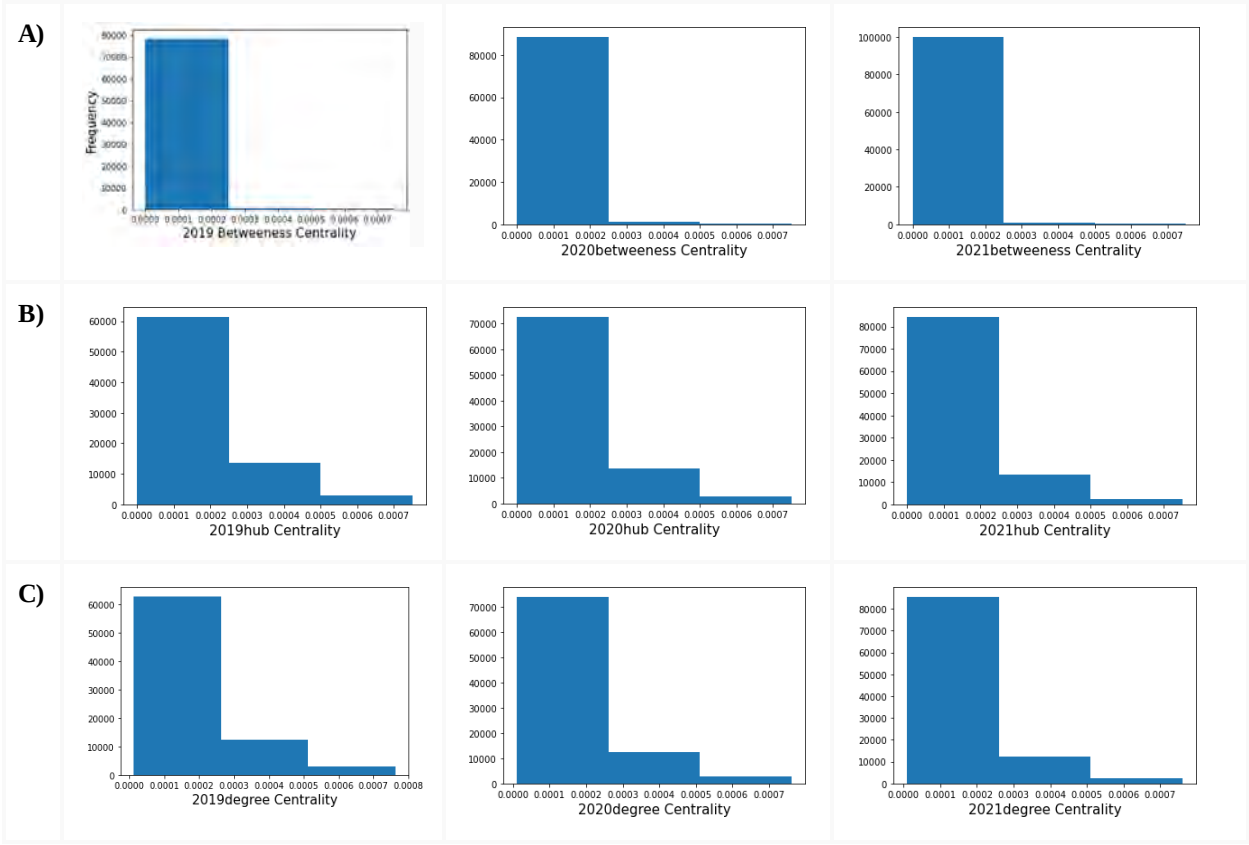

Figure 3: Distribution of centrality measures for 2019, 2020, and 2021 of a network developed by our data A) betweenness centrality B) hub centrality C) degree centrality

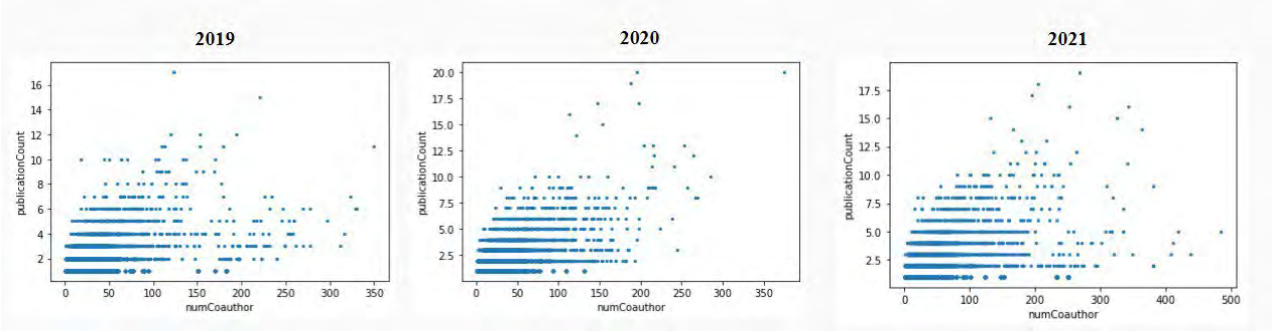

Figure 4: Scatterplot of authors based on number of coauthors and publication count for 2019, 2020, and 2021

References

1) Barabási Albert-László, Pósfai Márton.*Network Science*.Cambridge, United Kingdom: Cambridge University Press;2017.
2) Bikey Bonn Kleiford Seranilla. *Analysis on Collaboration and Co-Authorship Network Using Centrality Measures*. YouTube; 2020. https://www.youtube.com/watch?v=OYoCcFzewy8. Accessed July 27, 2022.
3) File:internet map 1024.jpg.*Wikipedia*.https://en.wikipedia.org/wiki/File:Internet_map_1024.jpg. Accessed July 31, 2022.

Morphometric Analysis of Normal Female Pelvic Anatomy Across Race in Young Adult Women

Anyssa R. Oden, High School Diploma[1], Shaniel T. Bowen, MS[2]
[1]University of Pittsburgh Hillman Cancer Center Academy, Pittsburgh, PA; [2]University of Pittsburgh, Pittsburgh, PA

Abstract

Current morphometric characterizations and analyses of Normal Female Pelvic Anatomy are based on clinical images of white women. However, having a diverse demographic as the basis for Female Pelvic morphometric analysis is important in establishing an inclusive "normal" for reference during restorative surgeries of Pelvic Organ Prolapse. This study uses MRIs from Young Adult Black and White women to compare morphometric features and determine if there are racial differences in the Pelvic Anatomy of these two groups.

Introduction

Pelvic Organ Prolapse is a Pelvic Floor Disorder characterized by weakened pelvic floor muscles, resulting in the displacement of the pelvic organs (i.e vagina, urethra, bladder, uterus, or rectum) from their "normal" positions. Approximately 1 in 10 women will undergo surgery for a pelvic floor disorder in their lifetime [1]. Up to 15% of the annually reported POP surgeries in the US will fail after 2 years [2] and nearly 12% will require another after 5 years [3]. Restoration of the pelvic floor muscles and vagina are believed to be vital for a successful POP surgery, yet there is no medically established norm for female pelvic anatomy. Additionally, these surgeries are known to cause alterations to patients' normal anatomical shapes and positions, hypothetically increasing the risk of further injury. Morphometric analysis provides a reliable 3D visualization and quantitative description of female pelvic anatomy. Unfortunately, there are little to no inclusive, comprehensive studies using this methodology for normal female pelvic anatomy and pelvic organ prolapse. Therefore, the purpose of this study is to compare the morphometry and shape variation of the vagina, clitoris, and urethra with respect to race in order to establish a standard for the characteristics of normal female pelvic anatomy across a diverse demographic of patients.

Methods

MRIs of anatomically normal patients were collected from the University of Alabama at Birmingham and UPMC Magee Womens' Hospital and de-identified by the Principal Investigator, Dr. Pamela Moalli, before co-investigators received them. Utilizing Slicer [4] and T2 axial scans from the MRIs, the urethra, vagina, and clitoris were segmented from the rest of the body tissue. Next, the auto generated 3D models based on the segmented pelvic organs were exported to Blender [5]. Geometries were remeshed and a smooth laplacian modifier was added for smoothing. The resulting stl files were imported into a Mathematica[6] code developed by Bowen to obtain morphometric measurements.. This was repeated for all 46 patients in the Young Adult (18-34 years) age range. Next, the mean and standard deviation were obtained for each morphometric measure in both groups. Using SPSS Statistics [7], an independent t-test was performed to compare measurements between young adult black and white women at a significance level of 0.05.

Results

Using the above methods, statistically significant (<0.05) differences in morphometric measurements were found in all focus pelvic organs between races. Figure 1 shows the Vaginal Apex Position X and Vaginal Position X which were found to be closer to Black patients' midline, while their Vaginal Position Y was more posterior. Also, their Upper Vagina Deviation Angle (Figure 2) was closer to 0° (straighter upper vagina). Figure 3 depicts the measurements for the Urethral Axis –Z-Axis Sagittal Angle and Mid-Urethra Centroid Y – angled posteriorly – and the Distal Urethra Centroid Y – angled anteriorly – also for the Black female patients. Lastly, multiple differences were found between the racial groups in the clitoral morphometry, depicted in Figure 4. For example, black women had an overall smaller clitoral anatomy, whereas their Clitoral distances like Crura-Vagina, Body-Vagina, Glans-Mid Urethra, and Vagina-Mid Urethra were all longer than the White group. All Figures were provided by Bowen.

Discussion

In this study, we successfully obtained morphometric measures and found significant differences in the normal position, shape, and size of the pelvic organs across races for this young adult sample of patients. The results suggest that race impacts the morphometry of the clitoris, vagina, and urethra; organs that are vital for normal gynecologic function. Black women could be at a higher risk for POP surgery failure due to surgeons' definition of "normal anatomy" revolving around white female patients. The results demonstrated the necessity of more studies on normal female pelvic anatomy, as well as the need for a diverse demographic of patients as the subjects for further translational research. Future research will be conducted with larger samples of patients with the same amount of diversity across older age groups for more comprehensive results.

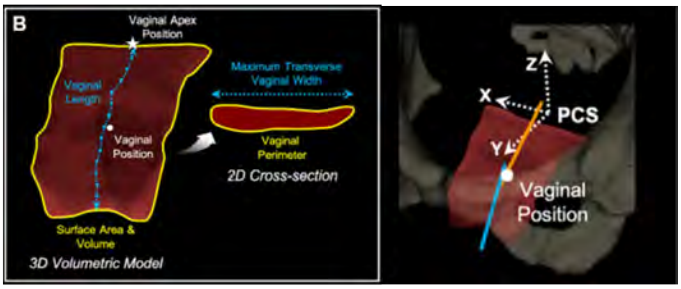

Figure 1. Visualization of morphometric measures taken from 3D reconstructions of the vagina.

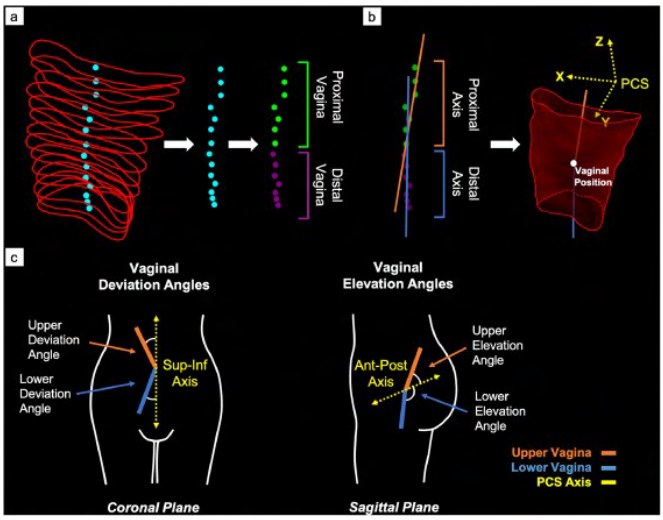

Figure 2 (Left). A and B) Another 3D depiction of how measurements are taken from the vagina. Splitting the vagina into its upper and lower parts makes it easier to find its multiple angles. **C)** Coronal and Sagittal views of how the separation of the vagina in Figure 2B is used to quantitatively characterize the proximal and distal deviation and elevation angles.

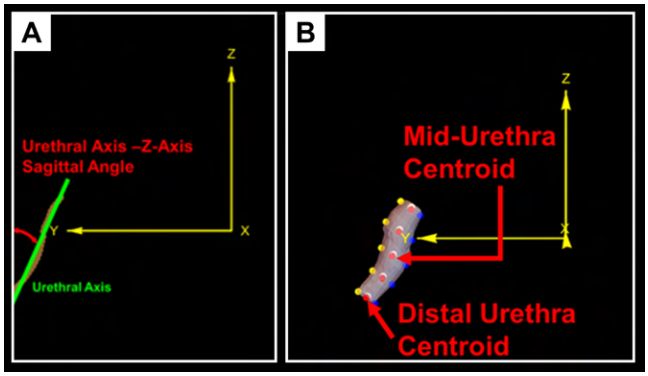

Figure 3 (Right). A)

Image of the Urethral Axis (in green) which is the overall slope of the urethra. **B)** Image of the points (red) that are considered the Distal Urethra Centroid (point at the middle end of the urethra) and Mid-Urethra Centroid (absolute center of the urethra).

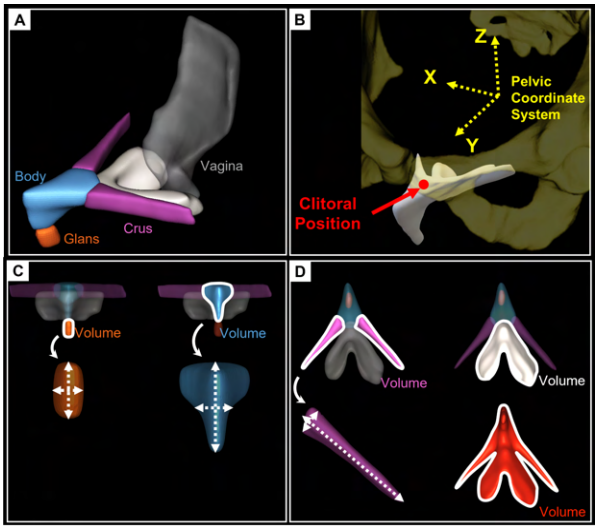

Figure 4 (Left). A) Anatomy of the clitoris which is broken into different parts to make morphometric analysis easier. **B)** Depicts the position of the clitoris in relation to the pubic bone and inside the pelvic region. **C and D)** How volume is determined for each part of the clitoris individually.

References

1. Wu JM, Vaughan CP, Goode PS, Redden DT, Burgio KL, Richter HE, et al. Prevalence and trends of symptomatic pelvic floor disorders in U.S. women. Obstet Gynecol. 2014a;123(1):141–8.
2. Barber, M. D., Brubaker, L., Burgio, K. L., Richter, H. E., Nygaard, I., Weidner, A. C., … Meikle, S. F. (2014). Comparison of 2 transvaginal surgical approaches and perioperative behavioral therapy for apical vaginal prolapse: The OPTIMAL randomized trial. *JAMA - Journal of the American Medical Association*, *311*(10), 1023–1034. https://doi.org/10.1001/jama.2014.1719
3. Jelovsek, J. E., Barber, M. D., Norton, P., Brubaker, L., Gantz, M., Richter, H. E., … Meikle, S. (2018). Effect of uterosacral ligament suspension vs sacrospinous ligament fixation with or without perioperative behavioral therapy for pelvic organ vaginal prolapse on surgical outcomes and prolapse symptoms at 5 years in the OPTIMAL randomized clinical trial. *JAMA - Journal of the American Medical Association*, *319*(15), 1554–1565. https://doi.org/10.1001/jama.2018.2827
4. Fedorov A., Beichel R., Kalpathy-Cramer J., Finet J., Fillion-Robin J-C., Pujol S., Bauer C., Jennings D., Fennessy F.M., Sonka M., Buatti J., Aylward S.R., Miller J.V., Pieper S., Kikinis R. 3D Slicer as an Image Computing Platform for the Quantitative Imaging Network. Magnetic Resonance Imaging. 2012 Nov;30(9):1323-41. PMID: 22770690. PMCID: PMC3466397.
5. Blender.org
6. Wolfram Research Inc. (2022). Mathematica for Macintosh (Version 13.1). Accessed through University of Pittsburgh Software Download.
7. IBM Corp. (2021). IBM SPSS Statistics for Macintosh (Version 28.0). Accessed through University of Pittsburgh Software Download.

A study of single cell RNAseq annotation using different methods

Scholar: Olutoba Ojo

High School: Newark Charter School, Newark, Delaware

Lab: Dr. Uma Chandran

Mentor: Alex Chang

Site: Biomedical Informatics

Background: All living systems are composed of cells, which contain crucial RNA molecules with important information and processes. In identifying and quantifying the expression levels of RNAs within a cell, by technologies such as RNA sequencing, scientists can infer the identity of a cell.

Single cell RNA sequencing, or scRNAseq, is a newer method that enables scientists to quantify the RNAs in individual cells and therefore infer more accurate identities for the cells in a sample. It enables scientists to deeper understand the complexity of cell types. In order to infer cell types as accurately as possible, the utilization of computational methods is essential. For this study, mouse motor cortex cell data is annotated utilizing three different annotation tools

Methods: Single cell RNAseq mouse motor cortex data was retrieved from the PanglaoDB database and annotated utilizing three computational methods: Azimuth, SingleR, and ScType. In contrast to the Azimuth method, SingleR and ScType required the normalization of data as a step prior to running completely. All three tools utilized the same reference mouse motor cortex file (SRS1915206) retrieved from the PanglaoDB database.

Results: Azimuth used an annotated mouse motor cortex reference as a basis for mapping, and outputted two plots visualizing celltype prediction. SingleR used reference transcriptomic datasets of pure cells for its annotation, and outputted a heatmap graph distinguishing the varying levels of expression among cell types, as well as a violin plot visualizing the distribution of cell type expression. ScType used a combinations from its cell marker database, and outputted a cluster graph of cell types, and a mapping classification graph

Conclusion: Based on our cell type annotation study, we are able to conclude that the usage of various computational annotation methods can directly lead to differing interpretations of data

Missense Variants: pathogenic or neutral

Scholar: Oluwatobiloba Olaore

High School: Pittsburgh Creative and Performing Arts

Lab: Ivet Bahar, PhD

Mentor: Anupam Banerjee

Site: Computational Biology

Background: Single-nucleotide polymorphisms are single DNA base pair changes: either germline variants or somatic variants. This can lead to the translation of a gene codon into a different amino acid than the wild type. Single amino acid variants (SAVs) are the most abundant form of known genetic variations associated with human disease. These genetic variations are important to study because by determining which missense variants (SAVs) are pathogenic or neutral, scientists can possibly use this information to discover a drug that can pair to the mutation and reverse the pathogenic effects. This research studies whether we can build a machine learning model that can accurately predict the pathogenicity of missense variants.

Methods: Using a data set of 20,312 single-amino acid variants that have already been determined pathogenic or neutral, we coded the hydrophobicity level, molecular weight, and BLOSUM62 score Then taking this information, we used the machine learning models K-Nearest Neighbor, Decision Trees, and Random forest, to create a model that will accurately sort and predict the pathogenicity of missense variants. To check the models, we used a 10-fold cross validation to check the accuracy, recall, and precision.

Results: With the machine learning models created, we got results in the form of accuracy, recall, and precision scores; the results go as follows: we got an accuracy score of 0.7, a recall score of 0.93, and a precision score of 0.713.

Conclusion: The research conducted shows that hydrophobicity levels, molecular weight, and BLOSUM62 scores can be used to determine the pathogenicity of single-amino acid variants. This is significant because these features can be coded from such variants and applied without much context.

Future Directions: Further research in this field can later on be of assistance to scientists and doctors; by determining which single-amino acid variants lead to pathogenic consequences, scientists can discover potential drugs and cures to illnesses.

PARL (Presenilins-associated rhomboid-like protein) inhibitor impairs mitochondria function and causes necrosis in cancer cells

Scholar: Oluwatomisin Olaore

College: Pennsylvania State University, University Park Pennsylvania

Lab: Dr. Yuan Liu

Mentor: Qing Cao

Site: Drug discovery

Background:

PINK1 (PTEN-induced putative kinase 1) is a mitochondrial kinase, performing an important role in mitochondrial quality control. Under healthy condition, PINK1 is imported into mitochondria and cleaved by mitochondrial proteases including PARL. This generates a 52-kDa PINK1 fragment, which will be further degraded by proteasome in the cytosol. However, in response to mitochondrial damage, the import of PINK1 will be closed, causing the accumulation of full-length PINK1 on the mitochondrial outer membrane and activating the downstream mitophagy pathway to remove damaged mitochondria. Overexpression of PINK level has been shown to protect neuron cells from oxidative damage in vitro. In this study, we identified mitochondrial protease PARL inhibitor that elevated Pink1 fragment level, but aggravated mitochondria damage induced by mitochondrial stressors. Also, we identified that inhibiting human PARL resulted in cancer cell death in a necrosis-dependent pathway.

Methods: Cellular Thermal shift assay (CETSA) was used to test the interaction between hit compounds and human PARL protein. Mitochondrial superoxide staining assay was used to examine the mitochondrial oxidative stress damage induced by CCCP or compounds. CellTiter-Glo 2.0 assay was used to evaluate the proliferation of cancer cells with dose-course and time-course compounds treatment. Annexin V apoptosis and Necrosis assay were used to determine the pathway of cell death.

Results: The human PARL protein demonstrated resistance to heat-induced protein denaturation with compound 8 treatment compared to DMSO treatment in HEK293 cell-based CETSA. PARL inhibitor pre-treatment further increased the production of mitochondrial superoxide induced by CCCP in Beas-2B cells. Compound treatment inhibited the proliferation of several cancer cells through necrotic pathway.

Conclusion: Our study discovered novel inhibitors of human PARL protein and revealed that inhibiting PARL impairs mitochondrial function and leads to the necrotic cell death in cancer cells. Further, we need to evaluate the downstream signaling pathway involving in necrosis.

The Differentiation of T-Cell Receptors by their Viabilities and the Sensitization of Target Leukemia Cells with the usage of IFN-γ

Scholar: Lea Omer

High School: Chartiers Valley High School, Bridgeville Pennsylvania

Lab: Dr. Sawa Ito, M.D., PhD

Mentor: Shirley Chang, Sawa Ito, Jui-en Ray Lee, Biswas Nepuane, and Kedwin Ventura

Site: Immunology and Cancer Immunotherapy

Background: Leukemia is a cancer of the blood characterized by the overproduction of mutated leukocytes. Stem cell transplant is the treatment that is focused on in the presentation, however, about 58% of patients die of a recurrence of leukemia post-transplant. To combat this issue, introducing ways to sensitize target leukemia cells is necessary. The protein CD69 acts as an activation marker for T-cells as well as IL-2. Both CD69 and IL-2 are presented when a T-cell receptor is with target leukemia cells. The amount of IL-2 and CD69 determines the affinity of the T-cell receptor. By priming the target leukemia cells with IFN-γ it is believed that the reaction of the T-cell receptor will be enhanced resulting in higher immunogenicity and a stronger immune cell reaction.

Methods: An Enzyme-Linked Immunosorbent Spot was used to determine the presence of IL-2 and CD69. The first test's goal was to identify if TCR 12 or TCR 539 had a higher affinity. There was a positive control PMA. The second ELISpot tested the effects of IFN-γ target cell sensitization for HA-1 T-cell receptor recognition and activation. The TCR with the highest affinity was used. There were alternating columns of target cells with target cells (+) IFN-γ.

Results: The first ELISpot proved that TCR 539 had a higher affinity on target cells than TCR 12. IFN-γ at a concentration of 1μg per mL increased the immunogenicity with THP-1 but did not seem to have a large effect on T2. Increasing the IFN-γ concentration cannot be done in the clinical setting.

Conclusion: The study proves that IFN-γ may be used to sensitize target leukemia cells to allow for better activation and initiation of an anti-cancer immune response. More information can be gathered from the clinical trial found online by searching NCT04628338.

Isolation and Characterization of Porcine Optic Nerve Head Astrocytes and Lamina Cribrosa Cells

Scholar: Arnav Patel

High School: North Allegheny Senior High, McCandless Pennsylvania

Lab PI: Jonathan Vande Geest, PhD

Mentors: Gabrielle Willson, Remi Shittu, Katarina Martinet, Ali Behrangzade

Site: Technology Drive

Background: Primary open-angle glaucoma (POAG) is a disease that causes gradual vision loss and is associated with intraocular pressure (IOP). The optic nerve head (ONH) contains more than a million retinal ganglion cells (RGC) which allows for sight. RGC transform visual information from the retinas to the brain. ONH contains the lamina cribrosa (LC), the primary site of injury in POAG. The LC yields two major cell types, ONH astrocytes and LC cells which synthesize extracellular matrix proteins to support and maintain the LC. As such, RGC, ONH astrocytes, and LC cells are needed to understand the mechanisms of POAG.

Methods: The LC was isolated from porcine eyes post-mortem. For LC isolation, the globe was cut at the equator. The vitreous, lens, and choroid were removed, the sclera was trimmed leaving the optic nerve and the lamina was isolated from the optic nerve using a 1mm biopsy punch. The LC explant was cultured in media to promote the growth of LC cells and ONH astrocytes. Cells of interest were preliminarily identified based on their morphology and passaged at 80% confluency. The cells were stained with GFAP and α-SMA. Six well plates were fully stained with each antibody and mounted with 4′,6-diamidino-2-phenylindole (DAPI), and six were left as a control group. Culture plates were imaged with an eclipse 90I microscope.

Results: Porcine ONH astrocytes are star-shaped while LC cells are elongated in shape. Similarly, they are glial fibrillary acidic protein (GFAP) positive and alpha-smooth muscle actin (α-SMA) positive respectively.

Conclusion: Our study allows for a straightforward technique to isolate both ONH astrocytes and LC cell types from a single dissected porcine ONH. Further studies will confirm this technique and will be able to use both cell types to conclude more tests.

Sources:

Tovar-Vidales, T., Clark, A. F., & Lopez, N. N. (2020, June 6). *Isolation and Characterization of Human Optic Nerve Head Astrocytes and Lamina Cribrosa Cells.* NIH. https://doi.org/10.1016/j.exer.2020.108103

Functional causal models for gene regulatory network inference in single cells

Name: Neil Porwal

Education: North Allegheny High School, Wexford, Pennsylvania

Mentors: Tyler Lovelace and Minxue Jia

Site: Computational Biology

Background: Casual networks can be used to test drug therapies, which is largely impaired because of regulations and restrictions prohibiting human trials. Furthermore, a very detailed simulation of genes' expression and interactions would allow for in-depth research.

Question: Can linear functional causal models, models that infer cause and effect relationships based on one cause directly affecting one effect, be used to infer gene regulatory interactions from observational single-cell data?

Methods: We are using Poisson distribution to represent gene expression and predict gene counts from sc-RNA-seq data. We are then modifying independent component analysis (ICA), breaking up a stream of data with multiple variables into singular components so that it can be applied to the Poisson distribution. We check the ICA's accuracy by getting its F1 score and finding the Amari distance between the mixing matrix, which is the matrix ICA attempts to recover, and the matrix of ICA components. We finally will run a modified LiNGAM program, a model that finds casual relationships in gene regulatory networks, on the independent components generated from the modified ICA to develop a causal model.

Results: Our modified ICA has more accurately recovered the mixing matrix as seen through an increased F1 score and decreased amari distance, allowing for a more accurate prediction of casual relationships between genes.

Conclusions: Functional casual models are a promising method for inferring gene regulatory interactions. Further optimization will result in models capable of allowing in depth study of gene interactions and the development of drug therapies through computational means.

Predicting postoperative lung cancer recurrence and survival using Cox proportional hazards regression and machine learning

Lucy Pu[1,2], Rajeev Dhupar, MD, MBA[3]
[1]North Allegheny Senior High School, Wexford, PA
[2]University of Pittsburgh Hillman Cancer Center Academy, Pittsburgh, PA
[3]Department of Cardiothoracic Surgery, University of Pittsburgh School of Medicine, Pittsburgh, PA

Abstract: *Surgery remains the optimal curative treatment for early-stage lung cancer. Unfortunately, recurrence rate after surgery is unacceptably high (30%–50%). When it comes back, lung cancer has often metastasized to brain, liver, or bones, and chances for a cure are slim. We used Cox proportional hazard regression analysis and machine learning methods to unveil risk factors associated with lung cancer recurrence. The goal is to personalize surveillance strategies and thus minimize lung cancer recurrence.*

Introduction: Available studies investigating the mechanisms of lung cancer recurrence have primarily focused on patient factors, the molecular or genetic characteristics of tumors, staging, and perioperative factors. Despite some progress, it remains elusive to accurately predict likelihood and timing of recurrence. While clinicians have some sense of the likelihood that a cancer may return based on pathologic staging and other characteristics of the cancer, overall it is not personalized medicine. We propose a different approach to predict postoperative recurrence by identifying novel image biomarkers from preoperative chest CT scans. The objective is to improve our ability to predict the likelihood and time of a seemingly "cured" cancer to come back and facilitate personalized surveillance of lung cancer recurrence.

Methods: A cohort of 309 patients were selected from 512 non-small cell lung cancer patients treated with lung resection. Patient demographics, pathological staging, and other clinical information (e.g., sugery method) were collected. Based on pre-treatment chest computed tomography (CT) scans, we computed five different body tissues and ten tumor characteristics. Univariate and multivariate Cox proportional hazard model analyses were used to identify factors that significantly impacted recurrence-free survival (RFS) and overall survival (OS). The associated variables are reported with their p-value and hazard ratios with 95% confidence intervals. A p-value < 0.05 was considered statistically significant. Kaplan-Meier curves of RFS and OS are presented as survival rates versus months after surgery among the different recurrence sites (local/regional versus distant recurrence and recurrence by organ site). Statistical analyses were performed using SPSS 27.0 statistics software. Cox proportional hazards models and three machine learning (ML) models – Support Vector Machine (SVM), Random Forest (RF), and Logistic Regression (LR) – were used to predict lung cancer recurrence in 2- and 5-year after surgery. Five-fold cross-validation was used to validate the performance of the prediction models. Receiver-Operator Characteristic (ROC) curves were used as the performance metrics to assess the performance of the models.

Results: In our cohort, 68.4% of the patients developed recurrence five years after surgery. RFS and OS for local/regional recurrence were significantly longer than those with distant disease ($p<0.05$). Patients with lobectomy surgical procedures are at a lower risk of local/regional recurrence than other types of surgery. Higher TNM staging is an independent factor associated with decreased RFS and OS for distant metastasis, and lymph node involvement is associated with decreased RFS and OS for local/regional metastasis. Interestingly, body composition also contributes to RFS and OS. Tumor characteristics (size, irregularity, pleural area, and ground glass opacity ratio) are associated with RFS and OS. ML-based approaches performed similarly in predicting lung cancer recurrence compared to the Cox regression models with an area under the receiver operative characteristic (ROC) curve (AUC) ranging from 0.75-0.77.

Discussion: Surgical procedure, TNM staging, lymph node involvement, body composition, and tumor characteristics are important determinants of the risk of both local/regional and distant recurrence for RFS and OS. ML-based approaches and Cox models exhibited similar performance. ML-based approaches may be a useful analytic tool for survival prediction in lung cancer recurrence. We are the first group that investigated the impact of body composition on postoperative lung cancer research. We expect that this computer tool could be an important addition to the clinical practice of lung cancer therapy and may improve treatment decision-making for patients, oncologists, and surgeons, ultimately improving patient long-term quality of life.

References

1. Thorsteinsson H, Alexandersson A, Oskarsdottir GN, Skuladottir R, Isaksson HJ, Jonsson S, Gudbjartsson T. Resection rate and outcome of pulmonary resections for non-small-cell lung cancer: a nationwide study from Iceland. J Thorac Oncol. 2012;7(7):1164-9. Epub 2012/05/18. doi: 10.1097/JTO.0b013e318252d022. PubMed PMID: 22592213.
2. Uramoto H, Tanaka F. Recurrence after surgery in patients with NSCLC. Transl Lung Cancer Res. 2014;3(4):242-9. Epub 2015/03/26. doi: 10.3978/j.issn.2218-6751.2013.12.05. PubMed PMID: 25806307; PMCID: PMC4367696.
3. Tolles J, Lewis RJ. Time-to-Event Analysis. JAMA. 2016 Mar 8;315(10):1046-7. doi: 10.1001/jama.2016.1825. PMID: 26954413.
4. Moncada-Torres A, van Maaren MC, Hendriks MP, Siesling S, Geleijnse G. Explainable machine learning can outperform Cox regression predictions and provide insights in breast cancer survival. Sci Rep. 2021 Mar 26;11(1):6968. doi: 10.1038/s41598-021-86327-7. PMID: 33772109; PMCID: PMC7998037.

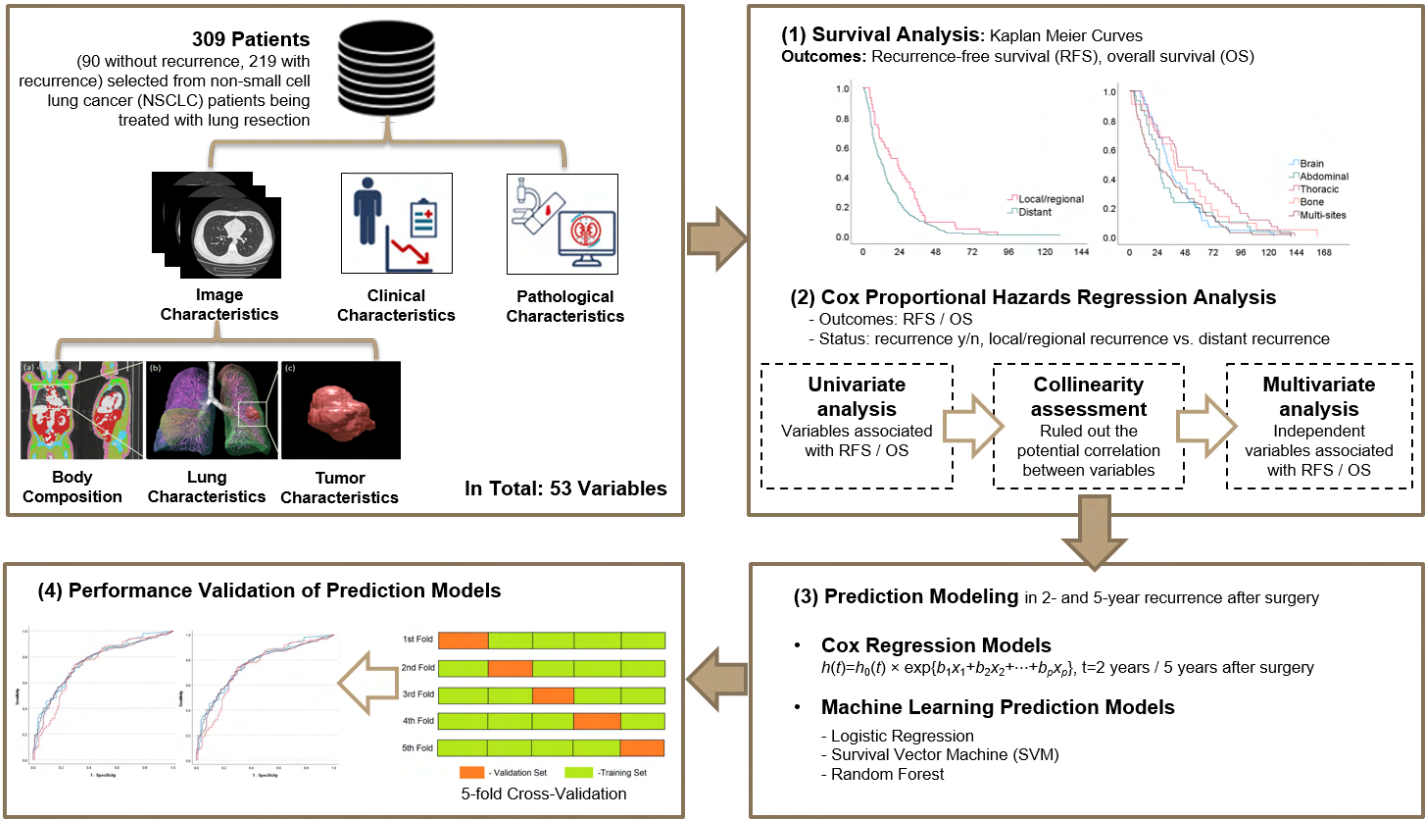

Figure 1. A flowchart showing the study design and its implementation. The key components include (1) cohort creation, (2) body composition and tumor feature computation, (3) time-to-event (or survival) analysis, (4) prediction modeling based on Cox regression model and machinle learning methods, and (5) performance validation.

Effect of Sulforaphane on Expression and Activity of Monoacylglycerol Lipase in Prostate Cancer Cells

Student: Jibraan Rahman
Group: Cancer Biology
Mentor: Dr. Krishna B. Singh
Site: Hillman Cancer Center (Dr. Shivendra V. Singh's lab)

Prostate cancer is the most common cancer in men. About 80-90% of prostate cancers are dependent on the sex hormones androgen at the initial diagnosis. Therefore, hormone/androgen deprivation therapy is often used as a first treatment. However, treatment of castration-resistant prostate cancer (CRPC) resulting from androgen deprivation therapy remains challenging. One of the key features of CRPC is associated with c-Myc mediated alterations of fatty acids metabolism. Prostate cancer cells have shown enhanced lipogenesis together with lipolysis to produce fatty acids that support malignancy. Monoacylglycerol lipase (MAGL) is a key lipolysis enzyme for conversion of monoglycerides into free fatty acids. Therefore, targeting fatty acid metabolic re-programming represents an attractive approach for prevention of prostate cancer. Sulforaphane (SFN) derived from broccoli sprout has shown inhibition of c-Myc expression and fatty acid synthesis and thus inhibit growth of prostate cancer cells *in vitro* and *in vivo*. The present study was designed to identify the correlation of c-Myc and MAGL protein expression in prostate cancer and mechanistic targets of SFN-mediated lipolysis inhibition in prostate cancer. Immunohistochemistry analysis revealed a positive correlation cMyc and MAGL in prostate cancer. In addition to this result, we also observed a positive interaction of SFN with the key residues of MAGL protein, suggesting its role in inhibition of MAGL activity. Western blot analysis revealed inhibition of MAGL protein expression by SFN treatment in PC-3 human prostate cancer cells. Since MAGL is known to be associated with the growth and metastasis of prostate cancer, SFN possibly prevent prostate cancer growth through inhibition of MAGL expression.

Identifying Immune Environment Interactions in Lung Cancer Development

Scholar: Maria Ramos

High School: Germantown Friends School, Philadelphia, PA

Site: Computer Science, Biology, and Biomedical Informatics (CoSBBI)

Mentor: Daniel Yuan, B.S., Joint CMU-Pitt Ph.D. Program in Computational Biology

Lab: Benos Lab, Department of Computational and Systems Biology, University of Pittsburgh, Pittsburgh, PA

Introduction: Lung cancer makes up 25% of all cancer-related deaths, and is one of the leading causes of death worldwide. Therefore, it is important to develop strategies for early detection and prevention for lung cancer. One key component in the development of cancer is the change in the immune environment. Through computational analysis, we investigate lung cancer immunoassay and flow cytometry data in order to determine if there are specific proteins and cell type changes and interactions that can help with uncovering components of the immune environment of lung cancer development.

Methods: The dataset analyzed for this project is from a study that followed high-risk patients, determined by smoking history, over several years. All patients were initially cancer-free. Cancer development status was recorded over the period and patient samples were collected at each screening. High throughput immunoassay and flow cytometry were used to measure immune protein and cell type abundances. The data was analyzed through the rCausalMGM and ssNPA packages developed by the Benos Lab. These computational tools allow researchers to identify directed relationships within the dataset and determine sample subtypes based on deregulation of the interaction network. We also replicated previous results through biostatistical analysis.

Results: - - -

Discussion: - - -

Future Directions: For this specific project, one possible future direction is to collect more information about proteins and cell types to refine the analysis. The identified tumor-associated immune interactions and proteins of this study could be used to help select therapeutic targets for future lung cancer studies.

Correlations Between Aortic Stiffness and Aortic Dissection
By: Narendra Ray, Ronald Fortunato, Spandan Maiti
Education: Canon McMillian High School, Canonsburg, PA
Site: Tech Drive X

Introduction:

Aortic Dissection, caused by a damaged aortic wall, is an acute tear in the aortic tissue that is fatal if not immediately treated. There exist numerous conditions/behaviors that increase the risk of an aortic dissection, such as smoking, age, aortic aneurysms (aortic diameter > 0.4 cm), and strenuous activity [1]. While multiple studies have and continue to be conducted to identify risk factors of aortic dissection, valve morphology continues to be debated. The common belief is that people born with a bicuspid aortic valve (BAV) are at higher risk than those with a healthy tricuspid aortic valve (TAV).

The contribution of this project is to search for possible correlations between aortic stiffness and aortic strength, to see if the stiffness of the aorta may have anything to do with the biomechanical stress that can be applied to the tissue before rupture. These metrics are measured by uniaxial tests on ex-vivo tissue or tissue that has been removed.

Methods

The data is split into three cohorts (TAV, BAV, and CTRL). The provided data set had 7 patients with a healthy Tri-cuspid aortic valve (CTRL), 7 aneurysmal tri-cuspid (TAV), and 7 aneurysmal bi-cuspid (BAV).
The main focus was on uniaxial testing data, and the administration of stress and the strain caused. The tissue was pulled circumferentially (CIRC) and length-wise (LONG) by clamps. A basic NumPy array was utilized within Python to construct a curve of the stress/strain data. Using the curve, the high strain/stretch stiffness was recorded within Prism. From there, statical analysis was performed on the data. T-tests were performed between the direction of the stress, and the correlations between stiffness and strength were tested. Lastly, a linear regression within Prism was also created to better create a more accurate metric.

Results

We found a positive correlation between high stretch stiffness and strength ($r = 0.577$). When separated into CTRL, BAV, and TAV the positive correlation remained (0.447, 0.755, 0.816) respectively. After linear regression, we found we could predict tissue strength by the equation: Strength=(1.585)*stiffness (kPa) + (1187) kPa. However, $R^2=(0.2928)$ suggests too high data variability for the model not to be affected by patient variability.

Conclusions/Discussion

The results provide a better understanding of the relationship between high stretch stiffness and strength. Ultimately, we would like to correlate high stretch stiffness with some in-vivo measured stiffness tool, for example, transthoracic echocardiogram. These results would then elicit dissection risk.

Acknowledgments

Research in this work was supported by the Hillman Academy

References

[1] Hirst, A et al. Medicine 37(3): 217-79, 1958.

Human in the loop cell segmentation method to study Lung Cancer cells and their Epithelial-mesenchymal transition.

Max Revis[1], Dante Poe…[2],

[1] The Potomac School, Mclean, VA, [2] University of Pittsburgh Hillman Cancer Center Academy, Pittsburgh, PA

Abstract:

Epithelial-mesencymal tranistion is very dangerous with cancer cells as it allows the cancer to spread. Image analysis is necessary to study the cancer cells as they take different pathways during the process. Cell segmentation is one of the better forms of image analysis. Cell segmentation is a tedious and time-consuming process that can cost precious time. Cellpose 2.0 allows us to create and train new models for our data and vastly improves cell segmentation

Introduction:

The Epithelial-mesenchymal transition (EMT) cycle is when cells lose their polarity and become invasive and migratory within the body. This is especially dangerous with cancer cells as it allows the cells to spread. Under a microscope you can image the cells during EMT and analyse them through various method. Cell segmentation is a method that allows us to separate each cell in the images and study them from image to image through the process. Manual cell segmentation was slow and tedious and forced the user to create their own model from scratch. Cellpose 2.0 is a new software that uses a machine learning method that is described as human in the loop training. Human in the loop differs from typical cell segmentation as the user trains a new model from a pre-existing one instead of creating a new one. This method allows the researcher to train a model for their own data and then automate the cell segmentation to their own liking, saving lots of time and effort.

Methods:

The lung cancer cells were placed under a microscope and then had photos taken. The images were split up into three channels. Channel 1 was the DIC channel. Channel 2 was the PCNA (cell cycle marker) channel. Finally, channel 3 was the vimentin and cytoskeleton gene channel. To begin to train the models for our images we needed to test which base models in cellpose 2.0's model zoo would be the best bases to train off of. The CP and LC3 models[1] were chosen after testing well on the separate channels individually. The CP model had been trained to segment the outlines of the cells and the LC3 model had been trained to segment the contrast differences between the cells and the bio-markers. Next was the training process of our new models. The training method for both models was the exact same although there were some slight differences in the duration of the training and the channels used. The CP model used all three channels while the LC3 model only used channels 2 and 3. This was because channel one added extra contrast to the image without changing the cell outlines, which would alter the accuracy of the LC3 model. The CP model used all 5 training images before it was performing at the desired accuracy while the LC3 model only took 3 training images before it was performing at a similar accuracy. First, we applied the base model to the first training image. After the base model had finished segmenting the image we altered and fixed any wrong ROIs or any cells that were missed. Then with your altered training image we trained a new model based off our changes. After the computer finishes training the new model you are able to select your trained model in the GUI. Then you can apply the new trained model to the next image, edit the ROIs if necessary and repeat until you believe the model is fully trained.

Results:

For cell segmentation it is difficult to actually quantify the accuracy of the models and the ROIs. But by looking at the images and ROIs you can tell which models are more effective for certain data than others. For the CP model (Figs 1 and 2) there are differences in how the cells are broken up. In fig 1 in the bottom right there is a cell that is split up by multiple ROIs, while in fig 2 it is only 1 ROI. Similar cases can be seen in the LC3 images as well. Seen in Figs 3 and 4 with some cells have 1 ROI in the original model then 2 in the trained model as it was actually two cells in close proximity instead of one. The models after training performed better to our data than the original models did.

Discussion:

The models were successfully trained for the lung cancer cells. This could allow quicker treatment for all cancer cells and help reduce the chances of cancer coming back and/or spreading as the EMT in the cells can be treated quicker and more efficiently. This new cell segmentation saves researcher valuable time and effort and can open up better treatment methods for cancer and other conditions that require image analysis.

Figures 1-3: Image T30 and the CP models

CP original model ROIs

CP Gen 5 Trained model ROIs

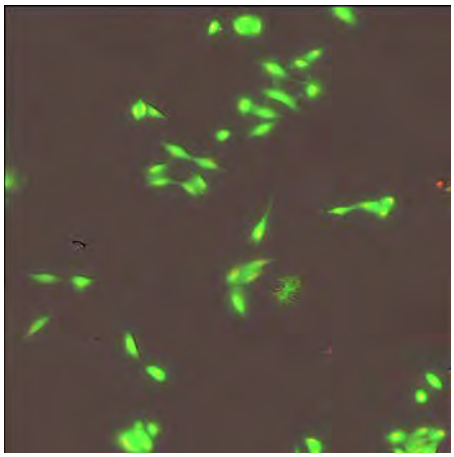

T30 all channels original image

Figures 4-6: Image T25 and LC3 models

LC3 original model ROIs

LC3 Gen 3 Trained model ROIs

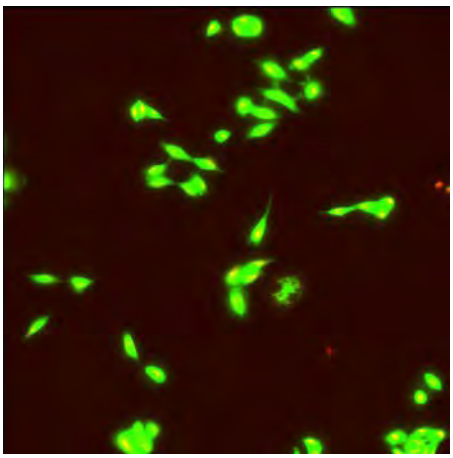

T25 Channels 2+3 original image

References:

1. Carsen Stringer, Marius Pachitariu. Cellpose 2.0: how to train your own model.
2. Original images from taken by Dante Poe.

Characterization of ER+ Tumors in a Rat Model of Breast Cancer

Scholar: Enysah Roberts

Highschool: The Ellis School, Pittsburgh, PA

Lab: Lee/Oesterreich Lab

PI of Lab: Adrian Lee and Steffi Oesterreich

Mentor: Neil Carleton

Site: Women's Cancer Research Center (WCRC)

Intro: Estrogen receptor positive (ER+) breast cancer is the most common subtype of human breast cancer. To better study ER+ breast cancer in the lab, effective animal models are needed that faithfully recapitulate the disease. The Lee/Oesterreich lab has previously established a carcinogen-induced tumor model in rats. These tumors warrant further characterization to ensure ER expression. To do this, experiments confirming the origin and subtype of induced tumor would need to be performed to ensure that the models being tested are in fact ER+.

Methods: We performed a number of experiments on our rat model tumors to test for ER positivity: (1) Western blot; (2) immunohistochemistry (IHC); and (3) qRT-PCR (assessing for *ESR1* level). Western blot and IHC will evaluate ER at the protein level - whereas in Western blotting, we will take extracted protein from tumor samples, IHC will look at ER protein using the tumor FFPE slide. Lastly, qRT-PCR will look for the *ESR1* mRNA level in the same excised tumor samples.

Results: The first two Western blots produced were inadequate because the negative controls were showing ER expression. With the third Western blot, another ER antibody was used which displayed valid results for the positive and negative controls, allowing further interpretation of the tumor samples in question. This now reliable Western blot showed faint bands that indicated

possible ER expression in rat samples 663 (organoid-implanted tumor model) and samples 010, 014, 019, and 021 (all carcinogen-induced tumors). The imaging of estrogen receptor-stained IHC slides from carcinogen-induced tumors had similar findings results with the Western blot and qRT-PCR.

Conclusions: These results show that three of the four carcinogen-induced tumor models could be considered ER+. Use of these tumors in future experiments can open new understandings of the most abundant breast cancer in women.

Using clinical data to estimate parameters for a computational model of SARS-CoV-2 infection dynamics

Akiva Rosenzweig[1 2], Ali Sinan Saglam[3], James Faeder[3]

[1]Montgomery Blair High School, Silver Spring, MD; [2]University of Pittsburgh Hillman Cancer Center Academy, Pittsburgh, PA; [3]Department of Computational and Systems Biology, University of Pittsburgh School of Medicine, Pittsburgh, PA

Abstract In this project, we created a TCL (target cell limited) model to fit SARS-CoV-2 data from a paper [1] published earlier this year. We performed parameter scans to understand the model's dynamics, tested the model with mock experimental data to understand its limitations, and fit the model to individuals' clinical Nasal CN (cycle number) data from the paper.

Introduction We created the TCL model in BNGL (BioNetGen Language, a Python-based modeling language being developed by my mentors), and performed the parameter scans, mock data analysis, and clinical data fitting with Python. The BNGL model uses ODE (ordinary differential equation) analysis to determine the end concentrations of molecules for given amounts of time elapsed. Our goals were to explore the TCL model's limitations and dynamics once recreated, and to succeed in fitting our model to clinical Nasal CN data of individuals. I believe it is worth mentioning that CN is tied to viral load inversely. Generally, a high CN value denotes a low viral load, and a low CN value denotes a high viral load. We found it was easier to fit the model using the CN values, so we included the logarithmic conversion between V (viral load) and CN provided by the paper into the model to make fitting to CN possible. In the model, T (target) cells are healthy cells susceptible to infection. E (eclipsed) cells are cells that the virus has entered, but are not producing new viruses yet. I (infected) cells are cells that are producing new viruses.

Methods First, we wrote the TCL model in BNGL (BioNetGen Language, a modeling language being developed by my mentors) as described in the paper. We borrowed the values for initial species states, static rate constants (eclipse period k and virus clearance rate c), and parameters to be estimated (virus binding rate β, infectious cell death rate δ, and infectious cell virus release rate π) for the starting model.

To explore the model's dynamics, we performed parameter scans on parameters β, δ, and π. The parameter scan sweeps through a range of given parameter values for a given parameter, then uses the model to generate and find the maximum or end concentrations of the given observables.

To understand and tune the model's parameter estimation limitations, we first generated mock experimental data by introducing noise to the model's CN values. Initial parameter values are given. Then, a cost function is defined to return the error between the mock experimental data and the model's values. Finally, the error from the cost function is minimized using the Nelder–Mead method to generate parameter estimates. The parameter estimates are compared to the initial parameter values to determine how accurate the estimations were. This process was then repeated, replacing the mock experimental data with individuals' clinical Nasal CN data.

Results As the virus binding rate β is increased, maximum concentrations of the virus, eclipsed cells, and infected cells increase, while end concentrations of target cells decrease (Figure 1a). Increasing the infectious cell virus release rate π has very similar effects (Figure 1c). As expected, increasing the infectious cell death rate has the opposite effect, decreasing maximum concentrations of the virus, eclipsed cells, and infected cells increase, while end concentrations of target cells increase (Figure 1b).

Through testing the model with mock experimental data, decreasing available data points and increasing noise in the data points both decreased accuracy in parameter estimations. We found that reducing the number of available data points below ten points caused the parameter estimation to fail. As expected, the model was able to successfully estimate parameters to fit the clinical Nasal CN data of patients with clear trends (Figures 2a, 2b, and 2c). When the clinical data was too noisy or indistinct, the model struggled to generate a suitable fit (Figure 2d).

Discussion This project has confirmed our expectations on the effect of virus binding rate β, infectious cell

death rate δ, and infectious cell virus release rate π on the concentrations of the virus, target cells, eclipsed cells, and infected cells. It has allowed us to find limitations of a TCL model of this type, such as the number of data points needed for a successful fit. Finally, the model we developed has the potential to assist in creating predictions for individual patients to help further our understanding of SARS-CoV-2.

Figure 1. Parameter scans of virus binding rate β, infectious cell death rate δ, and infectious cell virus release rate π

Figure 1a. Parameter β

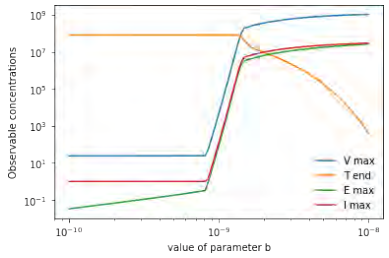

Figure 1b. Parameter δ

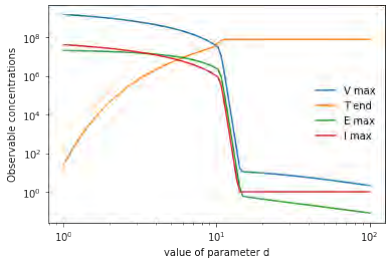

Figure 1c. Parameter π

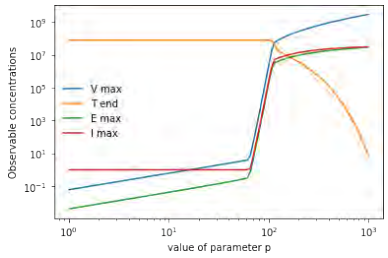

Figure 2. Experimental Data Fitting

Figure 2a. Successful Patient Fit

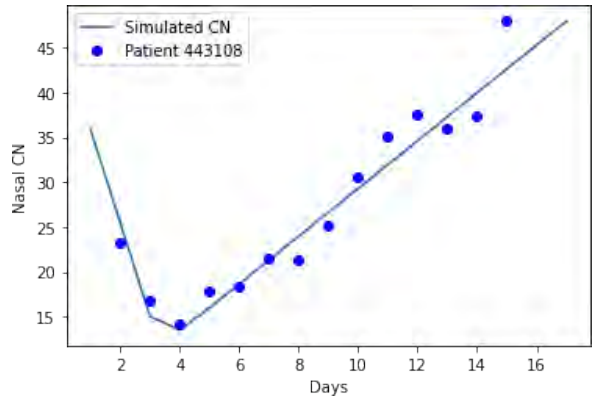

Figure 2b. Successful Patient Fit

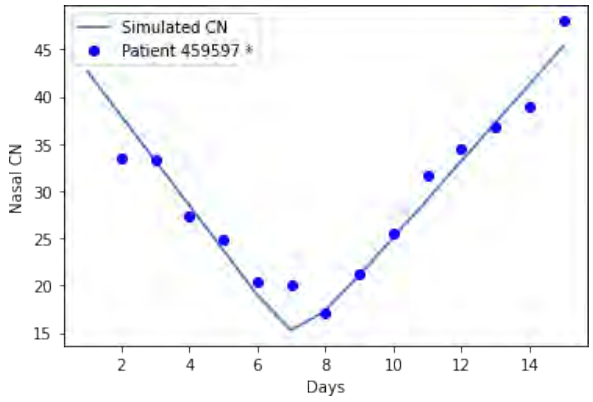

Figure 2c. Successful Patient Fit

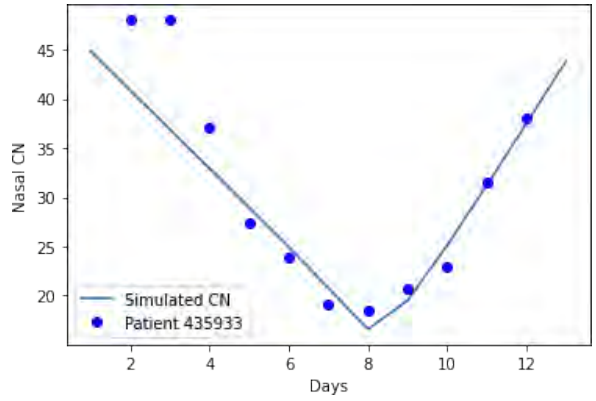

Figure 2d. Unsuccessful Patient Fit

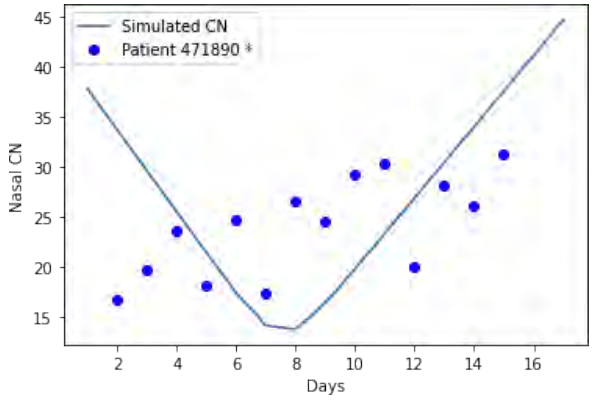

References

1. Ke R, Martinez PP, Smith RL, Gibson LL, Mirza A, Conte M, et al. Daily longitudinal sampling of SARS-CoV-2 infection reveals substantial heterogeneity in infectiousness. Nat Microbiol [Internet]. 2022;7(5):640–52. Available from: http://dx.doi.org/10.1038/s41564-022-01105-z

COVID-19's Impact on Pediatric Injury Patterns

Scholar: Sean Russell Jr

High School/College/City/State: Westinghouse High School, Pittsburgh, PA

Mentor(s): Christine M. Leeper, MD MSc, Stephen Strotmeyer, PhD, MPH.

Site: UPMC Department of Surgery, Division of Trauma and General Surgery

Introduction The COVID-19 pandemic led to schools and organized recreational activities temporarily closing. In 2020, many children in Allegheny County spent the entire year in lockdown. Bicycle injuries are a common trauma mechanism and popular recreational activity during the pandemic. We hypothesized that the COVID-19 pandemic affected pediatric injury patterns.

Methods UPMC's database from Children's Hospital of Pittsburgh was queried for children age<18 presenting to the ED from 2019-2020 that had bike-related injuries. The variables used included year, race, age, sex, ethnicity, emergency severity index (ESI), and trauma. Data were summarized using counts, percentages, mean (standard deviation), and median (IQR). The incidence and rates of bicycle accidents were compared between the two years using Chi-Square tests. The 2019 and 2020 cohorts were assessed for differences in demographics and outcomes.

Results There were 422 bike injuries/20,498 ER visits (2%) in 2019 compared to 630/17,336 ER visits (3.6%) in 2020 ($p<0.001$). There were no differences between 2019 and 2020 cohorts in terms of race (79% vs 80% white race respectively, $p=0.55$), age (median(IQR) years of age = 10(12-7) and 9(12-7) respectively, $p=0.75$) or urgent presentation (56% vs 57%, respectively; $p=0.93$). Females were involved in bicycle trauma more often in 2020 (30%) as compared to 2019 (25%) ($p=0.05$). Nearly every patient was treated and released the same day.

Conclusion There was an increase in bicycle accidents requiring Emergency Department visits in 2020 that may be attributable to the COVID-19 pandemic. An overall increase in unstructured outdoor recreational activities may be the underlying cause. Further research could look into other recreational-related trends over those two years, and data from subsequent years may be used to validate these findings.

Dose-response confirmation of small Molecules That Stabilize Mutant Triose Phosphate Isomerase (TPI) as Treatments for TPI deficiency

Scholar: Sidharth Sadashiv
School: Winchester Thurston, Pittsburgh, PA
PI: Andreas Vogt, Department of Computational and Systems Biology, University of Pittsburgh Drug Discovery Institute
Mentor: Laura Vollmer, University of Pittsburgh Drug Discovery Institute
Site: Hillman Academy, TDX

Introduction Triose Phosphate isomerase (TPI) is an enzyme involved in a critical energy-producing process known as glycolysis. Certain specific genetic mutations cause TPI deficiency (TPI-Df), an early childhood progressive degenerative neuromuscular disorder. Despite mutant proteins remaining active, these proteins are targeted by the protein quality control (PQC) pathway, leading to low levels of TPI within cells. There are currently no known medical treatments for TPI-Df. In order to find potential treatments for TPI DF, the Palladino laboratory in the Department of Pharmacology in collaboration with the University of Pittsburgh Drug Discovery Institute developed a high-throughput, high-content screening assay to identify compounds that increase cellular levels of mutant TPI. The goal of my project was to confirm the activity of selected hits from the primary screen in fibroblasts from TPI deficient patients.

Methods: Pilot screens were conducted on HEK293 and HeLa cells engineered to express the mutant TPI/E105D protein fused to a green fluorescent protein reporter (TPI/E105D- GFP). These assays functioned as a phenotypic screen for compounds that stabilize mutant TPI. The primary screens identified several compounds that increased levels of mutant TPI, which we tested in fibroblasts from a TPI-Df patient with the "common" mutation (E105D/E105D; FB303). Fibroblasts were cultured using standard methods (37°C, 5% CO2) in DMEM media. Cells were plated on a 384 well plate and treated with screening hits (Vincamine, Artesunate, and Vinpocetine) at varying concentrations in ten-point, two-fold concentrations gradients using a Beckman Coulter Biomek 2000 liquid handler. DMSO was used as a negative control and Luminespib was used as a positive control. Cells were then stained using anti-TPI antibodies (Invitrogen rabbit polyclonal, and Santa Cruz rabbit polyclonal) followed by a Cy3-conjugated secondary antibody. Plates were imaged on a PerkinElmer Opera Phenix high-content reader and analyzed by automated image analysis for levels of cellular mutant TPI.

Results Dose-response curves revealed that one of the agents tested (Artesunate) caused a dose-dependent increase in mutant TPI, although compared to our positive control Luminespib, at least 100-fold higher concentrations of Artesunate were required to increase mutant TPI levels. Both Luminespib and Artesunate reduced the number of cells, in the wells, possibly due to toxicity. Both antibodies gave identical results which were confirmed in a second, independent biological repeat.

Discussion Our results show that TPI levels increased in mutant patient Fibroblasts upon Artesunate treatment. Hence, Artesunate could be a promising new treatment for TPI-DF. Future studies would involve further confirmation in an orthogonal assay for TPI expression (Western blot) and testing in animal models of TPI-Df (fruit flies and mice).

Feature analysis for fall outcomes predicted by the Recurrent Neural Network (RNN) compared to the outcomes predicted by the CART Logit method

Richael Saka, Dr. Richard Boyce, PhD, Dr. Olga Kravchenko, PhD

St. Francis Desales High School, Columbus OH; [2]University of Pittsburgh Medical Center Aging Institute, Pittsburgh, PA, [3]University of Pittsburgh Hillman Cancer Center Academy, Pittsburgh, PA

Abstract

We used Long-Term Care Minimum Data Set (MDS) to predict falls in the nursing home facilities via Recurrent Neural Network (RNN) and compare results with predictions previously obtained via hybrid classification and regression tree (CART logit) method.

Introduction

Patients admitted into nursing homes often have an increased risk of falls due to various health conditions and/or adverse events resulting from medications. Fall events are dangerous and may lead to serious injury or death. Preventing these instances requires a holistic and unique approach for each patient that includes but is not limited to chart review, medication adjustment, physical and occupational therapy, etc. A validated machine learning model that uses nursing home data may help predict the probability of a fall in the near future and provide information that can be used by clinicians and nursing home staff to intervene. In order to develop effective intervention, it is important to understand the strengths and weaknesses of the model and determine which factors were most important for such prediction to be accurate.

Methods

The MDS dataset is a comprehensive survey that is completed by the nursing home staff for every patient who stays in a Medicare-certified nursing home in the United States. It includes more than 200 variables that include information about facility, demographics, cognitive status, medications, comorbidities, previous history of falls, and so on. Each patient has longitudinal data comprised of multiple records (up to 20) collected during regularly scheduled assessments. We hypothesized that a model such as RNN will outperform the CART logit model, because it can account for complex dependencies that develop over time. The data analysis was conducted using Python. We evaluated the performance of each model using F_1, precision, recall and specificity. We have used test sets for RNN and CART logit models to identify and run profile reports for each of the 208 features in each set.

Results

Running the performance characteristics for the CART logit model, we found the precision, recall, and F_1 to be 0.237, 0.637, and 0.346, respectively. Doing the same for the RNN model, the precision, recall, and F_1 were calculated to be 0.374, 0.559, and 0.448. From these numbers, it can be inferred that the RNN model performed significantly better than the CART.

Discussion

Our results show that RNN outperforms CART logit model in terms of F1 score, precision and recall, even though there is a small number of assessments for most patients. As the next step towards improving interpretability of the RNN model, we will investigate model features that have statistically significant differences between the test sets for both models, and then use logistic regression to identify which features were most significant in predicting the outcomes for the RNN model.

Determining the Optimal Chemotherapy To Be Used in TACE Therapy by Analyzing Patient Data

Jeremiah Satcho[1], Dr. Amar Zureikat, MD[2], Hussein Kachfe, MD[3], [1]North Allegheny Senior Highschool, Pittsburgh, PA, [2]UPMC Presbyterian Hospital, Pittsburgh, PA, [3]UPMC Presbyterian Hospital, Pittsburgh, PA

Abstract

TACE therapy or transarterial chemoembolization is a treatment for unresectable liver where chemotherapy and an emobolizing agent are injected through a catheter to directly combat and block off blood flow to the tumor. A lack studies determining the best chemotherapy has caused perscriptions of chemotherapy that may not be most beneficial for the patient. By collecting and analyzing data on patients who have recieved TACE therapy, the optimal chemotherapy can be discerned.

Introduction

The three different types of chemotherapy used in TACE therapy, streptozocin, doxorubicin or cisplatin, can lead to different lengths of overall survival, yet the decision of which chemotherapy to use is made by institutions without definite evidence from data sets to support the decision. The goal of this study is to determine which chemotherapy best compliments TACE therapy.

Methods

Data were collected on multiple, demographic, disease-related, and treatment-related variables from patients older than 18 with unresectable liver metastaseses treated with TACE using streptozocin, doxorubicin or cisplatin as the first-line agent, from 2002 to 2022. The patients' overall survival was measured from the time of diagnosis, metastatic disease, and time of start of TACE treatments.these along with univariable and multivariable analysis results based on the patients' data were used to compare each chemotherapy.

Results

P-value determines the statistical significance. The P-value for the overal survival from diagnosis was 0.939, from metastases diagnosis was 0.639, and from TACE start was 0.210. This indicates that there was no significant difference among the chemotherapies' patient overall survival because none of the values were <0.05.

Discussion

Based on the data analysis, there is no significant difference in survival associated with the three chemotherapy drugs. Thus, any of them can be used in TACE treatments to yield similar outcomes for the patient.

Figure 1: Multivariatte Analysis for overal survival from TACE completion

	Univariate				Multivariate			
	95% CI of HR				95% CI of HR			
	HR	Lower	Upper	p-valuer	HR	Lower	Upper	p-valuer
TACE Drug								
Cisplatin	REF				REF			
Doxorubicin	1.107	0.671	1.824	0.691	1.188	0.572	2.464	0.644
Strep	0.544	0.234	1.265	0.157	0.571	0.206	1.582	0.281
Sex (F)	1.388	0.876	2.199	0.162				
Primary Tumor Pathology								
Appendix	REF			0.000	REF			
Breast	2.173	0.217	21.793	0.509	0.169	0.002	18.210	0.457
Lung/Bronchial	1.179	0.261	5.313	0.831	0.101	0.011	0.899	0.040
Cholangiocarcinoma	5.035	1.045	24.254	0.044	0.172	0.014	2.113	0.169
Colorectal	2.539	0.601	10.716	0.205	0.143	0.021	0.945	0.044
Small Bowel	0.410	0.119	1.416	0.159	0.024	0.004	0.150	0.000
Gastric	4.373	0.830	23.049	0.082	0.468	0.056	3.895	0.483
Pancreas	0.560	0.168	1.872	0.347	0.014	0.002	0.093	0.000
Number of Mets								
1-5	REF							
6-10	0.988	0.332	2.939	0.983				
Innumerable	1.122	0.639	1.968	0.689				
Hepatic Steatosis	0.444	0.245	0.805	0.007	0.324	0.151	0.698	0.004
Surgery for Met before TACE	1.382	0.817	2.337	0.227				
Octreotide/Analogue	0.312	0.160	0.607	0.001	0.320	0.076	1.357	0.122
Everolimus	0.946	0.585	1.529	0.820				
Sunitinib	0.954	0.529	1.720	0.875				
Cytotoxic Chemotherapy	1.798	1.115	2.898	0.016	1.068	0.515	2.217	0.859
PRRT	0.366	0.199	0.671	0.001	0.538	0.265	1.095	0.087
Response after TACE Completion								
Response	REF				REF			
Stable Disease	2.123	1.053	4.280	0.035	2.032	0.877	4.708	0.098
Progression	4.337	2.246	8.372	0.000	3.927	1.639	9.410	0.002
Surgery for Met After Tace Completion	0.169	0.053	0.539	0.003	0.209	0.062	0.700	0.011

Figure 2: Overall Survival from TACE start

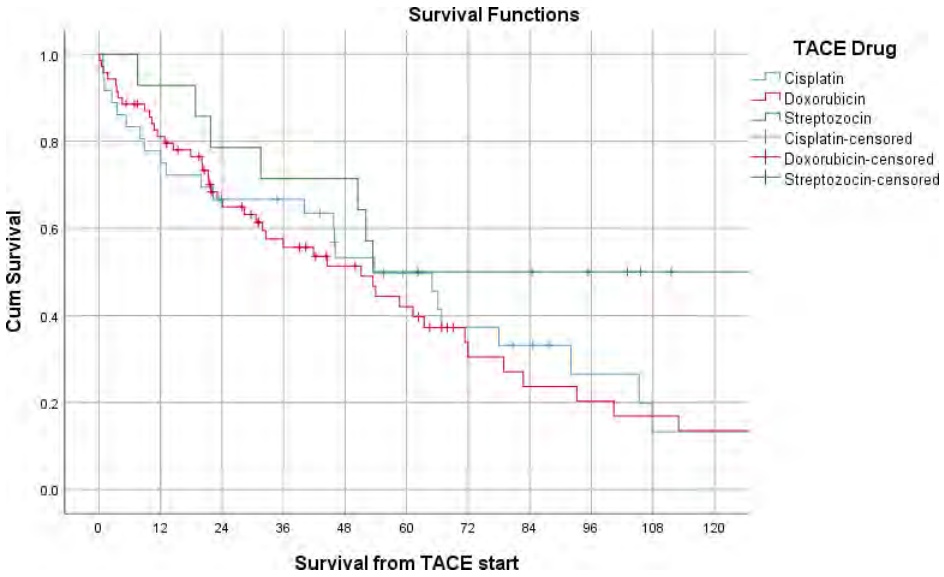

Title: The Effect of Serum Starvation on Regulatory T-Cells

Scholar: Jhanvi Sharma

High School/College/City/State: Obama Academy of IB International Studies

PI of group/lab/Mentor: Dr. Alison Kohan

Co-mentor(s): Apoorva Narain, PhD; Jitendra S Kanshana, PhD

Site: Immunology and Immunotherapy (ICI)

Introduction

T-lymphocytes make one half of the immune system, contributing crucially to host's defense mechanism. The two subtypes of T-lymphocytes CD4 and CD8 cells are primarily pro-inflammatory in nature. The only known/established anti-inflammatory subtype are regulatory T-cells (CD4+ CD25+ FOXP3+). These are essential to regulate the effect of pro- inflammatory cells in while mostly depending on lipids to fuel their metabolic processes. Earlier work in our lab has identified the role of lipids in regulating the anti-inflammatory role of Tregs.

In our study we intend to identify the physiological changes in Tregs upon serum starvation.

Methods

The splenocytes isolated from C57Bl/6J wild type mice were enriched for CD4+ population. After 24h the induced Tregs were split equally into serum starved (test) and complete media (control). The cellular pellet was processed for flow cytometric analysis and supernatant for ELISA. Trypan blue staining was performed for cell count.

Results

Upon comparing the Treg population the FOXP3+ and IL-10 expression was higher under serum starved conditions with 20-30% decrease in cellular proliferation.

Discussion

Depending on nutrient availability, Tregs can use alternate metabolic pathways for energy. Less cellular proliferation and an increase in both FOXP3 + IL10 expression under serum starved condition could be due to lipid unloading that triggers the synthesis of anti-inflammatory cytokines. The oscillation between mTOR and AMPK pathway is a driving force behind increased FOXP3 expression under nutrient rich conditions. As nutrient rich condition creates the possibility of overactivation of mTOR as well as subsided fatty acid oxidation rate. The results indicate towards the fact that the intracellular lipids play a direct role in imparting Tregs their established biomechanics.

Polymorphisms in DNA repair and oxidative stress genes associated with pre-treatment anxiety in breast cancer survivors: an exploratory study

Johnathan Z. Sherrill [1], [1]Power Center Academy High School, Memphis, TN

Dr. Susan M. Sereika1, Dr. Yvette P. Conley and Dr. Catherine M. Bender

University of Pittsburgh

Alexander W. Dreyfoos School of the Arts, Palm Beach, FL; University of Pittsburgh Hillman Cancer Center Academy, Pittsburgh, PA

Abstract In this project, secondary analysis of baseline data from a study investigating the effect of the adjuvant aromatase inhibitor therapy, anastrozole, on changes in cognitive function in postmenopausal women with breast cancer. The sample (N = 219) was comprised of three groups of postmenopausal women, two of these groups were women with early-stage breast cancer and women who received anastrozole alone. A third group of postmenopausal women were education-matched controls with no personal history of breast cancer. Anxiety was measured with the Profile of Mood States (POMS) Tension/Anxiety Subscale a self-report measure of anxiety.2 The POMS requires participants to rate their feelings (i.e., tense, shaky, panicky, restless, on edge) in the past week on a five-point Likert scale (not-at-all to extremely).. One-way analysis of variance was used to determine differences in anxiety between study groups. Linear regression was used to explore relationships between polymorphisms in oxidative stress and DNA repair genes and anxiety in postmenopausal women diagnosed with early-stage breast cancer. Results suggest that overall increases in anxiety levels based postmenopausal women who were prescribed more aggressive treatments for breast cancer such as anastrozole and chemotherapy

Introduction Breast cancer is the most common cancer in women and is the leading cause of cancer deaths among women worldwide. According to the World Health Organization, more than 500,000 people die annually from breast cancer. The term breast cancer refers to a malignant tumor that has developed from cells in the breast. The breast is composed of two main types of tissues, glandular and stromal tissues. Breast cancer is characterized by the unchecked growth of abnormal cells. Anxiety is a common symptom experienced by patients with cancer and leads to other internal issues. Studies have shown that high levels of anxiety are common among women with breast cancer at diagnosis, women with the disease are at a higher probability of experiencing extreme uneasiness and depression. Most women do not like to hear the word cancer and feel worried and stressed over it. In one study conducted by Ashbury et. al., 77 percent of 913 women with breast cancer recalled experiencing anxiety within 2 years of treatment. Nevertheless, the level of anxiety experienced by one person with cancer may vary from the anxiety experienced by another. Factors associated with this variability in the experience of anxiety in women with breast cancer are not entirely clear. Moreover, the mechanisms underlying anxiety in this population are not known. Emerging evidence suggests that oxidative stress and DNA repair may be associated with anxiety in women with breast cancer. The purpose of this study is to compare anxiety between two groups of women with early stage breast cancer and a control group of women without the disease and to explore relationships between polymorphisms in oxidative stress and DNA repair genes and anxiety in postmenopausal women diagnosed with early stage-breast cancer.

Methods This study was a secondary analysis of baseline data from a study investigating the effect of the adjuvant aromatase inhibitor therapy, anastrozole, on changes in cognitive function in postmenopausal women with breast cancer (R01 CA107408).1 The sample (N = 219) was comprised of three groups of postmenopausal women, two of these groups were women with early-stage breast cancer (women who eventually received the endocrine therapy agent, anastrozole and chemotherapy (N = 55), and women who received anastrozole alone (N=83). A third group of postmenopausal women were education-matched controls with no personal history of breast cancer (N = 81). All participants were no greater than 75 years of age, able to speak and read English, completed at least 8 years of education, and had no previous history of cancer, psychiatric illness, or neurologic disease/trauma at time of enrollment into the parent study. In addition, women with breast cancer had a diagnosis of estrogen receptor positive, early-stage breast cancer (stages 1, 2, or 3a) based on the Tumor, Nodes, Metastasis Classification of Malignant Tumors with no clinical evidence of distant metastases. This study was approved by the University of Pittsburgh Institutional Review Board. Informed consent was obtained from all individual participants. Anxiety was measured with the Profile of Mood States (POMS) Tension/Anxiety Subscale a self-report measure of anxiety.2 The

POMS requires participants to rate their feelings (i.e., tense, shaky, panicky, restless, on edge) in the past week on a five-point Likert scale (not-at-all to extremely). Genetic samples were collected from June 2008 to May 2014. Three milliliters of whole blood or two milliliters of saliva were obtained for genotyping. Data were analyzed using IBM® SPSS® Statistics Version 28.0.1.1(14). Descriptive statistics were used to describe the sample characteristics. One-way analysis of variance was used to determine differences in anxiety between study groups. Linear regression was used to explore relationships between polymorphisms in oxidative stress and DNA repair genes and anxiety in postmenopausal women diagnosed with early-stage breast cancer.

Results Women were on average 60.06 (SD=6.08) years of age with an average of 15.67 (2.78) years of education. At pretherapy, the groups differed significantly on anxiety (F = 5.67, p = .004) as measured by the POMS Tension/Anxiety score, with the group of women who would eventually receive chemotherapy plus anastrozole experiencing higher anxiety (mean = 9.61, SD = 6.14) compared to the anastrozole alone (mean = 6.97, SD = 4.65) and the control groups (mean = 6.61, SD = 5.63). Results of the exploration of the associations of polymorphisms of DNA repair and oxidative stress genes with anxiety, we found that ERCC5RS4150360 (B=5.137, p = .043) was significantly associated with anxiety, while the CATRS1001179 was marginally significantly associated (B=-2.062, p = .084).

Discussion These findings suggest that women with more aggressive breast cancer who are anticipating treatment with chemotherapy and anastrozole therapy have greater anxiety compared to women who are anticipating less aggressive cancer therapy without chemotherapy and compared to their counterparts without breast cancer. These results also suggest that the nucleotide excision repair pathway of the DNA repair system may play an important role in the experience of anxiety in postmenopausal women diagnosed with early state of breast cancer patients. In the future I will conduct another secondary analysis of follow up data from a study investigating the effect of the adjuvant aromatase inhibitor therapy, anastrozole, on changes in cognitive function in postmenopausal women with breast cancer at 6 months and 12 months follow up appointment intervals Please review the figures listed below regarding the POMS at baseline findings:

Figure One

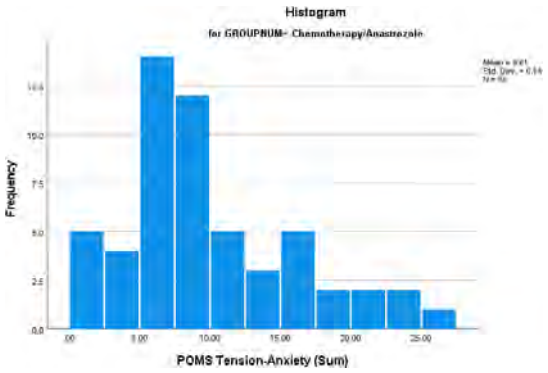

Figure Two

ANOVA

POMS Tension-Anxiety (Sum)

	Sum of Squares	df	Mean Square	F	Sig.
Between Groups	333.367	2	166.683	5.671	.004
Within Groups	6348.699	216	29.392		
Total	6682.065	218			

References

1. Bender C, Merriman J, Gentry A, Ahrendt G, Berga S, Brufsky A, Casillo F, Dailey M, Erickson K, Kratofil F, McAuliffe P, Ryan C and Sereika S. Patterns of change in cognitive function with anastrozole therapy. *Cancer*. 2015;121:2627-2636.

2. McNair D, Lorr M and Droppleman LF. *EdITS Manual for the Profile of Mood States*. San Diego: EdITS/Educational and Industrial Testing Service; 1992.

Use of Indocyanine Green Dye in Sarcoma Assessment

Maria Silvaggio[1,2], Tanya Heim MS[3], Brittany Royes MS[3], William Li MD[3], Matthew Gong MD[3], Richard McGough MD[3], Stella Lee MD[3], Brenda Diergaarde PhD[4], Kurt Weiss MD[3],
[1]Sewickley Academy, Sewickley PA; [2]University of Pittsburgh Hillman Cancer Center Academy, Pittsburgh, PA; [3]University of Pittsburgh Department of Orthopaedic Surgery, Pittsburgh, PA; [4]University of Pittsburgh School of Public Health, Pittsburgh, PA

ABSTRACT: Removing sarcomas with negative surgical margins is crucial in preventing recurrence. Indocyanine Green (ICG) is a fluorescent dye shown to concentrate in vascular irregularities. This study aims to determine if intraoperative fluorescent imaging with ICG can more accurately detect positive margins as compared to the current standard of care, which is largely based on the surgeon's subjective impression. This UPMC Hillman Cancer Center study is among the first to evaluate ICG use in sarcoma patients.

INTRODUCTION: Sarcomas are cancers of the soft tissue and bone that commonly metastasize to the lung. The primary goal of surgical resection in sarcoma is to remove the tumor with negative margins, indicating that the entire tumor has been removed. Margin assessment by frozen section is a common intraoperative procedure. However, the selected margin samples may not reflect the entire tumor bed which can result in false negative readings. Preclinical mouse studies demonstrated that ICG accumulates in sarcomas [1]. We hypothesize that residual tumor in the tumor bed can be identified by ICG and that use of ICG will be useful for evaluating surgical margins in sarcoma. In this study, the results of intraoperative ICG imaging of the tumor bed are compared to final pathology reports to assess its utility as a biomarker of positive surgical margins.

METHODS: Currently, 26 patients of varied ages and sarcoma types have been enrolled in our ongoing ICG clinical trial. ICG dye was injected intravenously into consented patients prior to start of surgery. Initially, 2.5 mg/kg of ICG dye was infused, but due to oversaturation of the dye, the dosage has since been decreased to 2.0 mg/kg. Start of infusion, end of infusion, and skin incision times were recorded. During surgery, both the tumor and the tumor bed were imaged with the Stryker SPY Portable Handheld Imaging System. Using a protocol originally described in breast cancer surgery, the most fluorescent region of the tumor was set to 100% prior to imaging the tumor bed. As with the breast cancer study, regions in the tumor bed that showed ≥ 77% fluorescence compared to this tumor reference point were assumed to contain residual tumor and surgical margins were classified as positive. If fluorescence was less than 77% within the tumor bed, the tumor was presumed to be removed with negative margins [2]. Immediately following resection of the tumor, surgeons completed a brief survey detailing their subjective assessment of tumor margins based on gross examination. Surgeons were blinded to the results of ICG imaging and no resection was made based on ICG imaging results. To represent whether ICG results matched with pathology, a system of 0s and 1s was used. ICG results that matched with pathology's assessment of margins were considered successful and assigned a 1, while unsuccessful cases were assigned a 0 (Table 1). Using final pathology results as the gold standard, the accuracy of ICG imaging was determined and sensitivity and specificity were calculated. We also explored whether ICG accuracy was affected by timing of ICG administration.

RESULTS: One patient experienced a burning sensation upon ICG infusion, and another patient's tumor margins were deferred by pathology. One patient was missing ICG assessment data, and another patient's pathology report had not yet been processed. This left 22 patients with final pathology reports as well as ICG imaging data. Margin assessment by ICG imaging and pathology aligned in 13 of the 22 cases for an accuracy of 59%. The sensitivity of ICG imaging to identify positive margins was 27% and the specificity was 91%. A correlation was identified between ICG accuracy and the time between the start of infusion and skin incision. For 21 (95%) of the 22 patients, timing data was available. Twelve cases had ≥ 2.5 hours between the start of ICG infusion and skin incision, and 9 of these 12 produced accurate ICG results (75% accuracy). Nine cases had < 2.5 hours between the start of ICG infusion and skin incision, and only 4 of these 9 produced accurate ICG results (44% accuracy). The sensitivity of ICG when ≥ 2.5 hours elapsed was 40%, and the specificity was 100%. The sensitivity of ICG when < 2.5 hours elapsed was 17%, and the specificity was 100% (Figure 1).

DISCUSSION: When considering ICG sensitivity and specificity, a higher sensitivity is desirable to reduce the chance of a false negative reading. The sensitivity and accuracy of ICG was highest in patients with ≥ 2.5 hours elapsed between the start of infusion and the skin incision, indicating a potential connection between ICG accuracy and timing. Increasing patient enrollment and further data collection, such as the exact time of tumor excision and imaging, is necessary in order to draw more firm conclusions about the efficacy of ICG imaging to determine margin status intraoperatively.

Table One

Patient ID	Start of Infusion	Time of First Incision	Time Between Infusion ≥ 2.5 Hours	Margins (Surgeon Opinion)	Margins (ICG)	Margins (Pathology)	ICG Success (Matches with Pathology)
ICG1	7:52 AM	10:20 AM	Yes	Negative	Positive	Positive	1
ICG2	6:44 AM	10:47 AM	Yes	Negative	Negative	Negative	1
ICG3	N/A	8:11 AM	N/A	Negative	Positive	Negative	0
ICG4	5:43 AM	8:25 AM	Yes	Positive	Negative	Positive	0
ICG5	11:00 AM	4:43 PM	Yes	Negative	Negative	Negative	1
ICG6	10:35 AM	3:05 PM	Yes	Negative	Negative	Negative	1
ICG8	7:15 AM	7:55 AM	No	Negative	Negative	Negative	1
ICG9	10:18 AM	12:58 PM	Yes	Negative	Negative	Negative	1
ICG10	8:00 AM	9:25 AM	No	Negative	Negative	Positive	0
ICG11	5:51 AM	8:00 AM	No	Negative	Negative	Positive	0
ICG12	8:20 AM	10:16 AM	No	Negative	Negative	Negative	1
ICG13	6:29 AM	9:36 AM	Yes	Negative	Negative	Negative	1
ICG14	6:15 AM	9:10 AM	Yes	Negative	Positive	Positive	1
ICG15	8:28 AM	12:25 PM	Yes	Positive	Negative	Positive	0
ICG16	5:35 AM	7:40 AM	No	Positive	Negative	Positive	0
ICG17	5:50 AM	7:22 AM	No	Negative	Negative	Positive	0
ICG19	5:55 AM	8:17 AM	No	Negative	Negative	Positive	0
ICG20	9:50 AM	12:20 PM	Yes	Negative	Negative	Negative	1
ICG21	7:55 AM	12:29 PM	Yes	Positive	Negative	Negative	1
ICG22	10:25 AM	1:43 PM	Yes	Negative	Negative	Positive	0
ICG24	6:25 AM	8:19 AM	No	Negative	Negative	Negative	1
ICG25	8:25 AM	9:41 AM	No	Negative	Positive	Positive	1

Data table with the timing of ICG and the comparison of sarcoma margin assessment between ICG and pathology.

Figure One

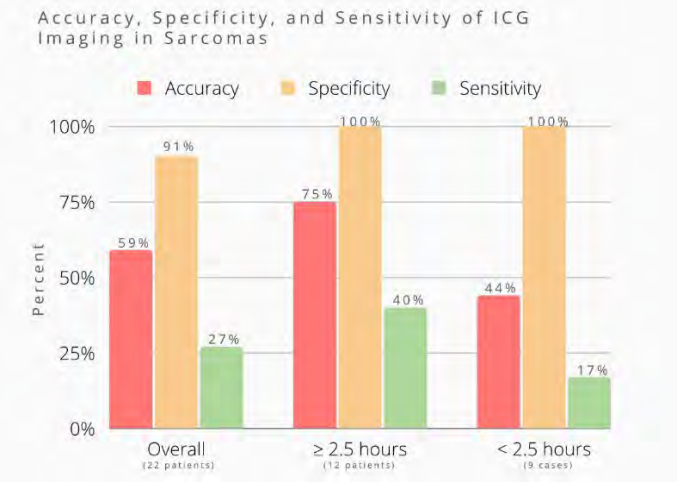

Bar graph comparing accuracy, specificity, and sensitivity of ICG as a method of sarcoma margin assessment across three groups.

References

1. Mahjoub A., Morales-Restrepo A., Fourman MS., M.Phil, Mandell JB., Feiqi L., Hankins ML., Watters RJ., Weiss KR. "Tumor Resection Guided by Intraoperative Indocyanine Green Dye Fluorescence Angiography Results in Negative Surgical Margins and Decreased Local Recurrence in an Orthotopic Mouse Model of Osteosarcoma." *Annals of Surgical Oncology*, vol. 26, 27 Dec. 2018, pp. 894-98, https://doi.org/10.1245/s10434-018-07114-9. Accessed 31 July 2022.

2. Veys I., Pop CF., Barbieux R., Moreau M., Noterman D., De Neubourg F., Nogaret JM., Libersle G., Lsrsimont D., Bourgeois P. "ICG fluorescence imaging as a new tool for optimization of pathological evaluation in breast cancer tumors after neoadjuvant chemotherapy." *PLoS One*, vol. 13, 2018, https://doi.org/10.1371/journal.pone.0197857. Accessed 31 July 2022.

Application of an OCT-based 3D reconstruction model to a quantitative assessment of corneal changes after stem cell therapy

Scholar: Skyler Spears

High School: Pittsburgh Science & Technology Academy

PI of group/lab Mentors: Moira L Geary (lab), Gary Yam (lab), Vishal Jhanji (clinical)

Site: Corneal Regeneration Lab

Introduction

Corneal scarring, due to different causes, like injury, infection and diseases, leads to impaired or loss of vision. The current treatment offered to rectify severe scarring cases is corneal transplantation using healthy donor corneas, however the global demand for donor tissues greatly exceeds its supply. Thus, our laboratory explores alternative strategies, including stem cell therapy. In a mouse model of corneal injury created by mechanical ablation, corneal stromal stem cells were applied to wound tissue. At time intervals, the corneal cross-sectional features were examined with a Spectral Domain Optical Coherence Tomography (SDOCT, Bioptigen). My study performed 3-dimensional reconstruction from serial OCT scans and measured the stromal volume changes after treatments.

Methods

Serial OCT images were processed using Fiji software (https://imagej.net). A full corneal view was obtained with tilt correction and centration, and the stroma was obtained after semi-manual segmentation to remove corneal epithelium, and clean-up. The stromal volume was measured using Metamorph image analysis software. The changes of stromal volume after treatment with reference to wound control were calculated and the statistical significance was analyzed using non-parametric Mann-Whitney U test, with $P<0.05$ considered to be significant.

Results

Serial OCT scans from 47 mouse corneas (6 wound controls and 41 corneas treated with 5 different batches of stromal stem cells) were 3D-reconstructed and the central stroma was segmented. After Metamorph measurement, stem cell-treated corneas generally had reduced stromal volume, when compared to wound controls. Among 5 different cell groups, treatment with HC618, 624 and 632 had significant volume reduction ($P<0.05$), whereas HC436 and 617 did not.

Conclusion

3D OCT reconstruction allowed a precise measurement of corneal stromal volume. After stem cell treatment, the reduced stromal volume illustrated a recovery from edema and/or fibrosis-related changes due to injury. This volume analysis could be a potential parameter to evaluate the treatment effectiveness in corneal wound management.

Title: Investigating the Relationship Between Senescence and PARPi Resistance in Triple Negative Breast Cancer

Scholar: Olivia St. Esprit

High School: Beaver Area Senior High School, Beaver, PA

Lab: Carola Neumann, MD

Mentor: Lisa Hong

Site: Women's Cancer Research Center

Breast cancer is the leading cause of cancer related death in women in the United States, with 1 in 8 women being diagnosed annually. Triple negative breast cancer (TNBC) is an aggressive type of breast cancer that is found to metastasize more quickly and has the worst prognosis compared to other breast cancer subtypes. TNBC also has fewer treatment options due to its lack of three receptors that are commonly associated with other types of breast cancers (ER, PR, HER2), which positive expressions enable more effective treatments. Poly-adenosine diphosphate ribose polymerase inhibitors (PARPi) are chemotherapeutics used to treat TNBC by inhibiting DNA repair, therefore preventing tumorigenesis. This project will examine whether cells that become resistant after PARPi treatment will demonstrate increased senescence activity. Senescence is a state of cell growth arrest, which prevents cell division. Senescence can be seen as a tumor suppressor by preventing tumor growth and metastasis. In contrast, senescence is also described as a tumor promotor due the senescence associated secretory proteome (SASP), which promotes tumorigenesis in neighboring cells. To test this hypothesis, using three TNBC cell lines (MDA-MB-231, MDA-MB-436, HCC1937), we performed western blotting to observe expression of p16 and p21 proteins, which are senescence markers, after treatment with various chemotherapeutics including cisplatin and three PARPi (talazoparib, olaparib, niraparib). Senescence activity was also measured under the same treatment conditions using β-Galactosidase staining. Our results indicate that PARPi-resistant cells do not exhibit a higher expression of p21 or p16 proteins. Similarly, β-Galactosidase staining did not show any significant induction of senescence after drug treatment, with few, visible senescent subpopulations in each treatment condition. In conclusion, senescence is not found to have a significant upregulation in PARPi resistant TNBC cells, which is influenced at least, in part, to cellular heterogeneity.

TNFR2 Expression on BRAF-Mutated Melanomas Mediates TNF-Driven Resistance to MAPK Pathway Inhibitors

Scholar: Jenna M. Trent

High School/College: 2022 Graduate of The Ellis School, Pittsburgh, PA/ First-year University of Virginia, Charlottesville, VA

Lab: Robert L. Ferris, MD, PhD

Mentor: Lazar Vujanovic, PhD

Site: Immunology and Cancer Immunotherapy (ICI)

Background: Melanoma is the most lethal form of skin cancer, that is responsible for 80% of skin-cancer related deaths. When exposed to numerous factors such as UV rays, the more likely mutations will result. One of which is the BRAF Mutation, that occurs in approximately 50% of melanoma cases that harbor mutations at position 600 of the BRAF gene (V600), the majority of which involve the substitution of valine by glutamic acid (V600E). Somatic mutation in BRAF, a key protein kinase in the mitogen-activated protein kinase (MAPK) signaling pathway (chemotherapy treatment used to treat melanoma patients) lead to oncogenic programming in pre-malignant melanocytes. The effectiveness of MAPK cascade-targeting inhibitors (MAPKi) used to treat patients with BRAF-mutant melanoma is limited by a range of resistance mechanisms, including soluble TNF (solTNF). solTNF signals through TNFR1, however, it can also bind to TNFR2, a receptor that is primarily expressed in immune cells. In this study, we are investigating the pattern of TNFR2 expression on human BRAFv600E melanomas and its role in resistance to MAPKi.

Methods: Identified TNFR2-negative BRAF V600E cell lines which include cell line SK-Mel 28. Treated these cell lines using BRAF and MEK inhibitors, as well as IFN-y in short-term cultures overnight. Flow cytometry was used to test TNFR2 expression in human BRAF-mutant melanoma. Utilized immunofluorescence microscopy to determine TNFR2 expression by melanoma in patients receiving MAPKi therapy.

Results: Recombinant human TNF induced BRAF and MEKi resistance only in TNFR1 and TNFR2 co-expressing BRAFV600E melanoma cell lines. Genetically modified melanoma cell line models indicate that TNFR1 and TNFR2 co-expression is necessary for TNF-induced resistance to BRAF inhibitors. BRAF and MEKi treatments do not directly induce TNFR2 expression on melanomas, but IFN-y does.

Conclusion: Our data suggest that TNFR2 could be essential to solTNF-induced MAPK pathway inhibitor resistance and a possible biomarker to identify melanoma patients that could benefit from TNF-targeting therapies.

Investigating Novel Biomarkers

Scholar: Michael Ulis

High School: Taylor Allderdice High School, Pittsburgh, Pennsylvania

Lab: Joseph Church, MD

Mentor: Joseph T. Church, MD

Site: Surgery Site

Background: Congenital diaphragmatic hernia (CDH) affects 1 in 2500 live births. It involves an opening in the diaphragm that allows abdominal organs to move into the thorax and has a mortality rate of 30%. Fetal endoscopic tracheal occlusion has shown promise as prenatal therapy but is invasive and often causes premature delivery. Other prenatal therapies are being investigated but may have optimal effects earlier in gestation than CDH is typically diagnosed (~20 weeks). Earlier diagnosis of CDH might therefore allow for expanded prenatal therapeutic options. We aim to identify new biomarkers to help diagnose CDH earlier in pregnancy.

Methods: Nitrofen was given to pregnant mice at E8 to produce CDH. Non-nitrofen-fed mice served as controls. Fetuses, amniotic fluid, and maternal blood were harvested at E16. The lungs were harvested from all the collected fetuses and fixed for 24 hours in 4% paraformaldehyde followed by 30% sucrose before being snap-frozen and cryosection. Slides were stained with hematoxylin and eosin and were imaged. The airspace width was systemically measured, and the Mean Linear Intercept was calculated using Image J. Maternal blood and amniotic fluid were centrifuged at 10,000rpm for 10 minutes to remove cellular debris, and the supernatants snap-frozen for future molecular analysis.

Results: Fetuses at E16 displayed lugs that were too underdeveloped to successfully image. None of the 10 nitrofen-fed mice were pregnant at the time of harvest.

Conclusion: E16 is too early for appropriate lung morphologic assessment but produces adequate amniotic fluid. Further results will be produced with the continuation of pregnancy after nitrofen administration.

Future Directions: We will repeat nitrofen-gavage with a new batch of nitrofen in case there was an error in concentration. We will also harvest on E17 instead of E16 to increase lung maturity. Amniotic fluid and maternal serum will then be analyzed for differences in transcription, including for microRNAs.

Effects of Matrix-Bound Nanovesicles on Myoblast Differentiation

Scholar: Nikita Venkatasamy

High School: Quaker Valley High School, Sewickley PA

Lab: Dr. Stephen F. Badylak

Mentor: Dr. Bill D'Angelo

Site: TDX

Background: Facioscapulohumeral muscular dystrophy (FSHD) is a genetic disease that causes progressive degeneration of skeletal muscle. The extracellular matrix (ECM), the protein meshwork surrounding cells, provides structural support and chemical queues to maintain tissue homeostasis, and exogenous ECM therapy has been investigated as a therapy for other volumetric muscle-loss pathologies. Embedded within the ECM are matrix-bound nanovesicles (MBV), a class of novel, distinct, highly-bioactive vesicle. Previous work has shown that MBV are able to recapitulate the immunomodulatory effects of whole ECM in mitigating the inflammatory phenotype of macrophages and promoting a constructive remodeling phenotype. The present study investigates the effect of MBV on C2C12 mouse myoblast differentiation and metabolism as a potential therapy for FSHD.

Methods: First, MBV were isolated from urinary bladder matrix (UBM) ECM. C2C12 myoblasts were then treated either directly with MBV or indirectly with conditioned medium from MBV-treated macrophages. Treated myoblasts were then examined for MBV uptake, metabolic activity using an alamar blue assay, and muscle marker expression using PCR and immunostaining.

Results: C2C12 cells were shown to internalize MBV by 1h post-exposure, with increased uptake evident at 6h. Cells exposed to MBV over a range of concentrations (1e9-1e11 MBV/ml) had increased metabolic activity 24h after treatment when compared to untreated controls. Expression of myoD, myogenin, and myosin heavy chain were not significantly altered by 24h treatment with MBV at a concentration of 1e11 MBV/ml. However, after 4 days of treatment with MBV, we observed increased desmin protein expression when compared to untreated cells.

Conclusion: These results indicate that direct treatment with MBV may promote differentiation. The effect of conditioned medium from MBV-treated macrophages on C2C12 differentiation is currently under investigation.

Defining How Recognition of Alloantigens Shapes Macrophage Immunometabolism

Marcus Waller, Dr. Heth Turnquist, Jordan Warunek
Brown University, Providence, RI; University of Pittsburgh Hillman Academy, Pittsburgh, PA

Abstract

In this project IC21 and bone marrow derived macrophages were treated with reparative and pro-inflammatory cytokines to observe the metabolic differences between them. Specifically, the uptake of glucose through Glut1and fatty acids through CD36.

Introduction

Macrophages differentiate into 2 types to be either pro-inflammatory or reparative. They differentiate depending on the cytokines in their environment that they bind to. What has previously been noticed is that M1 pro-inflammatory macrophages rely on glycolysis, while M2 reparative macrophages more heavily utilize fatty acid oxidation. During transplantation, we need these macrophages to be reparative because during this process the tissue receives trauma. This can be due to ischemia reperfusion injury or ice transport. Regardless, this tissue needs to repair itself once inside the recipient. Additionally, if the macrophages remain pro-inflammatory there is a higher chance for graft versus host disease. Our immune system often attacks transplanted tissue due to differences in alloantigens, as well as major and minor histocompatibility complexes. We hypothesize that macrophage recognition of allogeneic materials triggers glycolysis needed to support inflammatory differentiation, which then blocks metabolic reprogramming necessary for macrophage tissue repair.

Methods

IC21 macrophages were treated with four conditions. LPS and IFNy to induce a pro-inflammatory response, IL-4 to influence them to be reparative, allogeneic proteins from Balb C mice, and syngeneic proteins. They were then stained for Glut1 and CD36 to observe uptake using flow cytometry. Prior to this, we treated pro-inflammatory and reparative macrophages with 2NBDG, a fluorescent glucose, and bodipy a flurorescent fatty acid to be observed with cell imaging. However, these results were unreliable as there were no consistent readouts or numerical data produced.

Results

Despite being unreliable, we still noticed that all samples uptook more 2NBDG than bodipy. When we utilized flow cytometry we noticed that IL4 treated macrophages expressed more Glut1 and CD36.

Discussion

Our results from our IC21 macrophages were not what we expected, so we repeated the experiments with bone marrow derived macrophages as well. We recently performed flow cytometry on our samples and are currently analyzing the data.

Figure 1-4

Flow plot and graph for expression of Glut1

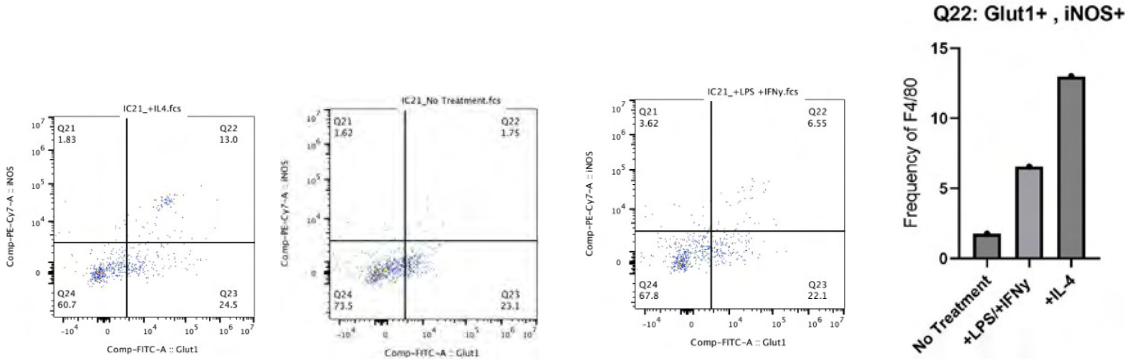

Figure 5-8

Flow plot and graph for expression of CD36

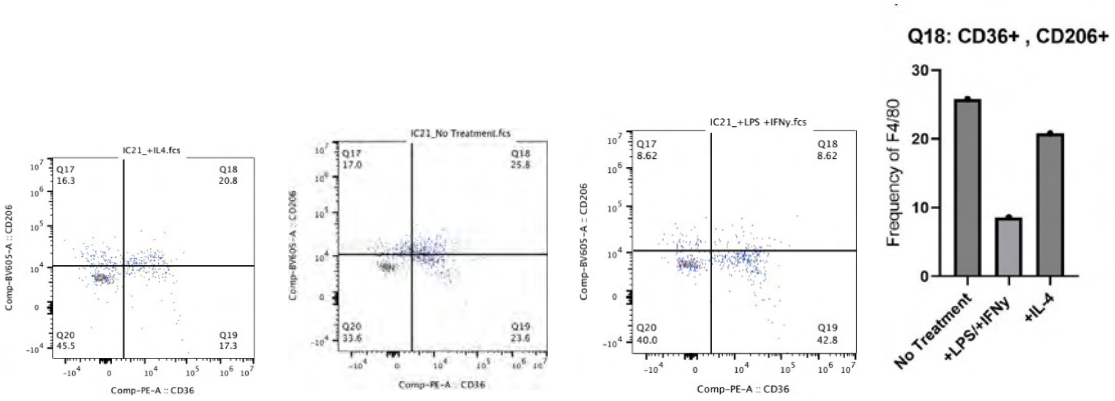

References

1. Ahl, P. J., Hopkins, R. A., Xiang, W. W., Au, B., Kaliaperumal, N., Fairhurst, A.-M., & Connolly, J. E. (2020). Met-flow, a strategy for single-cell metabolic analysis highlights dynamic changes in immune subpopulations. *Communications Biology*, *3*(1). https://doi.org/10.1038/s42003-020-1027-9
2. Artyomov, M. N., & Van den Bossche, J. (2020). Immunometabolism in the single-cell era. *Cell Metabolism*, *32*(5), 710–725. https://doi.org/10.1016/j.cmet.2020.09.013
3. O'Neill, L. A., Kishton, R. J., & Rathmell, J. (2016). A guide to immunometabolism for immunologists. *Nature Reviews Immunology*, *16*(9), 553–565. https://doi.org/10.1038/nri.2016.70
4. Van den Bossche, J., O'Neill, L. A., & Menon, D. (2017). Macrophage immunometabolism: Where are we (going)? *Trends in Immunology*, *38*(6), 395–406. https://doi.org/10.1016/j.it.2017.03.001
5. Zeiser, R., & Blazar, B. R. (2017). Acute graft-versus-host disease — biologic process, prevention, and therapy. *New England Journal of Medicine*, *377*(22), 2167–2179. https://doi.org/10.1056/nejmra1609337

Impact of COVID-19 Pandemic on Prostate Cancer Diagnosis

Scholar: Daniel Wang

School: Fox Chapel Area High School, Pittsburgh, PA

PI: Kathryn Demanelis

Mentor: Kathryn Demanelis

Site: Cancer Biology

Background: Prostate cancer (PCa) is the most prevalent cancer diagnosed in men and occurs most often in those over age 65, and early detection is crucial for improved prognosis. The COVID-19 pandemic greatly influenced hospital care for many chronic diseases, including cancer. As a result, patients with PCa may have experienced delayed diagnosis and treatment, although the extent of which is not known. Furthermore, the pandemic may have exacerbated PCa care disparities in Black and rural populations.

Objective: In this preliminary analysis, we sought to determine the extent to which patient-related and tumor-related factors differed between PCa tumors diagnosed before (January 2019-February 2020) and during (March-December 2020) the COVID-19 pandemic.

Methods: Data from 1384 PCa tumors (age ≥ 20 years and diagnosed after January 1, 2019) were available from the UPMC Network Cancer Registry. We used t-tests and chi-square tests to examine the association between being diagnosed during the pandemic and patient-related and tumor-related factors.

Results: Sample sizes for the pre-pandemic (control) and pandemic data (experimental) were 852 and 532 tumors, respectively. In all the variables assessed, only prevalence of family history in cancer was associated with being diagnosed during the pandemic (pre-pandemic: 64%, pandemic: 69% p=0.04). Overall, 80% of the tumors in the pre-pandemic group had late-stage cancer (stage 2-4), rising to 84% in the pandemic group (p=0.08). There was no association between clinical grade and being diagnosed during the pandemic.

Conclusions: While not many differences between the groups existed, a later stage of diagnosis was more frequent among tumors diagnosed in the pandemic. We could not examine socioeconomic status which may also contribute to cancer disparities. Future analyses will examine how the pandemic influenced time to treatment and prognosis.

Analyzing the Effects of Membrane Stressors on Biofilm Production in *Pseudomonas Fluorescens*

Julian J. Westray, Abigail Matela, PhD, Vaughn Cooper, PhD
Winchester Thurston, Pittsburgh, Pennsylvania; University of Pittsburgh Medical Center

Abstract

The Cooper Lab at the University of Pittsburgh studies microbiology and evolutionary genetics. Throughout the past few weeks, I have engaged in a series of experiments with bacteria pseudomonas fluorescens with the goal of finding mutants to study. I found 3 mutants which had a mutation in their cell membrane, (WT, wspF, and the double mutant) I grew these mutant colonies, and added ethanol and glycerol, two stressors to this bacteria's cell membrane. The goal of this project is to use a crystal violet assay to measure the amount of healthy cells and thus the biofilm production when these mutants come into contact with such stressors.

Introduction

Biofilm is the term that defines a group of microorganisms that grow and reproduce collectively on a surface. Many bacteria, such as pseudomonas fluorescens release biofilm that provides resistance to antibiotics or other harmful agents. These biofilms pose a serious threat to public health, as many bloodstream and urinary tract infections are both directly related to the production of biofilm. Gaining a better understanding of how to limit biofilm production could prove vital to healthcare.

Methods

First, in order to plate the bacteria, we must create agar plates made with half strength typtic soy agar. After the agar has been sterilized and poured into plates, we streak the plates with the 3 mutants of pseudomonas fluorescens that have been chosen for the experiment (WT, wspF, and the double mutant). We then allow the plates to grow for 2 days at 28 degrees Celsius. Single colonies from the mutant plates will be grown in experimental culture tubes filled with QB media, which will be incubated in a roller drum. After inoculation has finished, the bacteria cultures will be put into 96-well plates with QB media. Then, we will begin a dilution series for the experimental groups. After a day, we remove the contents from the well, submerge it in water, and add crystal violet. After 2 days, we add 95% ethanol to solubilize the crystal violet. Then, we use the Optical Density reader to measure the amount of health cells in the cell cultures.

Results

As of yet, there are no results. We just started this experiment on Monday, July 25, and we are still waiting to finish the crystal violet assay.

Discussion

These membrane stressors imitate the role of antibiotics used to kill bacteria. Bacteria are constantly growing, reproducing, and mutating, and researchers need to keep updating antibiotics to combat these mutations.

Epigenetic's: How Environmental Exposures and Sex-based Differences Regulate Macrophage Function

Scholar: Kamili Wiley

High school: Winchester Thurston

Lab: Dr. Adam Soloff

Mentor: Adam Soloff, Amy Powers, Seth Eisenberg, Sulwe Kauffmann-Okoko, Rajeev Dhupar

Site: Immunology and Cancer Immunotherapy (ICI)

Background

Macrophages are immune cells that can be found in all tissues in the body. Their role is to fight infection, tumors, and maintain immune tolerance. Functionally, macrophages protect from cancer through the phagocytosis of tumor cells and the production of inflammatory cytokines. Epigenetics regulation translates environmental exposures into altered gene expression. Epigenetic processes have been associated with the development of cancer and targeted for cancer therapy. We are exploring the impact of epigenetic regulation on macrophage function comparing female and male mice in response to toxin exposures.

Methods

To generate macrophages, we extracted bone marrow from female and male C57BL/6 mice and cultured them in complete DMEM and dosed with MCSF(20ng) for 5-6 days. Plated male and female cells in different plates. Each plate had Male/Female control and Male/Female toxin. For the toxins we exposed the cells to Diesel Exhaust Particulate (DEP;dose) and the organophosphate pesticide Malathion (dose). Plated cells were incubated for at 24 hours with or without toxins. Subsequently, supernatants were collected for CBA and cell pellets harvested for histone extractions using the (EpigenTek) total histone extraction kit. Scratch assays were performed to examine migration/wound healing. Cytokine analysis was performed using the mouse inflammation cytometric bead array and total H3 histone and H3 histone acetylation were determined by Elisa.

Results

The H3 histone levels for the cells that were dosed with toxins were lower than the cells that weren't dosed with toxins, The cells doused with LPS were also lower.

Conclusion

Our results showed that when out cells are exposed to environmental toxins, that the H3 levels will be lower. This can be a result of the activation of cells or damage to their nuclear contents or chromatins.

Characterizing Glaucoma Pathology, by Comparing the Retinal Nerve Fiber Layer (RNFL) Thickness of a Mouse Model with Wildtype Mice

Scholar: Samuel Wilson

High School: PA Leadership Charter School, Pittsburgh, PA

PI of Group/Lab: Yiqin Du, MD, PhD

Mentors: Yiqin Du, MD, PhD,
Sridhar Bammidi, PhD,
Site: Ophthalmology

Background: Glaucoma is a neurodegenerative disease causing irreversible vision loss. The retinal ganglion cells (RGCs), the innermost layer of the retina, are gradually damaged in glaucoma patients. RGCs and their axons that gather together to form the optic nerve are responsible for sending the information captured by the eye to the brain. This gradual cell death leads to gradual visual field loss that leading to blindness if leaving untreated. The RGCs and their axons together constitute the retinal nerve fiber layer (RNFL). In glaucoma, with the damage of the RGCs and their axons, the RNFL layer becomes thinner which could be an indicator of the glaucoma progress. Optical coherence tomography (OCT) is a non-invasive technique which uses light waves to take cross-section pictures of the retina. In human glaucoma patients, the RNFL thinning is not equal in the quarters of the retina. This study aims to compare the quarterly RNFL thicknesses of a mouse glaucoma model with myocilin mutation ($MYOC^{mut}$) and age-matched old wildtype (WT) mice. The RNFL of old WT mice and young WT mice was also compared which could indicate if aging could also induce RGC damage.

Methods: Animals were briefly anesthetized by injecting a cocktail of Xylazine and Ketamine and the pupils were dilated using Tropicamide and Phenylephrine eye drops. OCT recordings were taken at a wavelength of 576 nm, and the images were analyzed through Bioptigen software for measuring the thickness of the RNFL. The thicknesses were averaged quarterly using Excel and compared and statistically analyzed using PRISM.

Results: The RNFL thickness in the individual quadrants i.e. upper nasal, upper temple, lower nasal and lower temple for both the left and right eyes were clubbed together, for comparison. The lower temple and lower nasal quadrants showed a decrease in the trend of the RNFL thickness. The results were statistically analyzed for one-way ANOVA and Tukey's multiple comparisons test. Although there was no statistical significant difference among the groups, there was a trend with RNFL reduction in $MYOC^{mut}$ mice.

Conclusion: The $MYOC^{mut}$ animals showed a trend in decrease of the RNFL thickness. The degeneration of the RGCs in the RNFL layer in the $MYOC^{mut}$ animals shows the progression of Glaucoma. The lower number of positive and old WT mice analyzed for the RNFL thickness was a limiting factor for the lack of significance in the results obtained.

Reporting Macrophage M1 Inflammatory State Utilizing Inserted Fluorescent Reporting Gene in Mice

Scholar: Helen Zhang

Highschool: Winchester Thurston, Pittsburgh, Pennsylvania

Mentor(s): Rachel Gottschalk Ph.D., Karsen Shoger

Site: Immunology and Cancer Immunotherapy

Macrophages are the primary cells of the innate immune system. During immune response, macrophages polarize into a functional state which lies on a spectrum of M1, pro-inflammatory, and M2, tissue-repair. In both, there are biomarkers that indicate the polarization state, which include changes in transcription rate of certain genes. This study focuses on macrophage expression of the *Fth1* gene, which encodes a component of a major intracellular iron storage protein (ferritin) in relation to the M1 polarization state. The goal was to find a method of reporting M1 polarization through the use of a gene that encodes and produces a fluorescent protein, mScarlet. To do this, mice were genetically modified to have the gene placed in front of the *Fth1* gene along with a cleavage point so that when translation occurs, the cleavage point allows for mScarlet produced simultaneously with ferritin, thereby reporting how much transcription of *Fth1* occurs during macrophage functional states. The two primary methods used were Flow Cytometry and qPCR. Flow Cytometry was used to examine cell populations from the bone marrow and lung for mScarlet intensity. Some bone marrow monocyte populations were also stimulated with KLA, a component of bacterial cell walls, at various increments of time to initiate an immune response, thus causing differentiation into macrophages. qPCR was used to quantify *Fth1* expression in the stimulated samples. All experiments done on the genetically modified mice(*Fth1* mScarlet) were also performed on unadulterated wild type mice(WT), which served as the control. Through this, we found that various immune cell populations had noticeable differences in mScarlet intensity compared to the controls, with Alveolar Macrophages having the greatest intensity out of all the populations examined. Further studies would involve further validation testing of a larger pool and breeding with M2 Reporter Mice to make dual reporter mice.

\